Elastic Properties and Phases of Bent Core Liquid Crystal

A thesis submitted to The University of Manchester
for the degree of Doctor of Philosophy
in the Faculty of Science and Engineering

2016

Harry Liu
University of Manchester
School of Physics and Astronomy

Table of Contents

Chapter 3 Experimental techniques in investigating liquid crystal materials

Chapter 4 Investigation of unusual elastic properties in bent core liquid crystal

Tables and Figures

Elastic Properties and Phases of Bent Core Liquid Crystal

Harry Liu
The University of Manchester

Thesis for the degree of Doctor of Philosophy
2016

Abstract

The recent interest in bent core liquid crystal has shown many unique physical properties, such the anomalous behaviour of the elastic constants (Splay K_1, Twist K_2, and Bend K_3). In bent core liquid crystals it is observed that $K_3 < K_1$ contrary to what is observed in conventional calamitic liquid crystals. In this thesis we aim to understand how including an intrinsic bend affect liquid crystalline systems.

Mixtures of oxadiazole based bent core and calamitic liquid crystals were studied. Generally a stable nematic phase at room temperature can be achieved, however one unique phase was observed in one mixture which is studied in detail later. The mixture all show similar effects with increases in bent core dopant significantly lower values of K_3 and K_2. These results are expected as the lowering of K_3 is seen in many other studies, however generalising K_2 is more difficult due lack of studies of the K_2. The physical properties of four oxadiazole based bent-core liquid crystals were also examined. The materials are chosen to study the effects of terminal chain length, substitution with fluorine, and swapping alkoxy to alkyl. Changes in the terminal chain length and fluoro-substitution have been found to have little influence on the elastic constants at equivalent reduced temperatures. However, the material with an alkyl terminal chain exhibits much reduced elastic constants than the alkoxy terminal chain compounds. Importantly, using molecular field theory and atomistic modelling, the calculated elastic constants are in excellent agreement with the experimental values pointing to the importance of the bend angle. The elasticity in the nematic phase formed from bent-core molecules is not strongly influenced by changes to the terminal chains or the presence of fluorine.

The elastic properties of a bent-core thiadiazole nematic liquid crystal are also investigated. The elastic constants across the whole nematic range were studied. It was found that the thaidiazole bent core materials exhibited elastic properties similar to calamitic liquid crystals ($K_3 > K_1$). Such behaviour is analogous to calamitic liquid crystals but is in contrast to all other bent-core nematic materials reported to date. Such a result questions some of the current explanations for the elastic behaviour of bent-core materials. Using molecular field theory and atomistic modelling the different elastic behaviour predicted is again in excellent agreement with experimental results. The bend angle is again shown to be an important part in determining the physical properties of bent-core nematic liquid crystals.

In a mixture from an oxadiazole dopant and calamitic host liquid crystal, it was found that a filament structure appears in the nematic phase. The filaments appear to interfere with the measurements for elastic constants. In order to understand the filament structure many methods were used including SAXS, dielectric permittivity, and DSC. It was found that the mixture had formed a gel – like phase. The gel is composed of a liquid crystal network and a liquid crystal background, not seen before in any gel system. Due to the liquid crystalline properties both the network and the background can be aligned and manipulated. The new gel phase can possess many new unique properties which warrant further studies understand further into how fundamentally the phase is forming.

Declaration

No portion of the work referred to in the thesis has been submitted in support of an application for another degree or qualification of this or any other university or other institute of learning.

Copyright

Acknowledgement

Firstly I would like to offer my sincerest gratitude towards my supervisor Helen Gleeson, without her guidance, wisdom, and patience I would not be able to accomplish this work. I am also extremely grateful to Dr Rachel Tuffin and Merck Ltd for funding, providing support, and resources to help me with the work. Thanks to Prof Ferrarini for the calculation performed on the materials which proved invaluable in my work; and to Prof John Goodby, Dr Verena Gortz, Prof Seltmann, and Prof M. Lehmann for providing the materials used in this work. I must also thank my fellow group members especially Prof. Cliff Jones, Dr. Sarabjot Kaur, Dr. Mamatha Nagaraj, Dr. Linan Tian and Dr Zhaopeng Zhang for all the great discussions and help with my work; and past members Dr P. Brimiecombe for providing the programs for calculating the elastic constants.

I am grateful to my parents who each helped and supported me always unconditionally. I of course would like to offer a special thanks to my beautiful wife Lin who supported immensely me throughout my work.

Chapter 1 Introduction

Introduction

Matter can exist in many states, the most basic of which are the gas, liquid, and crystal states. In the liquid state, the molecules are in a state of complete disorder, whereas in the crystal state the molecules have complete positional and orientation order. A new state of matter was first discovered in 1888 by Friedrich Reinitzer, when he observed that a cholesterol derivative, found in plants, had two melting points [1]. The two melting points indicate that there is another state in-between the liquid and solid state, the intermediate state was later named the liquid crystal state, opening the way to a whole new area of research. The liquid crystal state is a state of matter existing below the temperature range of the liquid phase, and above the temperature range of the crystal phase. Liquid crystalline materials exhibit the properties of both the liquid and crystal states, where molecules have some order, but maintain the diffuseness associated with liquids.

Liquid crystals have risen to prominence with their application in display devices. Liquid crystal displays are relatively cheap, simple, and thin making them the ideal candidate for a range of displays. The most common display made from liquid crystals is the Liquid Crystal Display (LCD) television; almost every household has a LCD TV. There are several limitations with LCD technology; however, such as slow switching speed and ambient light dependency; in order to overcome these difficulties, a large level of research currently exists. The liquid crystal state is also extremely sensitive to temperature changes; at higher temperatures there are more molecular movements, which reduce the order in the liquid crystal phase. Small changes in the phase order can influence bulk properties of the material, such as changing the colour exhibited by the liquid crystal. Due to the sensitivity of the liquid crystal state to temperature changes, liquid crystals have also found many applications in temperature sensing. The temperature dependent colour changes in liquid crystals was utilised in mood rings and other novelty products. The sensitivity to temperature can also produce a map of different temperature regions; this is especially useful in applications such as monitoring complex electrical circuits. Regions with shorts or bad connections will have higher temperatures, and can be seen without the need to check each individual component [2, 3]. Liquid crystals also possess many optical properties making them ideal for manipulation of light, such as waveguides [4, 5], optical attenuators [6], shutters [7], and many more. The other major use for liquid crystals is in soaps and detergents, and they dominate the market for liquid crystals, ton for ton outselling the liquid crystals sold for displays and other uses. There are also other unique liquid crystals such as Kevlar, a synthetic

fibre made from liquid crystals. Kevlar is made from a nematic solution, due to the long polymer molecules, they are ordered in the solution to form a nematic phase. The synthetic fibres are then spun from the liquid crystal solution to give highly oriented fibres. Kevlar has extremely high tensile strength, and when spun into ropes have found a wide range of uses, from protective armour to bike tires. Liquid crystal materials' many interesting unique properties have led to the prominent use of liquid crystals for many aspects of industry, science, and everyday life.

With the prominent use of liquid crystal based materials throughout everyday life, there has been intense research in liquid crystals to improve their current function and to find new uses. The ongoing research has led to the discovery of new liquid crystal phases formed by complex molecules such as bent core molecules, explained later in this chapter. This thesis aims to investigate the new unique behaviour from introducing bend into common liquid crystal phases, and attempts to understand the physics behind these behaviours. This chapter will aim to introduce some basic concepts of liquid crystals, which will be built upon when investigating the bent core liquid crystals.

Calamitic liquid crystal

There are many types of molecules that can form liquid crystalline phases and they all share one common attribute, the anisotropy of the molecular shape. The anisotropy of the molecule promotes certain orientations and positions, creating the order that differentiates this phase from the liquid phase.

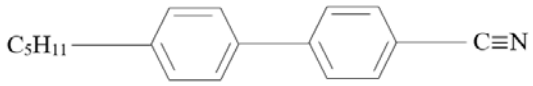

Figure 1 The structure of a calamitic liquid crystal molecules 5CB.

The most common type of liquid crystal molecule is the calamitic liquid crystal, shown in Figure 1, which is typically a long rod-like molecule. Calamitic liquid crystal molecules generally have a rigid core to maintain the anisotropic shape and often have flexible side chains. The side chains exists to encourage more disorder in the material to prevent crystal formation [8]. Figure 1 shows the molecular structure of a 5CB molecule, a room temperature liquid crystal discovered in 1973 [9], and were among the first commercially viable liquid crystals.

Basic phases formed by calamitic molecules

Liquid crystal phases can form in two ways, thermotropic and lyotropic. Thermotropic liquid crystal phases are dependent on temperature and are split further into two groups, enantiotropic and monotropic. Enantiotropic liquid crystals exhibit liquid crystal phases on both heating and cooling, while monotropic liquid crystal phases can be observed on cooling below the melting point of the material. These phases are metastable and will revert to a crystalline state over time. Most of the liquid crystal phases studied in this thesis is thermotropic and enantiotropic in nature.

Lyotropic liquid crystal phases are dependent on the concentration of the liquid crystal molecules in a solvent. Once above a certain threshold, the bulk material exhibits a liquid crystal phase. Lyotropic liquid crystals are very common in everyday life, with most detergents composed of molecules that can form lyotropic liquid crystals.

The simplest liquid crystal phase exhibited by calamitic molecules is the nematic phase, commonly denoted by the symbol N, shown in Figure 2. In the N phase, the molecules are distributed randomly similar to liquids but with the molecular long axis pointing in one common direction, referred to as the director, and denoted by the symbol $\hat{n}$, thus $\hat{n}$ is an average of the molecular long axis in space and time. It is important to note that, due to the lack of physical polarity in the phase, $\hat{n} = -\hat{n}$.

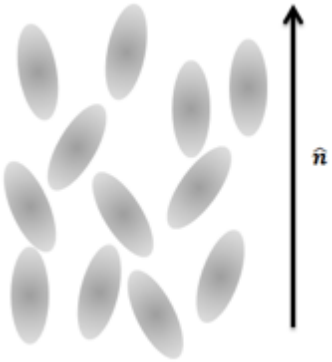

Figure 2 Nematic liquid crystal phase with orientation order but no positional order, the director $\hat{n}$ is shown by the arrow.

Although locally there are more variations in the orientation of the molecular long axis, but when averaged over long distances the orientation of the molecules is along $\hat{n}$. To specify the amount of

orientation order within a liquid crystal phase it is helpful to define an order parameter. The most useful way is to find the average of the second Legendre polynomial,

$$S = \langle P_2(\cos\alpha)\rangle = \langle \frac{3}{2}\cos^2\alpha - \frac{1}{2}\rangle,$$

Where α is the angle between the molecular long axis and the director.

S can take values between 1 and 0, 1 defines complete order such as solids and 0 defines complete disorder such as liquids. Liquid crystals typically have S values between 0.3, and 0.8.

There are also more ordered liquid crystalline phases, where there exists both structural and orientation order such as the smectic phases. In the smectic A (SmA) phase, the molecules are oriented in layers with the molecular long axis parallel to the layer normal as shown in Figure 3 (Left). The order within the layers only exists over a few molecular centres [10] thus there is no periodic structure within each layer. In reality the actual layers are not well defined, and is more accurately described as a density wave[11]. There are also further variations in the smectic phases, such as the smectic C (SmC) phase, where the director is tilted with respect to the layer normal shown in Figure 3 (right).

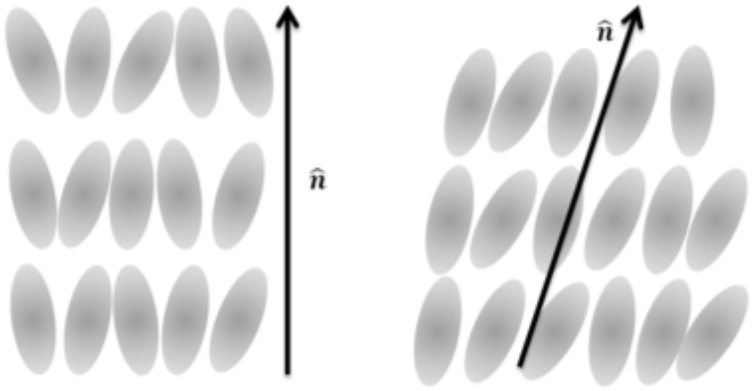

Figure 3 (Left) Smectic A phase where the molecules lie parallel to the layer normal (Right) Smectic C phase where the molecules are tilted with respect to the layer normal.

There are many other smectic phases where there also exists positional order within the layers, such as the smectic B (SmB) phase, where the molecules arrange themselves in a hexagonal order

within each layer [10, 12]. The more ordered a phase is, the closer it is to exhibiting properties similar to a crystal phase, whereas a less ordered phase such as the N is similar to the liquid state.

Chirality

Further changes to the molecular orientation can exist with chirality. A chiral object is defined to be distinguishable from its mirror image, and the classic example are the human hands. Usually chirality is composed of liquid crystal molecules that have an intrinsic chirality within the molecular structure, causing a bulk chirality throughout the material. Chirality can also be induced by introducing chiral dopants to a system with an achiral liquid crystal host, and note the dopants do not necessarily need to be liquid crystal themselves. Introducing chirality in liquid crystal systems can cause a dramatic change in its properties, and the chiral phases are typically denoted with *.

For nematic phases with chirality (N*) the structure is shown in Figure 4(a, b). The molecules form a helical structure with the helix axis perpendicular to the molecular long axis[13]. The director therefore follows a continuous twist along the helical axis, and the distance over which the director is rotated by 360^{o} is called the pitch length p. However, we note that the structure actually repeats every 180^{o} due to $\hat{n} = -\hat{n}$. In chiral nematics can be made from equal amounts of both left and right handed molecules, such systems are referred to as racemic systems. In racemic systems, the mixture is innately mixed and the system has infinite pitch, thus the phase can no longer be described as a chiral nematic phase. In some situations, racemic mixtures are made from achiral molecules which give rise to different domains of handedness; these are separated by defects where the director is undefined and separate the different handedness of chirality. This latter case is an unusual situation but can form in bent core systems.

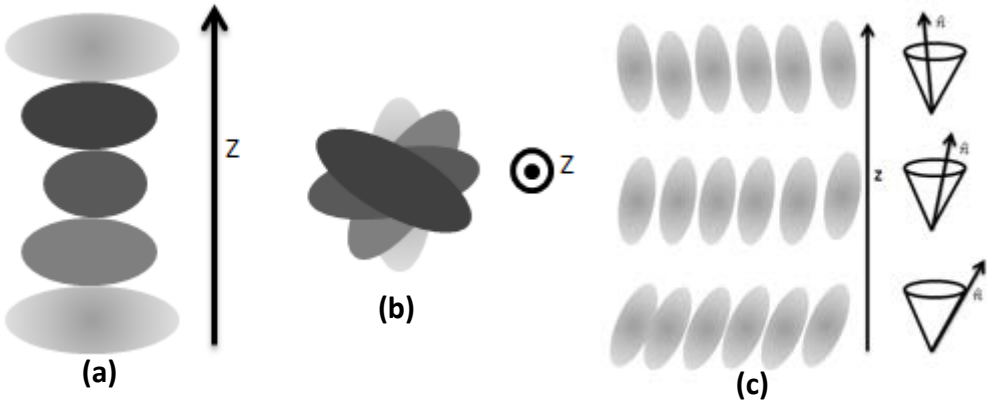

Figure 4 (a) The chiral nematic phase, seen from side with the helical axis in the azimuthal direction z. (b) The same chiral nematic phase, with the helical axis through the page. (c) The smectic C phase, with the director rotating as it recesses from one layer to the next. (z represents the helical axis)

Smectic phases can also exhibit chirality; however, any deviation of the director within the layers will be incompatible with the layer structure, so the director can only rotate in between layers. In the case of a smectic C* phase, the resultant structure is shown in Figure 4(c) where there is a conical rotation of the director. If we consider a similar approach for smectic A* phases, then it is obvious there is no change in the structure since the structure is degenerate about the helical axis.

Bent core liquid crystals

Calamitic liquid crystal was the focus of early research, because any deviations from the rod-like shape were considered to destroy the liquid crystallinity of the material. Thus molecules which break the shape symmetry like board shapes or bent shaped molecules, were not considered to be good candidates to exhibit liquid crystal behaviour. Even though the first bent core liquid crystal material was created in 1929 [14], it's properties were not properly investigated until much more recently. It was not until the polar switching properties [15] were discovered in 1991 that bent core liquid crystals became a popular area of research. Bent core liquid crystals, similar to calamitic liquid crystal, have a rigid core with the bend in the core with flexible side chain as shown in Figure 5.

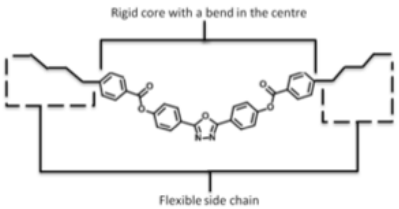

Figure 5 A bent core molecule with an oxadiazole core.

Due to the anisotropy in the short axis and the long axis of the molecules, there are many phases formed by the bent core molecules that are biaxial; this is where the molecules have an orientation order for the long axis and the short axis. This is different than in conventional calamitic liquid crystals, where the phases seen are usually uniaxial. In this case, there in only one axis, the long axis, the orientation order exists.

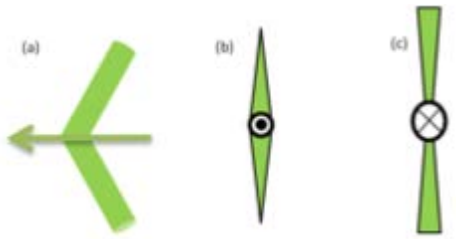

Figure 6 Definition of polar orientation for different geometries; (a) molecule with polar order pointing to the left of the page, (b) molecule with polar order pointing out of the page, (c) molecule with polar order pointing into the page.

The anisotropy in the short axis induces the polar ordering shown in Figure 6. The polar order is an important property in the bent core liquid crystal phases and is differentiated from the conventional phases discussed previously. The more complex phases will be explored in chapter 4.

Optics of liquid crystals

Birefringence

Due to the anisotropic nature of liquid crystal phases, the properties exhibited are also anisotropic. A prominent property of anisotropic materials is birefringence. Birefringence in crystals causes a well-known phenomenon called double refraction; this is where an incident beam is split, each with distinct polarisation and each traveling along different paths. This results in two images being observed. Birefringence is an important property that liquid crystals possess, and the phenomenon is observed during liquid crystal formation through cross polarising microscopy.

In cross polarising microscopy, a liquid crystal material is placed between crossed linear polarisers and observed with a microscope setup. The linearly polarised light (upon entering the material) is split into two orthogonal components, the ordinary ray, which follows the Snell's law, and the extraordinary ray, which only follows Snell's law when light travels along the optic axis of the material. For anisotropic materials the refractive index experienced by the ordinary ray n_o is different

than the refractive index experienced by the extraordinary ray n_e. Each component of light is slowed by a different amount depending on the refractive index that they experienced.

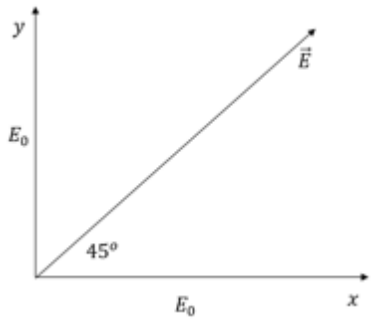

Figure 7 light propagating at 45^o to the director (y axis).

Consider an incident light travelling through a nematic liquid crystal material, with the incident light polarised at 45^o to the director parallel to the y axis shown in Figure 7. The components of the electric field as it enters the materials, where the frequencies are the same, but each possess a different wavelength and velocity. Thus the electric field can be expressed as

$$\mathrm{E_x}(z,t) = E_0\cos(\omega t) = E_0\cos(n_\perp k_0 z - \omega t),$$

$$\mathrm{E}_y(z,t) = E_0\cos(\omega t) = E_0\cos(n_\parallel k_0 z - \omega t).$$

Where E_0 is the amplitude, $n_\parallel, n_\perp$ is the refractive index parallel and perpendicular to the molecular long axis, ω is the angular frequency, k_0 is the wavenumber, and z distance travelled.

The amplitudes of the two components are the same since the light is polarised at 45^o to the director. The polarisation emerging from the liquid crystal materials can be found by simply substituting $z = d$ where d is the thickness of the material.

$$\mathrm{E_x}(z,t) = E_0\cos(n_\perp k_0 d - \omega t),$$

$$\mathrm{E}_y(z,t) = E_0\cos(n_\perp k_0 d - \omega t) = E_0\cos(n_\perp k_0 d - \omega t + \Delta n k_0 d),$$

where $\Delta n = n_e - n_o$ is defined as the birefringence.

The phase difference between the beam components is [16]:

$$\Delta\phi = \frac{2\pi\Delta \mathrm{n} d}{\lambda_0},$$

Where λ_0 is the vacuum wavelength of the incident light.

When components of the incident beam recombine, the polarisation is changed. Generally, the combined light is elliptically polarised however there are special cases such as when the phase difference between each component is a multiple integer of the wavelength. In the case of:

$$m\lambda_0 = \Delta nd.$$

There is no change in the polarisation with respect to the incident light. Since the second polarizer is perpendicular to the incident light when the components recombine, minimum transmission occurs. If the difference in retardation is a half integer multiple of the wavelength:

$$(m + \tfrac{1}{2})\lambda_0 = \Delta nd,$$

The change in polarisation would mean that the outgoing light would have the polarization rotated by 90^o and that means that it is parallel to the second polarizer and passes through unhindered; in this case we observe the maximum intensity for the outgoing beam.

Polarising microscopy

A polarising microscope, shown in Figure 8, is simply a microscope setup with a linear polarizer perpendicular to a second polarizer called an analyser. The analyser is placed perpendicularly to the polarizer, this means that any isotropic material, such as air, in between the polarisers would result in minimum light transmitted. This is only true if the polarizer and the analyser are perpendicular to each other; if an arbitrary angle exist between the polarizer and analyser then the transmitted intensity obeys Malus's Law, which is $I(\theta) = I_0 \cos^2(\theta)$, when $\theta = 90^o$ then $I = 0$. The microscope has two modes, a reflection mode and a transmission mode. For the most of the work in this thesis, the transmission mode is used. There is also a camera which can take images in situ monitoring any texture change, and due to the temperature sensitivity of liquid crystal materials a heating stage, this is used to control the temperature of the sample.

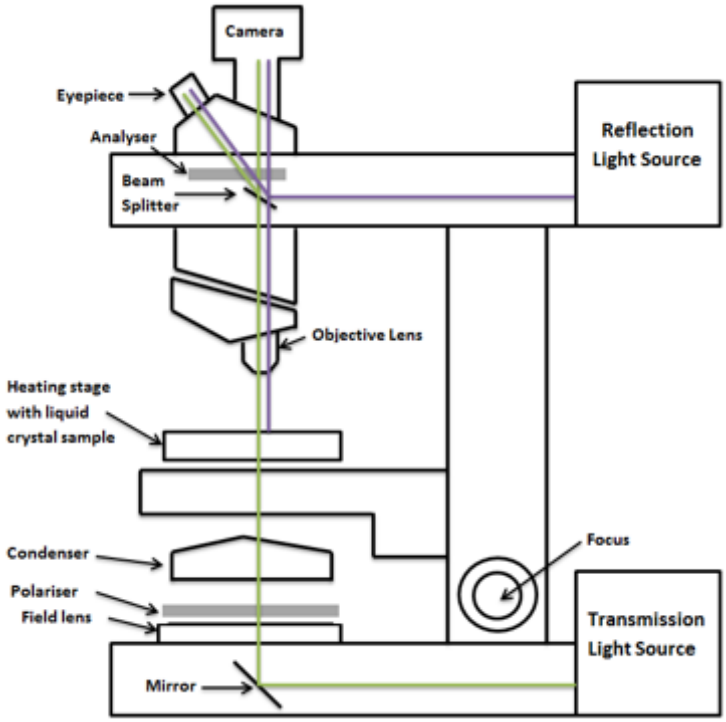

Figure 8 Polarising microscope setup with transmission and reflection modes

Using a crossed polarising microscope, only those properties which change the polarisation of light can be observed, making it a powerful tool for studying liquid crystalline systems, due to the inherit birefringence of the liquid crystal. Depending on the orientation of the liquid crystal director, different textures can be observed. From those textures, the average director profile can be assessed and the basic structure of the liquid crystal can be probed by observing the texture. Any isotropic material would not alter the polarisation. As a result, the texture observed in isotropic systems would be dark since no light can be transmitted. This is also the case for birefringent materials with optical axes parallel to the incoming beam; along its optical axis, the birefringent material is isotropic. For example in nematic phases the optical axis is along its director, and thus if place in a crossed polarising microscope with the director orientated normal to the polarisers, no light would be transmitted.

Optical properties of chiral nematics

Introducing chirality to nematics produces some unique optical properties when light is propagating along the helical-axis of the chiral-nematic liquid crystal. In the case where the pitch of the chiral nematic is much larger than the wavelength of the incoming light, the light can travel the distance of several wavelengths while experiencing very little director changes. This special case can be simplified to light propagating through infinitesimal slices of nematics with slight changes in $\hat{n}$

between each slice. The plane of these slices is perpendicular to the helical axis and the light propagation shown in Figure 9.

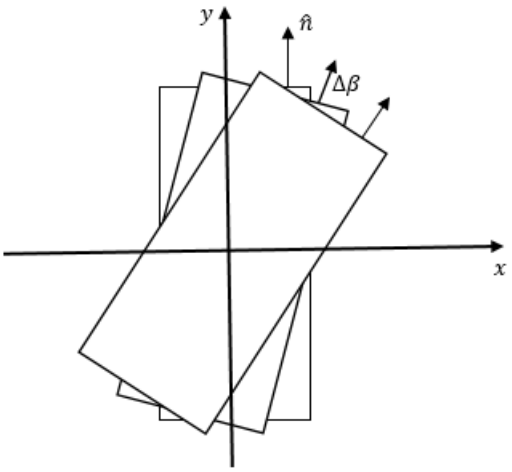

Figure 9 Nematic slices of a chiral nematic liquid crystal, with $\hat{n}$ initially y axis and $\Delta\beta$ the angle of director of the second slice to the y axis.

Consider an incident light polarised parallel to y axis, it will propagate through the first slice without any changes in polarisation. Since the director of the second slice is oriented at $\Delta\beta$, there must be two components of the electric field, one perpendicular to director, $E_0 \cos(\Delta\beta)$, and the other parallel, $E_0 \sin(\Delta\beta)$. So the components emerging from the second slice are

$$\mathrm{E_x}(z,t) = E_0 \sin(\Delta\beta)\cos(n_\perp k_0 d - \omega t),$$

$$\mathrm{E}_y(z,t) = E_0 \cos(\Delta\beta)\cos(n_\perp k_0 d - \omega t + \Delta n k_0 d).$$

Therefore, the emerging light is polarised elliptically, with β being the angle between the angle of the semi – major and x axis where

$$\beta = \frac{1}{2}\tan^{-1}\left(\frac{2E_{0x}E_{0y}\cos\Delta\phi}{E_{0x}^2 - E_{0y}^2}\right).$$

Applying the limits $p \gg \lambda_0$ and $\Delta n k_0 d \ll 1$, β can be approximated to be

$$\beta \approx \frac{1}{2}\tan^{-1}(-\tan(2\Delta\beta)) \approx \begin{cases} -\Delta\beta \\ \frac{\pi}{2} - \Delta\beta \end{cases}.$$

Since β is the angle between the semi – major axis and the x axis, and $\Delta\beta$ is small, the first result would mean that the resultant polarisation is nearly parallel to the x axis. This results does not make sense since the incident light is polarised along the y axis. This means that the only real result is $\frac{\pi}{2} - \Delta\beta$ where the emerging ligh is near parallel to the y axis. As a result, the light emerging from the infinitesimal nematic slice has its director rotated slightly and since $\Delta n k_0 d$ is extremely small the light is still linearly polarised. The overall effect is that of an optical rotator, with the linear polarisation rotating with the director. This is called a waveguide regime for propagation and is commonly used in display devices where it is required to rotate the polarisation by 90^o or 270^o causing the light to emerge with polarisation perpendicular to the incoming light [2].

For short pitch lengths the optical response is much more complicated, however due to the periodic nature of the phase, a special case arises when the wavelength of incident light $\lambda_0 = np$. The special case is also the condition for Bragg's law; this causes the complete reflection of one handedness of circular polarisation of that wavelength, and is commonly referred to as Bragg reflection[17].

Basic construction and geometry of liquid crystal devices

In the discussion so far, liquid crystal directors have been assumed to be perfectly uniform. In reality this is rarely the case without a surface treatment or external fields. In order to utilize their potential, liquid crystalline materials need to be confined, and using surface treatments on the boundaries of the liquid crystal, its properties can then be manipulated.

Liquid crystal cell

The most common way to confine and manipulate liquid crystal is by using a liquid crystal cell. A basic cell schematic is shown in Figure 10. The cell is composed of several layers. First the glass substrate forms a basis for everything to be built upon, it is transparent so that any optical change can be observed. Then a layer of Indium Tin Oxide (ITO) is used as electrode to apply an electric field

across the cell, which is transparent as well. Finally, a layer of alignment is used to influence the director orientation.

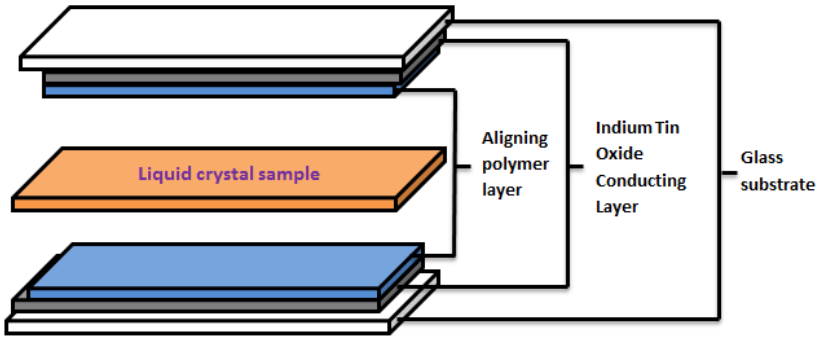

Figure 10 Experimental cell used to study liquid crystalline materials.

The two most common and simplest orientations of molecules are the planar and homeotropic alignment, which are induced from the alignment layer. Planar alignment is where the molecule's long axis lies in the plane of the cell. To achieve planar alignment, a thin layer of polymers like polyvinyl alcohol (PVA) or polyimide materials are deposited onto the glass substrates. The alignment layer then needs to be rubbed; the rubbing process causes microgrooves to form along the rubbing direction [18]. The typical way to create the grooves is to rub with a velvet cloth. One of the reasons why rubbing works for aligning liquid crystals is that the micro-grooves are rubbed into the alignment layer and this causes the molecules to lie in parallel to the grooves[19-22]. The influence from the alignment layer deteriorates with increase the cell gap, and at distances above $50\mu m$, the alignment layer has little to no effect on the director orientation[23, 24].

To achieve homeotropic alignment, hydrophobic or hydrophilic materials such as lecithin [25] are used. The material is usually dispersed in water then the solution is evaporated. The process causes the alignment molecules to lie with its molecular long axis perpendicular to the surface as shown in Figure 11. The structure formed by the alignment layer then forces the liquid crystal molecules lie perpendicularly to the glass surface.

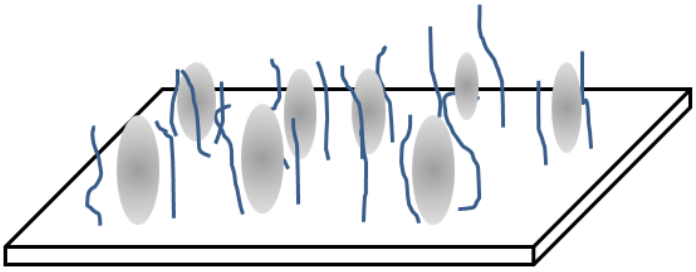

Figure 11 Homeotropic aligned calamitic molecules lying perpendicular on glass substrate.

Indium Tin Oxide (ITO) is a transparent conducting material that is most commonly applied to the glass substrates, to act as electrodes, allowing observations of electric field effects in situ.

The thickness of the liquid crystal layer in the cell can be set from the cell gap. The cell gap in turn is determined from spacers, which are either dispersed throughout the cell or just at the periphery of the cell. The spacers are made from hard materials typically silicon or Mylar so that the cell gap is not easily distorted. Spacers dispersed throughout the cell could distort the local director field around the spacer and could be detrimental in certain situations.

There are some limitations with this simple device geometry. Firstly, the alignment only causes a uniform director field throughout the cell; any other complex director field is unable to be achieved with this simple construction. Secondly, the electrodes can only produce electric fields perpendicular to the cell plane, and are unable to produce any field in the plane of the cell. More complex arrangements of the cell will be explored in the next section.

Twisted Nematic (TN) alignment

In addition to the two most common alignment geometries, the planar and homeotropic, there are many other types of alignments which create a complex director field for a range of purposes. One such alignment is the Twisted Nematic (TN) alignment. In the TN cells, the alignment direction on each of the glass substrates is at 90^{o} to each other as shown in Figure 12.

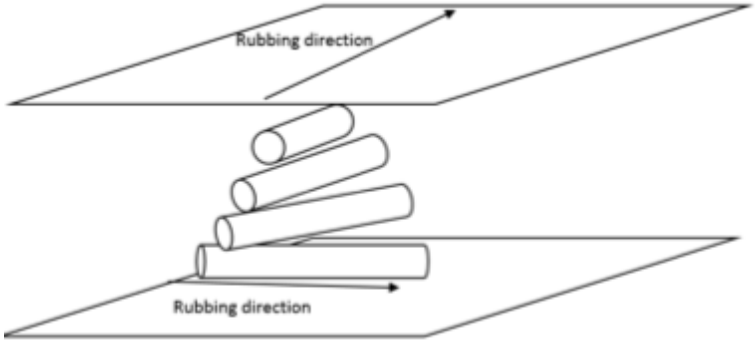

Figure 12 The perpendicular alignment between the top and bottom glass substrate causes a twist in the nematic structure of the liquid crystal

Near the surfaces, the alignment layer forces the liquid crystal molecules to align along the rubbing direction, therefore rotating the director by 90^o through the cell from one substrate to another. Thus, in TN cells there is an intrinsic twist deformation occurring throughout the cell. As discussed earlier, when the condition $p > \lambda_0$ is met, the liquid crystal acts as a polarisation rotator. In a twisted nematic cell, the $p = \frac{d}{4} \gg \lambda_0$, conditions enables any liquid crystal to act as rotator. When TN cells are placed in between crossed polarisers, there is a maximum transmission when the alignment direction is either perpendicular or parallel to the polarisers. The maximum transmission state is in contrast to the planar cells where this would produce a dark state where no light is transmitted. Interestingly there is no dark state for the TN cells in between cross polarisers and minimum transmission occurs when the TN alignment is 45^o to the polariser direction. These cells are commonly used in display devices, since TN cell would be in a transmission mode without any electric field application. TN cells are commonly used in "passive" displays [26] as they require little power to operate and useful for devices which run on battery to reduce the need to frequently change the battery.

Interdigitated cells

One way to obtain electric fields within the plane of the cell is to use interdigitated cells referred to as In-Plane Switching (IPS) cells. In IPS cells, the electrodes the red and black regions seen in Figure 13, are etched into an interdigitating pattern shown in Figure 13 (Bottom).

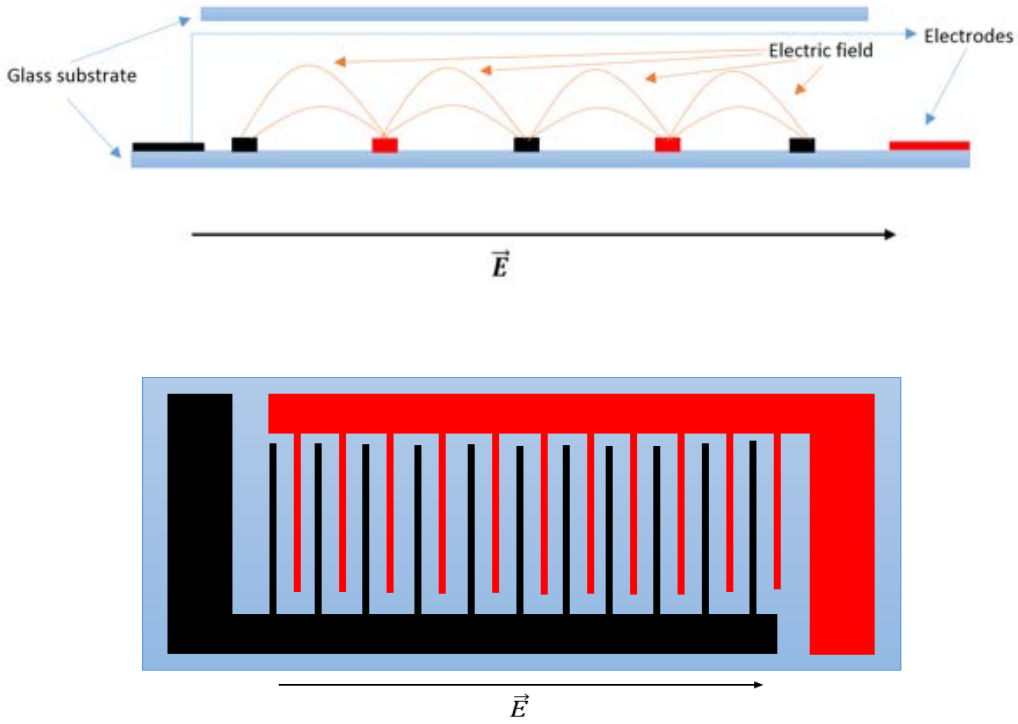

Figure 13 (Top) A side on view of an IPS cell where the black regions are the negative electrodes, red regions are the positive electrodes (the electric fields are as shown), and $\vec{E}$ is the overall electric field. (Bottom) a top down view of the IPS cell where the interdigitated electrodes can be seen.

In this way an electric field $\vec{E}$, shown in Figure 13, can be produced in the plane of the cell. The electric field strength is dependent on the electrode gap and the electrode width. The major drawback to IPS geometry is the non-uniformity of the field induced shown by the field line in Figure 13 (Top). Since the electrodes cannot be extended in height to infinity, there exists a non-uniform field produced from the edges of the electrode. The non-uniform field leads to a higher electric field region near the electrode edges. The non-uniform field also complicates any effect from the liquid crystal, but these cells are simple to construct and uniform over large regions.

Summary

In this chapter we have discussed some basic concepts of liquid crystals. Many important fundamental properties, like birefringence and chirality are introduced. Basic investigation techniques have been discussed which will be employed later to understand more complex properties of liquid crystals. In the future chapters, investigations based on the fundamentals presented here are built upon to develop an understanding of the behaviour of complex liquid crystals such as bent core liquid

crystals. The next chapter will explore in detail the properties which arise from the nematic phase of the liquid crystal.

Outline of thesis

Chapter 2: Physical properties of nematic liquid crystals

To understand how introducing intrinsic bend into liquid crystal phases will affect the phase, first the properties of a conventional liquid crystal must first be understood. The theory of elasticity will be introduced in this chapter. How distortions to the director within the nematic phase will affect the liquid crystal systems. Then, the effect of electromagnetic fields on the director will also be examined. Finally, flexoelectric effect will also be theoretically explored and its electro-optic effects.

Chapter 3: Experimental techniques in investigating liquid crystal materials

In this chapter several techniques to measure the properties of liquid crystals will be explored. Experiments will be conducted by finding the elastic constants of liquid crystals and tested on calamitic liquid crystal 5CB. X-ray diffraction is also used when investigating the structure of liquid crystals; this will also be explored and some fitting processes are developed.

Chapter 4: Investigation of unusual elastic properties in bent core liquid crystal

Many bent core liquid crystals have shown unique properties even in the nematic phase. This suggests that introducing bend into liquid crystal phases can alter their phase significantly. There are anomalous elasticity behaviours seen in bent core liquid crystals. The elastic constant in mixtures of bent core and calamitic liquid crystal is also measured and the anomalous behaviour is seen to increase with increasing bent core dopant. The elastic constants in a series of oxadiazole based liquid crystal and thaidiazole based liquid crystal is measured and the anomalous behaviour is only seen in oxadiazole materials. Theoretical calculations are performed and compared with experimental data, origin of the anomalous behaviour is discussed.

Chapter 5: Investigating the filament structure in mixture of bent core and calamitic liquid crystals

A unique filament structure is seen in one of the mixtures of bent core and calamitic liquid crystals studied in chapter 4. The structure is investigated with several techniques. Polarising microscopy is used to explore the nature of the phase and shows that it differs from the nematic phase. X-ray diffraction was performed to analyse the structure of the phase. The dielectric properties will also be analysed and the nature of the filament is discussed.

Chapter 6: Unusual Flexoelectric Switching

Introducing bend in even the simplest liquid crystal phase, the nematic phase, has already shown to significantly alter the phase. Introducing the bend into a chiral nematic phase can show as the flexoelectric effect, which has been speculated to be great in bent molecules. The flexoelectric effect studied in a few mixtures of dimers and calamitic liquid crystals have shown to produce an unusual switching mechanism from an electric field. The unusual switching effect of some mixtures is explored and attempt to resolve the origin of such effects.

Chapter 7: Summary and future works

Introducing bend into liquid crystal phases have been shown to alter even the simplest nematic phase. Here we will review and summarize the work, how bend changes the phases and discuss any future work possible to further our understanding of these systems.

References

1. Reinitzer, F., *Beiträge zur Kenntniss des Cholesterins.* Monatshefte für Chemie und verwandte Teile anderer Wissenschaften, 1888. **9**(1): p. 421-441.
2. Collings, P.J. and M. Hird, *Introduction to liquid crystals : chemistry and physics*. 1997, London: Taylor & Francis.
3. Zhuk, V.V. and G.I. Natanson, *The Inverse-Theorems of the Constructive Theory of Functions for Periodic Equidistant Splines.* Vestnik Leningradskogo Universiteta Seriya Matematika Mekhanika Astronomiya, 1983(2): p. 11-16.
4. Skivesen, N., Tetu A., Kristensen, M., Kjems, J. and Borel , P.I., *Photonic-crystal waveguide biosensor.* Optics Express, 2007. **15**(6): p. 3169-3176.
5. Hu, X.S., O. Hadaler, and H.J. Coles, *High Optical Contrast Liquid Crystal Switch and Analogue Response Attenuator at 1550 nm.* Ieee Photonics Technology Letters, 2011. **23**(22): p. 1655-1657.
6. Shih, C.S. and R. Alben, *Lattice Model for Biaxial Liquid-Crystals.* Journal of Chemical Physics, 1972. **57**(8): p. 3055- 3061.
7. Warr, S.T., M.C. Parker, and R.J. Mears, *Optically Transparent Digitally Tunable Wavelength Filter.* Electronics Letters, 1995. **31**(2): p. 129-130.
8. Collings, P.J., *Liquid crystals : nature's delicate phase of matter*. 2nd ed. ed. 2002, Princeton, N.J. ; Oxford: Princeton University Press.
9. Gray, G.W., K.J. Harrison, and J.A. Nash, *New Family of Nematic Liquid-Crystals for Displays.* Electronics Letters, 1973. **9**(6): p. 130-131.
10. Gray, G.W. and J.W.G. Goodby, *Smectic liquid crystals : textures and structures*. 1984, Glasgow: L. Hill.
11. Oseen, C.W., *The theory of liquid crystals.* Transactions of the Faraday Society, 1933. **29**(140): p. 883-899.
12. Pindak, R., Moncton, D.E., Davey, S.C., and Goodby, J.W., *X-Ray-Observation of a Stacked Hexatic Liquid-Crystal B-Phase.* Physical Review Letters, 1981. **46**(17): p. 1135-1138.
13. Goodby, J.W., *Volume 1 Fundamentals,* in *Handbook of Liquid Crystal*, J.W. Goodby, Gray, G.W., Spiess, H.-W., and Vill, V. , Editor. 1998, Wiley-VCH Verlag GmbH, Weinheim. p. 115-132.
14. Vorländer, D., *Die Richtung der Kohlenstoff-Valenzen in Methan-Abkömmlingen.* Berichte der deutschen chemischen Gesellschaft (A and B Series), 1929. **62**(10): p. 2824-2831.
15. Kuboshita, M., Y. Matsunaga, and H. Matsuzaki, *Mesomorphic Behavior of 1,2-Phenylene Bis[4-(4-Alkoxybenzylideneamino)Benzoates]*. Molecular Crystals and Liquid Crystals, 1991. **199**: p. 319-326.
16. Dierking, I., *Textures of liquid crystals*. 2003, Weinheim ; [Cambridge]: Wiley-VCH.
17. Goodby, J.W., Collings, P.J., Kato, T., Teschierske, C., Gleeson, F.H., and Raynes, E.P., *Handbook of liquid crystals*. Second completely revised and greatly enlarged edition. ed.
18. Kim, Y.B., Kim, H.S., Choi, J.S., Matuszczyk. M., Olin, H., Buivydas, M., and Rudquist, P., *Atomic force microscopy of rubbed polyimide aligning films for liquid crystal displays.* Molecular Crystals and Liquid Crystals Science and Technology Section a-Molecular Crystals and Liquid Crystals, 1995. **262**: p. 89-98.
19. Kumar, S., J.-H. Kim, and Y. Shi, *What Aligns Liquid Crystals on Solid Substrates? The Role of Surface Roughness Anisotropy.* Physical Review Letters, 2005. **94**(7). 077803:p. 1-4.
20. Wolff, U., W. Greubel, and H. KrÜGer, *The Homogeneous Alignment of Liquid Crystal Layers.* Molecular Crystals and Liquid Crystals, 1973. **23**(3-4): p. 187-196.
21. Berreman, D.W., *Solid Surface Shape and the Alignment of an Adjacent Nematic Liquid Crystal.* Physical Review Letters, 1972. **28**(26): p. 1683-1686.
22. Ishihara, S., Wakemoto, H., Nakazima, K., and Matsuo, Y., *The effect of rubbed polymer films on the liquid crystal alignment.* Liquid Crystals, 1989. **4**(6): p. 669-675.
23. Naemura, S., *Measurement of Anisotropic Interfacial Interactions between a Nematic Liquid-Crystal and Various Substrates.* Applied Physics Letters, 1978. **33**(1): p. 1-3.

24. A.I.Hopwood, *electro-optic effects in polymer liquid crystal solutions*. 1985: United Kingdom. p. 54.
25. Hiltrop, K. and H. Stegemeyer, *Contact Angles and Alignment of Liquid-Crystals on Lecithin Monolayers.* Molecular Crystals and Liquid Crystals, 1978. **49**(2): p. 61-65.
26. Schadt, M. and W. Helfrich, *Voltage-Dependent Optical Activity of a Twisted Nematic Liquid Crystal.* Applied Physics Letters, 1971. **18**(4): p. 127-128.

Chapter 2 Physical properties of nematic liquid crystals

Introduction

Since this thesis focuses on the nematic phase of bent core liquid crystals, a basic understanding of the physical properties of nematics must be developed. In chapter 1, some fundamentals of liquid crystals were discussed. Within a nematic liquid crystal, the molecules on average point along $\pm\hat{\mathrm{n}}$ in a uniaxial system. Nematic liquid crystals in the presence of limiting surfaces and external fields will result in some form of distortion in the director field which may permeate throughout the material. One way of understanding the changes to the director is to use continuum theory, starting with examining the free energy of a nematic liquid crystal system.

Continuum theory

Free energy of nematic liquid crystals

As seen commonly in nature, any system will adopt the configuration that has the lowest free energy. By determining the free energy of nematic liquid crystals, the conditions for which the free energy is minimised will be the configuration the system adopts. This process was originally explored in papers by Frank [1], Oseen [2], and Zocher [3]. The detailed mathematical processes are given by those papers and repeated in many text books on liquid crystal such as "Physics of Liquid Crystal" By P. G. de Gennes and J. Prost [4], but here we follow the approach found in "Introduction to Liquid Crystal: Chemistry and Physics" by P. J. Collings and M. Hird [5]. There are three components of the director and three physical dimensions in the reference frame; together, this makes a vast number of combinations of configurations possible. However, there are certain limits on the possible distortions:

- There can be no term for which $\hat{n}$ and $-\hat{n}$ give different energy values.
- There can be no linear terms of variation of the director except for within chiral systems; in chiral systems one linear term is allowed.
- The configuration has to obey Stoke's theorem where the divergence integrated over the volume must be equivalent to the surface integral.

The restriction to the configurations reduces the free energy per unit volume to three terms:

$$F_v = \frac{1}{2}K_1[\nabla \cdot \hat{n}]^2 + \frac{1}{2}K_2[\hat{n} \cdot (\nabla \times \hat{n})]^2 + \frac{1}{2}K_3|\hat{n} \times (\nabla \times \hat{n})|^2, \quad 2.1$$

Here K_1, K_2, K_3 are analogous to the spring constant in classical mechanics, and are referred to as elastic constants in liquid crystal systems. Their corresponding factors describe the types of distortion possible for the director to make, in a nematic liquid crystal. The elastic constants' specific value describes the susceptibility to each distortion, the larger the value to more resistant to the distortion. The exact meaning of the corresponding factors can be found by considering the director along the z-axis. Therefore the first derivative of n_z with x, y, z is zero at this point, and evaluating each derivative gives:

$$[\nabla \cdot \hat{n}]^2 = \left[\left(\frac{\partial n_x}{\partial x}\right)_{y,z} + \left(\frac{\partial n_y}{\partial y}\right)_{x,z}\right]^2,$$

$$[\hat{n} \cdot (\nabla \times \hat{n})]^2 = \left[\left(\frac{\partial n_y}{\partial x}\right)_{y,z} - \left(\frac{\partial n_x}{\partial y}\right)_{x,z}\right]^2, \quad 2.2$$

$$[\hat{n} \times (\nabla \times \hat{n})]^2 = \left(\frac{\partial n_x}{\partial z}\right)^2_{y,z} + \left(\frac{\partial n_y}{\partial z}\right)^2_{x,y}.$$

The distortions possible are shown in Figure 14. They have been named splay, twist, and bend. Thus K_1 is the splay elastic constant, K_2 is the twist elastic constant, and K_3 is the bend elastic constant.

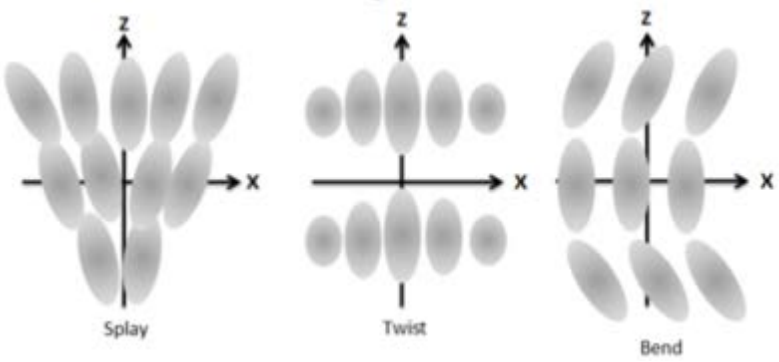

Figure 14 The three types of distortions (left) splay, (middle) twist, and (right) bend.

The splay distortion describes the tilt of a director's long axis away from the z axis, as shown in Figure 14 (left). The twist deformation is the gradual rotation of the long axis of the director with respect to the same short axis direction as shown in Figure 14 (middle). Bend is the deformation where there is a tilt of the director's short axis away from x axes as shown in Figure 14 (right).

Energy due to electromagnetic field in nematic liquid crystals

External fields are often used to manipulate liquid crystals. Understanding how electromagnetic fields interact with liquid crystals is important since most liquid crystals molecules contain a permanent dipole, commonly along the molecular long axis. When the dipole is placed in an electric field, the dipole will try to align parallel to the electric field to minimise the free energy. To find the energy due to an electric field, we follow the process in [5].

If we consider the effect of $\vec{E}$ on a nematic director $\hat{n}$ and then the electric displacement $\vec{D}$ induced is:

$$\vec{D} = \varepsilon_{\parallel}\vec{E}, \qquad \text{if } \vec{E} \text{ is parallel to } \hat{n}$$

$$\vec{D} = \varepsilon_{\perp}\vec{E}, \qquad \text{if } \vec{E} \text{ is perpendicular to } \hat{n}$$

where ε is the dielectric constant of the material, and $\varepsilon_{\parallel}, \varepsilon_{\perp}$ describes the components of the dielectric constant parallel and perpendicular to the director respectively. If $\vec{E}$ makes an arbitrary angle with $\hat{n}$, then the electric displacement $\vec{D}$ becomes

$$\vec{D} = \varepsilon_{\perp}\vec{E} + (\varepsilon_{\parallel} - \varepsilon_{\perp})(\vec{E} \cdot \hat{n})\hat{n},$$

Often in nematic liquid crystals the dielectric anisotropy is positive $\Delta\varepsilon > 0$; thus the free energy of the system is found to be:

$$F = F_v - \int_0^E \vec{D} \cdot d\vec{E} = F_v - \frac{1}{2}\varepsilon_{\perp}\vec{E}^2 - \frac{1}{2}\Delta\varepsilon(\hat{n} \cdot \vec{E})^2.$$

The term $\frac{1}{2}\varepsilon_{\perp}\vec{E}^2$ is independent of $\hat{n}$ and may be omitted for the rest of the discussion. The term of interest is the last term $\frac{1}{2}\Delta\varepsilon(\hat{n} \cdot \vec{E})^2$, describing the energy induced by an electric field within a

nematic liquid crystal. We note that for $\hat{n}$ parallel, the energy due to an electric field $\vec{E}$ is 0 as expected.

Similarly, an expression for energy from an applied magnetic field can be derived. For magnetic fields, the effects are derived from the molecular structure of the liquid crystal, which commonly are aromatic and diamagnetic. If a magnetic field $\vec{H}$ is perpendicular to the plane of a benzene ring (a common component of calamitic liquid crystals), then the current will be induced in the ring and produce an opposing magnetic field. Similar to the case in electric fields, the ring prefers to align itself parallel to the magnetic field. Through a similar mathematical process, the energy from a magnetic field can be found to be:

$$\frac{1}{2}\Delta\chi\left(\hat{n}\cdot\vec{H}\right)^2.$$

Analogous to the term for the energy from an electric field, when the director is parallel to the magnetic field the energy is 0 as expected.

Fréedericksz Transitions

In most real life situations liquid crystal experiencing external forces will be confined in a cell device as discussed in chapter 1. Thus the limiting surface will affect how the bulk liquid crystal is reacts to the external field. Now consider an electric field that is applied in the plane of a cell to the liquid crystal within a cell.

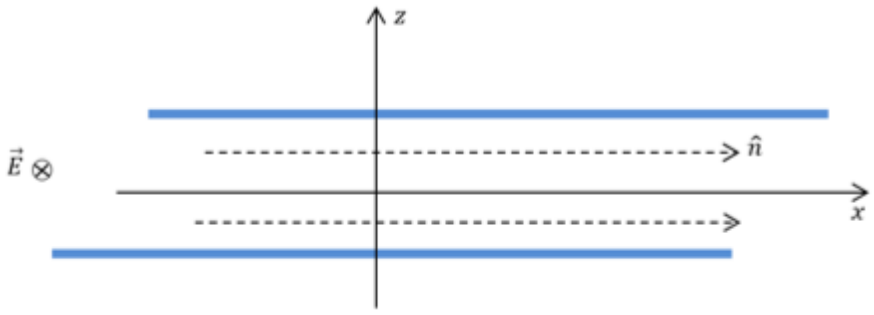

Figure 15 A perpendicular electric field through the page is applied to a planar aligned nematic cell.

Let us consider the geometry shown in Figure 15 where the liquid crystal has a positive dielectric anisotropy. Initially n̂ is constrained to point along the x-axis, and an electric field $\vec{E}$ is applied

perpendicularly to $\hat{n}$ along the z axis into the page. We define an angle Θ as the angle between the director and the x-axis [5].

To simplify the situation let us assume that the anchoring energy from the alignment layer is infinite so that $\hat{n}$ is constrained to the x-axis then at the boundaries $\Theta = 0$, Θ would increase along z until it reaches a maximum at $z = \frac{d}{2}$, where d is the cell gap, and then begins to decrease until $z = d$, where $\Theta = 0$. We can calculate the elastic energy associated with the distortion since

$$n_x = cos[\Theta(z)], \qquad \text{and} \qquad n_y = sin[\Theta(z)].$$

Each of the free energy component from equation 2. 2 the derivatives are calculated to be

$$\nabla \cdot \hat{n} = 0,$$

$$\hat{n} \cdot (\nabla \times \hat{n}) = \frac{d\Theta}{dz},$$

$$[\hat{n} \times (\nabla \times \hat{n})] = 0.$$

Clearly only the twist deformation exists, this is expected as the electric field would only rotate the director causing only the twist deformation to occur if a sufficient field is applied. Now consider the total energy of the system. The energy per unit volume of the total system is the sum of the energy from electric field and the elastic energy. Equation 2. 1 becomes

$$F = \frac{1}{2} K_2 \left(\frac{d\Theta}{dz}\right)^2 - \frac{1}{2} \varepsilon_0 \Delta\varepsilon E^2 \, sin^2 \Theta,$$

where $\varepsilon_0 = 8.854 \times 10^{-12} \, Fm^{-1}$ is the permittivity of free space.

Minimum energy of F is the most favoured state, and since Θ is a function only dependent on z, we need to find the function $\Theta(z)$ which yields a minimum energy. Since the variation is only in z we need only to consider the free energy per unit area

$$F_A = \int_0^d \left[\frac{1}{2}K_2\left(\frac{d\Theta}{dz}\right)^2 - \frac{1}{2}\varepsilon_0 \Delta\varepsilon E^2 \sin^2\Theta\right] dz\ .$$

To minimise F_A, variational calculus is employed, by using the Euler-Lagrange equation. This will yield a $\Theta(z)$ function with minimum energy

$$K_2 \frac{d^2\Theta}{dz^2} + \varepsilon\Delta\varepsilon E^2 \sin\Theta\cos\Theta = 0. \qquad 2.3$$

Making equation 2. 3 dimensionless would simplify it by making it easier to understand. This is accomplished by substituting

$$\varsigma = \frac{z}{d}, \qquad \text{and} \qquad \xi = \frac{K_2}{\varepsilon_0 \Delta\varepsilon E^2}$$

into equations 2.3. The latter can also be made dimensionless with

$$\xi_d = \frac{\xi}{d}.$$

The simplified equation of 2. 3 has the form

$$\xi_d^2 \frac{d^2\Theta}{d\varsigma^2} + \sin\Theta\cos\Theta = 0. \qquad 2.4$$

It is not difficult to obtain a numerical solution to equation 2. 4 by using appropriate values of ξ_d and guessing a value $\frac{d\theta}{d\varsigma}$ at $\varsigma = 0$. When going through the numerical procedures, it is quickly realised that if $\xi_d > \frac{1}{\pi}$, then $\theta(\varsigma) = 0$ everywhere. This means that below certain electric field strengths, no distortion takes place, known as the Fréedericksz threshold. It is then possible find a solution in terms of elliptic integrals and can find the threshold field as

$$E_t = \frac{\pi}{d}\sqrt{\frac{K_2}{\varepsilon_0 \Delta\varepsilon}}.$$

For different orientations of the electric field with respect to the director, the threshold electric field needed to reorient liquid crystal molecules depends on different elastic constants. For planar aligned cells with electric field perpendicular to the plane of the cell the threshold, the field becomes $E_t = \frac{\pi}{d}\sqrt{\frac{K_1}{\varepsilon_0 \Delta\varepsilon}}$, for homeotropic aligned cell and electric field in the plane of the cell then the threshold field becomes $E_t = \frac{\pi}{d}\sqrt{\frac{K_3}{\varepsilon_0 \Delta\varepsilon}}$.

Flexoelectric effects in liquid crystals

In most calamitic liquid crystal phases there is degeneracy about the molecular long axis. If a transverse dipole exists, then introducing an electric field will break the degeneracy due to the induced polarization; this in turn will give rise to many structures that can affect the properties of the phase. In liquid crystals, elastic strain coupled with electric polarization can lead to other deformed structures. Similarly, a deformed structure can lead to a permanent polarization. Originally predicted by Meyer *et al* [6], this phenomenon is now commonly accepted as flexoelectricity [7]. The flexoelectric effect is highly dependent on molecular shape and transverse dipole, thus can be particularly strong in bent core liquid crystals. Similarly, there also may be a strong flexoelectric effect in tear shaped molecules with a longitudinal dipole. Using Meyer notation, the flexoelectric polarization is defined to be:

$$P_{flexo} = e_1(\nabla \cdot \hat{n})\hat{n} + e_3(\nabla \times \hat{n}) \times \hat{n}, \qquad 2.5$$

where e_1, and e_3 are the splay and bend flexoelectric coefficients respectively.

In many cases the flexoelectric contribution to free energy can be ignored either due to the flexoelectric coefficient being too small or the effect is outweighed by the dielectric polarization effect. However in some circumstances the inclusion of the flexoelectric free energy contribution is important to describe the complete electric field induced distortion in liquid crystals [8, 9].

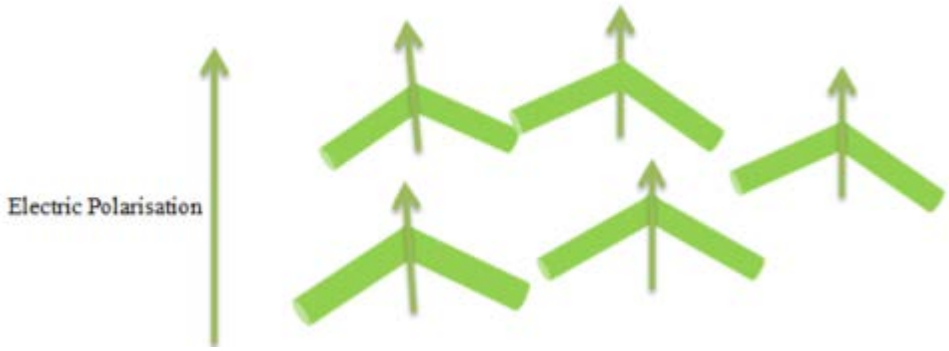

Figure 16 bend molecules with polar ordering inducing an electric polarisation in the same direction.

Flexoelectricity is an example of the electromechanical properties of liquid crystals [10]. Since bent core liquid crystals have an innate polarity due to their molecular shape, this is expected to promote flexoelectricity in molecules that have a strong transverse dipole as shown in Figure 16. It is easy to see that with polar ordering there would be a spontaneous electric polarisation due to the alignment of the dipoles. The reverse is also true to electric field applications as it would induce ordering in the material due to the coupling of molecular shape and dipole.

Flexoelectricity in chiral nematics

The flexoelectric effect is observed as an electro-optic effect in chiral nematic liquid crystals. When a chiral nematic is placed in a homeotropic cell like those discussed in chapter 1. The chiral nematic exists in a structure shown in Figure 17.

Figure 17 The ULH structure of chiral nematic liquid crystal in a homeotropic cell with the optical axis along the helical axis.

The structure, referred as the Uniform Lying Helix (ULH), is incompatible with the planar boundary conditions and is splayed and bent in the regions near the boundaries [11]. Thus according to equation 2. 5, the flexoelectric polarisation can arise in those regions and interact with the electric

field. The ULH orientation is not the preferred orientation for chiral nematic liquid crystals in conventional cells. Many methods have been explored to achieve ULH, cycling temperature under voltage application[12-14], periodic boundary conditions[15], and tri-electrode cells[16]. In this geometry when a field is applied perpendicular to the cell plane, due to the flexoelectric deformation near the surface regions, the optical axis does not coincide with the initial orientation of the helix but forms an angle Ψ shown in Figure 18. This was first observed by Patel and Meyer [17].

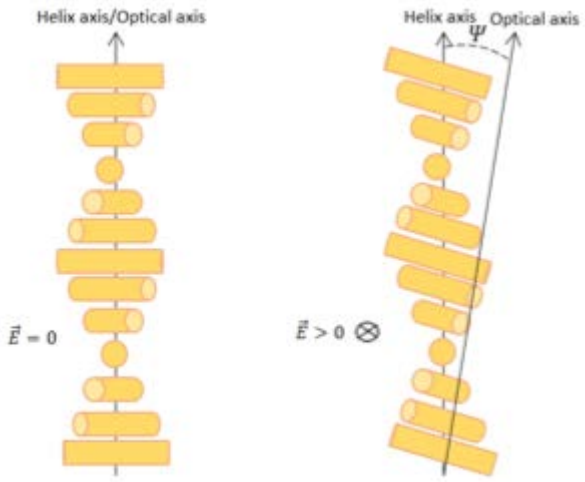

Figure 18 ULH structure under electric rotates the optical axis by an angle Ψ.

The free energy of the system in an electric field is the combination of elastic, dielectric, and flexoelectric contribution.

$$F = F_v - \vec{P}_{flexo} \cdot \vec{E} - \vec{P} \cdot \vec{E} \qquad 2.6$$

The first term is simply the free energy due to elastic properties, the second describes the flexoelectric coupling between strain and polarisation, and the last term is the free energy from the dielectric response. Since dielectric contribution is much larger than flexoelectric contributions in most cases, the flexoelectric effect is only prominent in materials with low $\Delta\varepsilon$ where dielectric response is small. To see the consequence of the flexoelectric effect, equation 2. 6 is simplified by assuming that $\Delta\varepsilon > 0$, thus $K = K_1 = K_3$, and $e = e_1 = e_3$. For director components parallel to the cell plane, x, y-plane, and $n_z = \cos\varphi$, $n_y = \sin\varphi$, the free energy now becomes:

$$F = \frac{1}{2}K\left(\frac{\partial\varphi}{\partial y}\right)^2 \pm \frac{1}{2}K_2\left(\frac{2\pi}{p} - \frac{\partial\varphi}{\partial x}\right)^2 - eE\frac{\partial\varphi}{\partial y} + \frac{1}{8\pi}\Delta E^2 \sin^2\varphi$$

The first two terms are the energy from the elastic properties, and the last term is the flexoelectric response. Upon minimising the free energy, this results in $\frac{\partial \varphi}{\partial x} = \frac{2\pi}{p}$ and $\frac{\partial \varphi}{\partial y} = \frac{eE}{K}$. If the rotated helical axis is represented by the wave vector $\vec{k}$, then $\left|\vec{k}\right| \cos \Psi = \frac{2\pi}{p}$ and $\left|\vec{k}\right| \sin \Psi = \frac{eE}{K}$, and the rotation angle is given by:

$$tan(\Psi) = \frac{epE}{2\pi K},$$

What is observed as a consequence of the flexoelectric effect is the tilt of the optical axis perpendicular to the electric field and in the plane of the cell by angle Ψ as observed. In situations where the splay and bend elastic constant, and flexoelectric coefficient are not equal, the equation becomes [18],

$$tan(\Psi) = \frac{(e_1 - e_3)pE}{2\pi(K_1 + K_3)}.$$

Raman Scattering

When a light source is incident on a material, most of the scattering that occurs is elastic, where there is no energy transfer. This is commonly called Rayleigh scattering. However there are many inelastic scattering modes in which energy is transferred to the molecules [19]. One of the inelastic scattering modes is Raman scattering. Raman scattering is an interaction between the photons of an incident beam and the phonons of the molecular resonance vibrations and rotations. The molecules can absorb the resonance energy from the incident photon, called Stokes Raman scattering, resulting in a lowering of the reemitted photon energy. The molecule can also transfer the resonance energy to the incident photon, called anti – Stokes Raman scattering, resulting in an increase in the remitted photon energy. The Raman scattering modes causes the remitted light to have a shift in wavelength with respect to the incident beam, and thus Raman scattering is a powerful diagnostic tool for identifying chemical species [20]. The intensity of the scattering is dependent on the polarisation of the incident light and the director. This property of the Raman scattering can be utilised in creating a director profile for the nematic liquid crystal, and will be used in chapter 5 for trying to understand the director profile while undergoing electric field induced switching.

Summary

In this chapter the physical properties of nematic liquid crystals have been reviewed. Minimising the free energy derives the expressions for the three eigen-distortions possible in nematic liquid crystal. Then how the elasticity influences the liquid crystals response to external fields resulting in the Fréedericksz transition was overviewed. Flexoelectricity in chiral nematics is also discussed due to the unique electro-optic effect it produces. Raman scattering and how it can be used in analysing director profile was also briefly discussed. Now that basic properties of nematic liquid crystals are understood, the methods used to find these physical properties can be explored.

Reference

1. Frank, F.C., *On the Theory of Liquid Crystals.* Discussions of the Faraday Society, 1958(25): p. 19-28.
2. Oseen, C.W., *The theory of liquid crystals.* Transactions of the Faraday Society, 1933. **29**: p. 0883-0898.
3. Zocher, H., *The effect of a magnetic field on the nematic state.* Transactions of the Faraday Society, 1933. **29**: p. 0945-0957.
4. Gennes, P.-G.d., *The physics of liquid crystals*. 1979, Oxford: Clarendon Press.
5. Collings, P.J. and M. Hird, *Introduction to liquid crystals : chemistry and physics*. 1997, London: Taylor & Francis.
6. Meyer, R.B., *Piezoelectric Effects in Liquid Crystals.* Physical Review Letters, 1969. **22**(18): p. 918-921.
7. Gennes, P.G.d. and J. Prost, *The physics of liquid crystals*. 2nd ed. Oxford science publications. 1993, Oxford New York: Clarendon Press ; Oxford University Press. xvi.
8. Cazabat, A.M., Delabre, U., Richard, C., and Sang, Y.Y.C., *Experimental study of hybrid nematic wetting films.* Advances in Colloid and Interface Science, 2011. **168**(1-2): p. 29-39.
9. Oldenbourg, R. and G. Mei, *New Polarized-Light Microscope with Precision Universal Compensator*. Journal of Microscopy-Oxford, 1995. **180**: p. 140-147.
10. Shribak, M. and R. Oldenbourg, *Techniques for fast and sensitive measurements of two-dimensional birefringence distributions.* Applied Optics, 2003. **42**(16): p. 3009-3017.
11. Blinov, L.M.l. and V.G. Chigrinov, *Electrooptic effects in liquid crystal materials*. 1994, New York ; London: Springer-Verlag.
12. Rudquist, P., L. Komitov, and S.T. Lagerwall, *Linear Electrooptic Effect in a Cholesteric Liquid-Crystal.* Physical Review E, 1994. **50**(6): p. 4735-4743.
13. Musgrave, B., P. Lehmann, and H.J. Coles, *Flexoelectro-optic properties of a series of novel chiral nematic liquid crystals.* Molecular Crystals and Liquid Crystals Science and Technology Section a-Molecular Crystals and Liquid Crystals, 1999. **328**: p. 309-316.
14. Patel, J.S. and R.B. Meyer, *Flexoelectric electro-optics of a cholesteric liquid crystal.* Physical Review Letters, 1987. **58**(15): p. 1538-1540.
15. Hedge, G.a.K., L., *Periodic anchoring condition for alignment of a short pitch cholesteric liquid crystal in uniform lying helix texture.* Applied Physics Letters, 2010. **96**(113503): p.1-3.
16. Gardiner, D.J., Morris, S.M., Hands, P.J.W., Castles, F., Qasim, M.M., Kim, W.S., Choi, S.S., Wilkinson, T.D., and Coles, H.J., *Spontaneous induction of the uniform lying helix alignment in bimesogenic liquid crystals for the flexoelectro-optic effect.* Applied Physics Letters, 2012. **100**(6) 063501: p.1-4.
17. Patel, J.S. and R.B. Meyer, *Flexoelectric Electrooptics of a Cholesteric Liquid-Crystal.* Physical Review Letters, 1987. **58**(15): p. 1538-1540.
18. Salter, P.S., Kischka, C., Elston, S.J., and Raynes, E.P., *The influence of chirality on the difference in flexoelectric coefficients investigated in uniform lying helix, Grandjean and twisted nematic structures.* Liquid Crystals, 2009. **36**(12): p. 1355-1364.
19. Brown, J.M., *Molecular spectroscopy*. 1998, Oxford: Oxford University Press.
20. Ferraro, J.R. and K. Nakamoto, *Introductory Raman spectroscopy*. 1994, Boston ; London: Academic Press.

Chapter 3 Experimental techniques in investigating liquid crystal materials

Introduction

In chapter 2 the responses of an electric field for the nematic liquid crystals were discussed. In particular, the importance of the Fréedericksz transition in electro-optic responses was detailed. In order to understand how including bend into the bulk nematic structure will affect the fundamental properties of liquid crystals, its conventional behaviour needs to be examined. Most liquid-crystal-based display devices rely on the electro-optic responses; understanding the Fréedericksz transition is not only important for understanding its fundamental properties, but also for practical device development. In this chapter the measurement techniques relevant to determining the fundamental properties, such as elastic constants, will be explored. Small angle x-ray scattering (SAXS) can reveal details of the molecular orientation of liquid crystals, will be a powerful tool in understanding how phases are altered with the inclusion of bend. A method to analyse the SAXS pattern will be discussed. Many of these methods will be utilised in measuring properties of bent core nematic systems.

Measuring elastic constants of nematic liquid crystals

There are many techniques that measure elastic constants of liquid crystals. Since the Fréedericksz transition is dependent on the elastic constant, this is a popular approach to measuring the elastic constants relying on determining the threshold voltage of the nematic liquid crystal. Depending on the geometry of the nematic phase, only one elastic constant can be determined from the Fréedericksz threshold. A capacitance – voltage [1] fitting method can be employed to find both the splay and bend elastic constants in a planar cell. The twist elastic constant is more difficult to find and two methods, an In-Plane Switching (IPS) cell [2] and a Twisted Nematic (TN) cell [3], of measuring the twist elastic constant will be explored; both methods are utilised in later chapters in exploring the properties of bent core liquid crystals.

Capacitance - Voltage fitting method to find splay and bend elastic constants

Consider the cell geometry described in chapter 1 with planar alignment and the electric field applied perpendicularly to the cell, the structure of the cell in this case is very similar to a parallel plate capacitor. The capacitance of a parallel plate capacitor is

$$C = \frac{\varepsilon_0 \varepsilon_r A}{d}, \qquad 3.\ 1$$

where ε_0 is the dielectric permittivity of free space, ε_r is the relative dielectric permittivity, A is the active area, and d is the distance between the parallel plates. The only term of interest is ε_r, as this is the relative dielectric constant of the medium between the electrodes. Since the medium is liquid crystalline, and is thus anisotropic, the relative dielectric constant is dependent on the orientation of the director. By analysing the director's orientation under the influence of an electric field, as described in chapter 2, the elastic properties can be determined.

In the initial state of a planar aligned cell, the director is lying parallel to the plane of the cell and perpendicular to the applied field, in this case $\varepsilon_r = \varepsilon_\perp$. If a voltage greater than the threshold voltage is applied to the cell, then the ε_r will increase, if $\Delta\varepsilon > 0$, since the director will try to align parallel to the electric field. The director can be considered to be completely constrained at the boundaries for the condition of infinite anchoring; making it is impossible to completely align the director throughout the cell. Thus with increase to high field strengths there is a limit to the maximum ε_r, an asymptote of $\varepsilon_\parallel$.

To determine ε_r, the other terms in equation 3. 1also need to be accurately measured. Measuring the active area and the cell gap may introduce many other sources of error, however by comparing the capacitance of a filled cell with that of an empty cell the other terms can be eliminated. The capacitance of an empty cell is defined to be

$$C_{empty} = \frac{\varepsilon_0 A}{d}. \qquad 3.\ 2$$

The other terms can be eliminated by simply dividing the equation 3. 2 by equation 3. 1 $\frac{C}{C_{empty}} = \varepsilon_r$. The capacitance is measured from a bridge circuit; the equipment consists of an Agilent Precision LCR Meter E4980A which measures the dielectric permittivity across the frequency range 20 Hz – 2

MHz using a 0.05 V_{ac} probe voltage, where necessary in the presence of an AC electric voltage of up to 20V. The typical relative dielectric constant response to an applied voltage is shown in Figure 19.

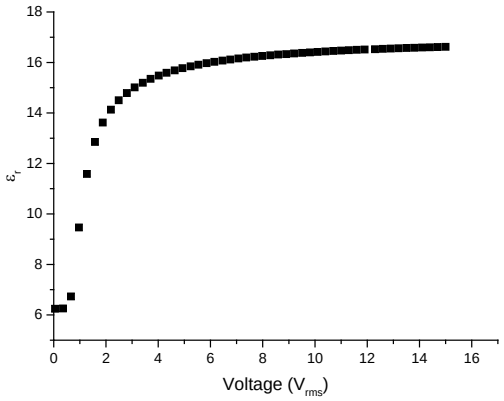

Figure 19 The relative dielectric constant of 5CB (molecular structure shown in chapter 1) at room temperature as a function of different voltages

Initially from Figure 19 the dielectric permittivity perpendicular ($\varepsilon_\perp$) can be determined as the value that is initially measure at $V_{rms} \approx 0$ which remain constant below threshold voltage. In chapter 2 the threshold voltage V_t was found to be

$$V_t = E_t d = \pi \sqrt{\frac{K_1}{\varepsilon_0 \Delta\varepsilon}}. \qquad \textbf{3. 3}$$

At voltages where $V < V_t$ then the dielectric permittivity is in-between the parallel ($\varepsilon_\parallel$) and perpendicular components $\varepsilon_\parallel > \varepsilon_r > \varepsilon_\perp$, in this region there should exist some combination of perpendicular and parallel component of the dielectric constants, this should give a curve that gradually approaches the asymptote of $\varepsilon_\parallel$. Thus $\varepsilon_\parallel$ can be approximated from the value at high voltages. The full curve is actually dependent on $\frac{K_3}{K_1}$ so using the previously obtained K_1 from the threshold voltage it is possible to find K_3 from equation [4]

$$V\Big/_{V_t^{K_1}} = 2\pi^{-1}(1 + \gamma sin^2\psi_m)^{1/2} \int_0^{\pi/2} (\frac{F_k}{F_\varsigma F_\gamma})^{1/2} d\psi, \qquad 3.4$$

where $F_k(\psi) = 1 + k sin2\psi_m$, $F_\zeta(\psi) = 1 - sin2\psi_m$, $F_\gamma(\psi) = 1 + \gamma sin2\psi_m$, $k = (K_3/K_1) - 1$, $\gamma = (\varepsilon_\parallel/\varepsilon_\perp) - 1$ and ψ_m is the director angle in the centre of the liquid crystal layer in case of planar alignment. The curve is dependent on different elastic constants and that depends on the geometry of the cell and orientation of liquid crystal. In a planar cell geometry with positive dielectric material the splay elastic constants, K_1 and the bend elastic constant K_3 are calculated.

The data can be fitted using a computer program, the program used in this thesis was written by *P. Brimecombe (University of Manchester)*. By using nonlinear fitting, the data can be fit to obtain values for the elastic constants. This is done by creating a dummy set of data from the equations describing the threshold, and the gradient to the asymptote. Then nonlinear fitting will attempt to find the values of the variables: $\varepsilon_\perp, \varepsilon_\parallel, K_1, K_3$ which will give the dummy data closest to the actual data.

Another important aspect of the fitting process is to be able to accurately determine K_1, since K_3 is dependent on K_1. To be able to determine an accurate K_1, a clear threshold voltage must be obtained. In order to get a good fitting, more data needs to be recorded around the threshold voltage. By using a logarithmic scale to determine the voltage intervals measured, we can ensure more data is taken in the regions close to the Fréedericksz transition to give a reliable fitting. The expected result would be a sudden and sharp increase of the dielectric constant at the threshold voltage. However, what is often seen is a smooth transitional increase in the dielectric constant; this is because there is a slight molecular shift so that the director is not perfectly aligned parallel to the glass surface called a pre-tilt. The pre-tilt means that there is no perfectly sharp Fréedericksz transition at the threshold voltage. Using this fitting method gives an error of 5% for K_1 and 8% for K_3, this is because K_1 only depends on the threshold voltage while K_3 depends on the gradient and K_1 giving it a larger error. The dielectric anisotropy can also be fit with an absolute uncertainty of 5%.

Before investigating complex liquid crystal such as bent core liquid crystals, it is important to understand how conventional calamitic materials behave. A common liquid crystal is 5CB, discussed in chapter 1. 5CB exhibits only a nematic phase at room temperature making it very easy to work with. Using the capacitance method discussed and fitting the resultant curve K_1 and K_3 can be determined. In Figure 20 the elastic constants of 5CB are plotted together with data taken from *Bunning et al* [5].

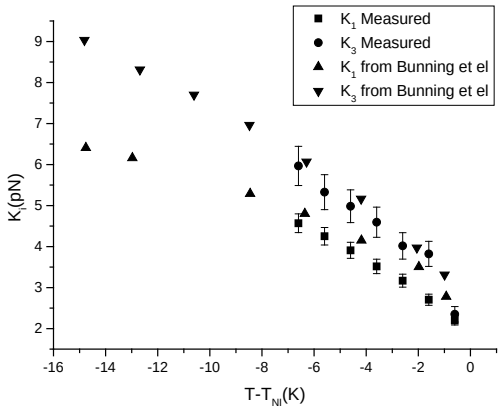

Figure 20 Measured K_1 and K_3 values for 5CB using fitting method compared to results from *Bunning et al* [5]

The elastic constants were obtained using the Fréedericksz transition with magnetic field in *Bunning et al* and they fitted the threshold and the entire curve in a similar fashion to what was described in this section. *Bunning et al* measured the entire nematic range of 5CB. The measurements I carried out were only above room temperature. Both measurements are in excellent agreement with each other, since the experiments utilised similar methods, one with an electric field and the other magnetic field, the data is expected to be in excellent agreement.

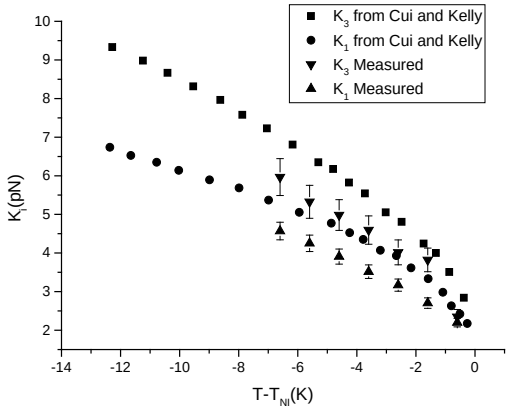

Figure 21 Measured K_1 and K_3 values for 5CB using capacitance voltage fitting compared to results from *Cui and Kelly* using light scattering [6].

Figure 21 shows the capacitance voltage fitted elastic constants with data obtained using a light scattering technique to measure K_1(circle), and K_3(square) of 5CB. In Figure 21 there is a discrepancy between the elastic constant measured to the values from *Cui et al.* Since the light scattering method of measuring elastic constant is dependent on different parameters, the errors involved are distinct and

there is a discrepancy in the absolute values between the methods. The temperature dependence in the data is still very similar for both measurement methods, thus the relative error for both methods are good and in agreement.

The capacitance voltage fitting method in determining splay and bend elastic constants is consistent, and reliably gives the temperature dependence when compared to other methods. In this study, the calamitic liquid crystal properties will first be determined by using the capacitance voltage fitting methods and then compare them to the values in bent core liquid crystal giving an accurate comparison.

Measuring twist elastic constant

The methods discussed here can only provide measurements of K_1 and K_3. The reason of that is that K_2 is difficult to measure, mainly due to the difficulty in producing a planar field. In-Plane Switching (IPS) cells can be used to achieve an in-plane field, however it is non-uniform. Another way to overcome this difficulty is to use Twisted Nematic (TN) cells; the Fréedericksz transition in this geometry is dependent on all three elastic constants. Since K_1 and K_3 are simple to determine using the capacitance-voltage fitting method, this implies that K_2 can be determined. IPS and TN methods will be explored in this section in order to find the viability of using such methods in determining the twist elastic constant in bent core liquid crystals.

Measuring K_2 using Twisted Nematic (TN) cells

In chapter 1, the geometry of TN cells was discussed, where the alignment direction on the two glass substrates is perpendicular to each other. The difference in alignment induces an intrinsic twist to the liquid crystal layer between the glass substrates causing the director to rotate by 90^o. By minimising the free energy of the TN cell, a modified threshold voltage for a TN cell configuration can be obtained [3, 7, 8]. The threshold voltage V_{th}^{TN} in a TN cell is dependent on all three elastic constants. Using TN cell to measure K_2 method can be used since K_1 and K_3 can be measured in the capacitance voltage fitting method.

$$V_{th}^{TN} = \frac{\pi}{\sqrt{\Delta\varepsilon\varepsilon_0}}\left[K_1 + \frac{(K_3 - 2K_2)}{4}\right]^{\frac{1}{2}}, \qquad 3.5$$

The experimental setup consists of measuring the transmission of a light source through a TN cell between cross polarisers under different voltage applications. An in-house built photodiode is used to

measure the transmitted intensity through the cell. A sine wave of 1 kHz is applied from an Agilent 33220A waveform generator, and the photodiode signal was measured using an Agilent 34410A multi-meter.

In a cell that is twisted by 90^o, there is no orientation of the director that produces a dark state. As discussed in chapter 1, the TN cell rotates the polarisation of any linearly polarised light by 90^o. If the alignment direction is initially parallel or perpendicular to the polariser then there is maximum transmission. If the alignment direction is 45^o, then there is minimum transmission. The Fréedericksz transition is found by finding the voltage for which there is a change in the transmission, indicating the change in the director due to an applied voltage.

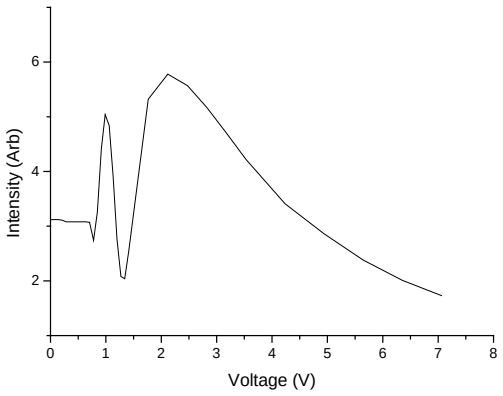

Figure 22 The transmitted intensity of 5CB in a TN cell with increase in applied voltage.

A typical voltage response from a TN cell filled with 5CB is shown in Figure 22. At high voltages, where the directors are mostly aligned parallel to the electric field, the transmission is at a minimum as expected. Due to some residual background light the intensity does not reach zero. The variation of intensity results from changes to the different wavelengths of the transmitted light. The different transmitted wavelengths are due to the birefringence of the liquid crystal between the cross polarisers. As discussed in chapter 1, the maximum transmitted intensity occurs for wavelengths that follow the relation $m\lambda_0 = \Delta nd$. Therefore, as the voltage increases the birefringence changes, thus changing the wavelengths of the transmitted intensity. The photodiode sensitivity is different for different wavelengths, so it apparently decreases in intensity at 0.76V and 1.36V and increases at 0.99V and 2.12V. There changes are attributed the sensitivity of the photodiode.

Ideally the intensity would behave as the inverse of Figure 19, where the intensity would start at the maximum transmission and suddenly decrease at the threshold voltage, and then gradually decrease until it reaches minimum transmission. The important factor would be that for the voltage at which the intensity changes from the initial value, the threshold voltage is irrespective of the subsequent curve. Using TN cells to calculate K_2 also requires K_1 and K_3 which are obtained from the capacitance – voltage fitting methods, however this would introduce new sources of error and is dependent on those values.

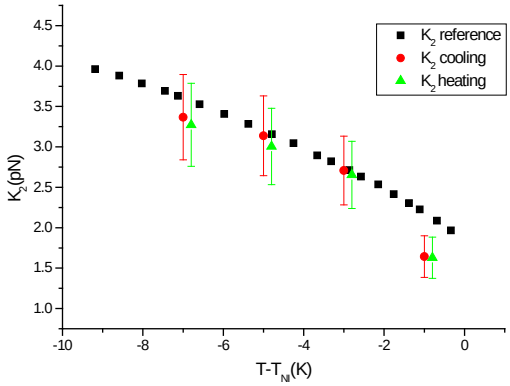

Figure 23 K_2 measured 5CB from a TN cell compared to a previous study of 5CB [9].

In Figure 23, the resultant K_2 is shown as determined using equation 3. 5. They are in good agreement with the data obtained by Coles *et al* [9] in which a light scattering technique was used to determine the twist elastic constants. The uncertainty in K_2 is calculated from the propagating uncertainties of the elastic constants, dielectric anisotropy, and threshold voltage. It is found to be ~15.7%. Measuring the threshold voltage of liquid crystal in a TN cells is a viable way of measuring the twist elastic constant. Many of the bent core liquid crystals have negative dielectric anisotropy so this method is unable to be used to measure those materials, thus perfecting this method, such as by using filters to produce a better curve, was not prioritised.

Measuring K_2 using interdigitated cell

Another way to measure K_2 is to use an IPS cell. IPS cells have interdigitated electrodes to produce an overall in-plane field, however, locally there is strong nonlinearity in the electric field produced. Using the in-plane field to induce a twist distortion, it can also be induced into an aligned liquid crystal; this interaction is simply the Fréedericksz transition. The threshold voltage from the IPS cells is calculated to be [2]

$$V_{th} = \frac{\pi l}{d}\sqrt{\frac{K_2}{\Delta\varepsilon\varepsilon_0}}, \qquad 3.6$$

where l is the electrode gap, and d is the cell gap.

The experimental setup that uses planar alignment, and an aligned cell, with the alignment in the plane parallel to the electrodes, is perpendicular to the electric field. The cell is oriented so that it is initially in the dark state when the alignment direction is parallel or perpendicular to the polarisers. In this position, any twisting of the director would produce more transmitted intensity due to the birefringence altering the incoming polarisation.

The response from 5CB in an in-plane cell can be seen in Figure 24. In contrast to the behaviour of the cells used in previous sections, the electric field produced by IPS is independent of a liquid crystal normal. Therefore, the threshold in IPS is not governed by the voltage, but by its electric field [2]. Initially the cell is in the dark state and the transmitted intensity is ~ 400 (this is the background noise). As mentioned earlier, in a planar cell the non-sharp Fréedericksz transition is due to the pre-tilt in the alignment, however, in this case the non-sharp Fréedericksz transition is due to a non-uniform field.

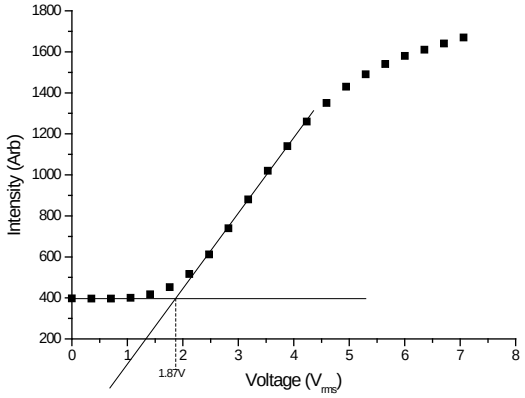

Figure 24 Transmitted intensity with increasing voltage application for 5CB at room temperature in IPS cell.

Equation 3.6 for a Fréedericksz threshold in IPS cells only takes into account of the field strength in between the electrodes where there exists a relatively uniform field. The non-uniform field means that the Fréedericksz transition occurs at different regions between the two electrodes on increasing voltages, this is shown in Figure 24 as a smooth transition. We tested whether extrapolating from the

linear portion of the graph to the baseline is a good estimate of what would be seen from the uniform field. Using this method gives large absolute uncertainties in the measured K_2.

The error in the threshold voltage can be calculated by examining the difference in the electric field strength between the non-uniform region and the uniform region. Using IPS as a method to measure K_2 gives absolute error ~33% which is much larger when compared to other methods like using TN cells.

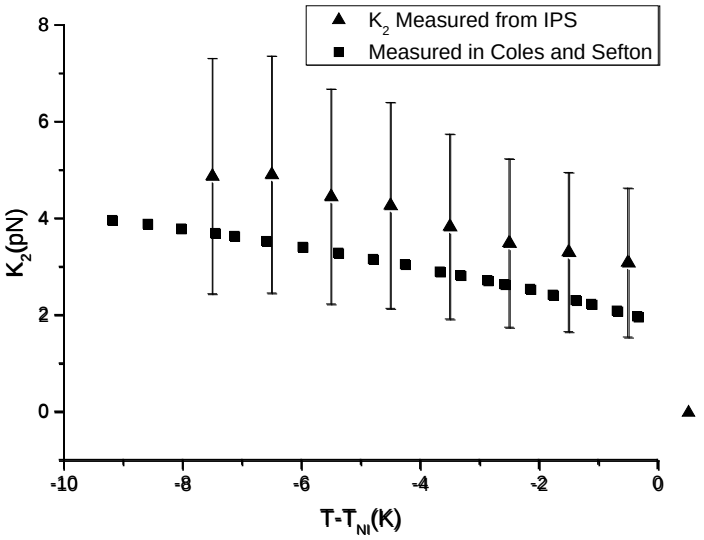

Figure 25 K_2 Measured K_2 using IPS cells threshold voltage compared to *Coles and Sefton* using light scattering [9]

The temperature dependence of K_2 of 5CB is shown in Figure 25. Using IPS to measure the temperature dependence of K_2, the resulting data is in good agreement with the data obtained from *Coles and Sefton* [9]. The uncertainty associated with using IPS cells to measure K_2 is very large. This is mainly due to the inhomogeneous field applied. The replicated behaviour means that the relative error at different temperatures and using the same method is very good. Even for distinct materials will demonstrate good understanding the changes between materials so long as the same method is used. Using IPS methods to determine absolute values is less accurate. In this study, we are investigating the influence of introducing intrinsic bend into liquid crystal IPS cells; this can be a powerful tool for understanding these effects. In bent core liquid crystals, the simple geometry of the cell is also advantageous in reducing external influences which complicates the experimental process.

Small Angle X-ray Scattering (SAXS)

X-rays are able to interact with the electron densities within molecular units. This makes it a powerful tool to probe any short range periodic ordering such as those seen in smectic phases. Using the Bragg equation, the scattering distance can reveal periodic lengths within the molecular structure:

$$n\lambda = 2Dsin(\chi),$$

where λ is the wavelength of the incoming beam, D is the periodic spacing, and χ is the scattering angle.

For the nematic phase the molecules are oriented in a specific order which results in a slight molecular periodicity along the direction perpendicular to the director, and somewhat less so in the direction parallel to the director. In the nematic phase the x-ray diffraction exhibits both small and wide angle peaks shown in Figure 26.

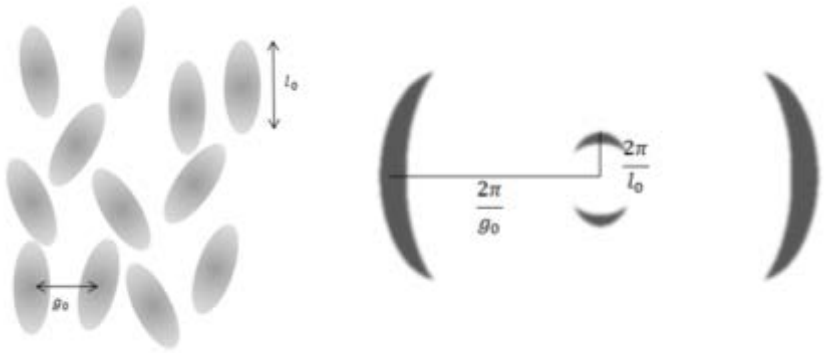

Figure 26 (left) nematic liquid crystal ordering, (right) and the corresponding x-ray diffraction.

Detailed analysis of x-ray diffraction patterns is explored in *Leadbetter et al* [10] which details finding periodic structures and finding the order parameter. The angular distribution can be used to determine order parameters and the radial distribution can give the size of the periodicity of the short range order. SAXS is a powerful tool in analysing any periodic structures such as smectic phases. The SAXS pattern is also dependent on the sample preparation, in an aligned sample the position of the scattering can also reveal the direction of the structure, as seen in Figure 26(right) where scattering pattern shows a vertically aligned nematic phase seen in Figure 26(left). In powder or bulk samples,

however, the scattering pattern is isotropic due to random orientations of molecules but the periodic spacing are consistent thus producing an image of a ring shown in Figure 27.

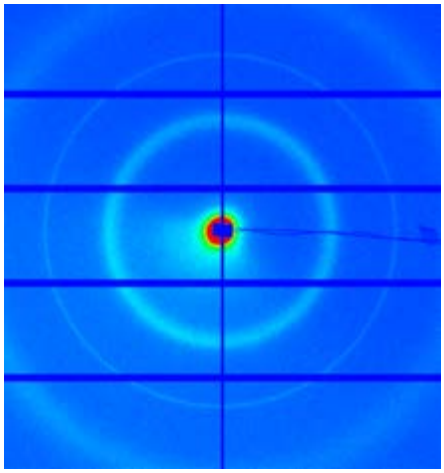

Figure 27 SAXS image of a bulk sample of mixture of bent core and calamitic liquid crystals.

In this thesis only the radial distribution is utilised for finding periodic structures in the bent core liquid crystals. To analyse the x-ray signal, first a calibration of the X-ray is required. Silver behenate is a silver salt of long-chain fatty acids, and is usually used since its periodic spacing is well defined in other methods to be 48.68 Å [11-14]. Powder sample's x-ray scattering gives a symmetric image, as is the case for silver behenate; the intensity can be integrated over all angles adding all the radial contributions to create a stronger signal. The integrated signal from silver behenate measured at ESRF, Grenoble, is shown in Figure 28.

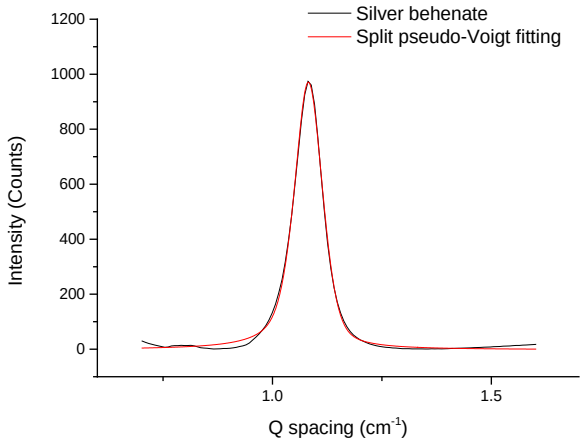

Figure 28 The peak from the integrated signal from sliver behenate.

The peak produced from integrating the signal is asymmetric [14], which can be attributed to severe axial divergence. Thus the fitting of the peak needs to be asymmetric also, such as a split pseudo-Voigt function

$$A\left(\mu\left(\frac{2}{\pi}\right)\left(\frac{w}{4(x-x_c)^2+w^2}\right)+(1-\mu)\left(\frac{2}{\pi w}\right)e^{-\left(4\frac{ln(2)}{w^2}\right)(x-x_c)^2}\right),$$

where w is the full width half maximum (FWHM), x_c is the peak centre, μ is the amount of Lorentzian content in the function, A is the height of the peak.

The split pseudo-Voigt function is a simple addition of Gaussian and Lorentzian functions, with different a parameter left of the peak centre and right of the peak centre. The Gaussian and Lorentzian functions are constrained to have the same height, and same FWHM to obtain a peak function. Only μ, the lorentzian content of the function is changed on either side of the peak centre. As seen in Figure 28 as the red line, the pseudo-Voigt function is a good fit for the sliver behenate and will be used in analysing the peaks from other liquid crystalline sources.

Summary

Various methods to measure the splay bend and twist elastic constants have been discussed in this chapter. Splay and bend elastic constants can be measured using the capacitance response to the applied voltage. The difficulty in measuring twist elastic constant is overcome by utilising two cell geometries using, a TN cell or an IPS cell. To measure flexoelectric coefficients, an electro-optic effect in the analysis method of X-ray images for fitting an integrated intensity from an x-ray image have also been explained. Many methods for measuring constants that define the physical properties of liquid crystal were discussed in this chapter. The methods discussed in this chapter will be used to measure the properties of bent ore materials in later chapters. SAXS will be used to understand new structures formed in mixtures of bent core and calamitic liquid crystals.

References

1. Maze, C., *Determination of Nematic Liquid Crystal Elastic and Dielectric Properties from the Shape of a Capacitance-Voltage Curve*. Molecular Crystals and Liquid Crystals, 1978. **48**(3-4): p. 273-287.
2. Ohe, M. and K. Kondo, *Electro-optical characteristics and switching behavior of the in-plane switching mode.* Applied Physics Letters, 1995. **67**(26): p. 3895-3897.
3. Leslie, F.M., *Distortion of Twisted Orientation Patterns in Liquid Crystals by Magnetic Fields*. Molecular Crystals and Liquid Crystals, 1970. **12**(1): p. 57-72.
4. Blinov, L.M.l. and V.G. Chigrinov, *Electrooptic effects in liquid crystal materials*. 1994, New York ; London: Springer-Verlag.
5. Bunning, J.D., T.E. Faber, and P.L. Sherrell, *The Frank Constants of Nematic 5CB at Atmospheric-Pressure.* Journal De Physique, 1981. **42**(8): p. 1175-1182.
6. Cui, M. and J.R. Kelly, *Temperature Dependence of Visco-Elastic Properties of 5CB.* Molecular Crystals and Liquid Crystals Science and Technology. Section A. Molecular Crystals and Liquid Crystals, 1999. **331**(1): p. 49-57.
7. Nehring, J., A.R. Kmetz, and T.J. Scheffer, *Analysis of Weak-Boundary-Coupling Effects in Liquid-Crystal Displays.* Journal of Applied Physics, 1976. **47**(3): p. 850-857.
8. Yang, K.H., *Freedericksz Transition of Twisted Nematic Cells.* Applied Physics Letters, 1983. **43**(2): p. 171-173.
9. Coles, H.J. and M.S. Sefton, *Determination of Twist Elastic and Viscotic Constants Using Electric-Field Dynamic Light-Scattering.* Molecular Crystals and Liquid Crystals, 1985. **1**(5): p. 151-157.
10. Leadbetter, A.J. and E.K. Norris, *Distribution Functions in 3 Liquid-Crystals from X-Ray-Diffraction Measurements.* Molecular Physics, 1979. **38**(3): p. 669-686.
11. Blanton, T.N., Huang, T.C., Toraya, H. Hubbard, C.R., Robie, S.B., Louër, D., Göbel, H.E., Will, G., Gilles, R., and Raftery, T., *JCPDS—International Centre for Diffraction Data round robin study of silver behenate. A possible low-angle X-ray diffraction calibration standard.* Powder Diffraction, 1995. **10**(02): p. 91-95.
12. Meyer, T., Marcus, R., Berk, M., Patel, J., Dinicola, G., and Sareli, P., *The Beneficial Hemodynamic-Effect of Rapid Atrial-Pacing in Severe Acute Aortic Regurgitation (Ar).* Journal of the American College of Cardiology, 1987. **9**(2): p. A84-A84.
13. Salter, P.S., Elston, S.J., Raynes, P., and Parry-Jones, L.A., *Alignment of the Uniform Lying Helix Structure in Cholesteric Liquid Crystals.* Japanese Journal of Applied Physics, 2009. **48**(101302): p. 1-5 .
14. Patel, J.S. and R.B. Meyer, *Flexoelectric Electrooptics of a Cholesteric Liquid-Crystal.* Physical Review Letters, 1987. **58**(15): p. 1538-1540.

Chapter 4 Investigating elastic properties of bent core mixtures and compounds

Introduction

Bent core liquid crystals have been a research topic of great interest recently. Introducing a relatively small change to the molecular structure, such as inducing a bend at the core, has produced some rather unique behaviours, even in the simplest nematic phase. In many studies, the nematic phase of bent core liquid crystals have indicated bi-axiality [1, 2], unusual Kerr effect [3], and electro-convection [4]. Another of these unique behaviours is the anomalous elastic behaviour, where the splay elastic constant K_1 is greater than the bend elastic constant K_3 [5-12]. This is contrary to conventional calamitic liquid crystals. In this chapter, the origin of the anomalous behaviour will be investigated using the methods discussed in Chapter 3.

First an introduction of some of the unique phases that bent core liquid crystals exhibit is given, and then a view of the existing research on the unusual elastic constant behaviour in bent core liquid crystals will be developed. Bent core liquid crystals are difficult to study due to their negative dielectric anisotropy, and high nematic temperature range. Due to the difficulty in measuring elastic constants, there are limited reports of the elastic properties of pure bent core materials. There are however several studies relating to mixtures of bent core and calamitic liquid crystals; consequently, these mixtures were initially investigated. The influence of introducing dopants with intrinsic bend into a calamitic liquid crystal systems can be assessed relatively simply due to well-understood properties of the hosts such as 5CB.

Even though pure bent core liquid crystals are difficult to measure, there are some methods that can be used to investigate the systems. A series of oxadiazole-based bent core compounds with varying terminal chain lengths are investigated with the aim of understanding the effect of further molecular shape changes on the elastic constants. Calculations that include information relating to conformations of the molecules can also be used to predict the elastic behaviour. Thus, calculations considered in conjunction with experimental results, allows an understanding of the effect of introducing bend in the system on the elastic behaviour.

In the final part of the chapter, measurements of the elastic constants in a thaidiazole bent core compound are reported. This bent core compound is of particular interest because the elastic properties seen are similar to those in calamitic nematic liquid crystals. By comparing the structural differences between oxadiazole and the thiadiazole compounds, and considering the calculations of the elastic constants, a consideration of whether the behaviour is unique to this particular bent core compound or a more general property arising from the bent core structure, or indeed other factors, can be made.

The splay and bend elastic constants of the thaidiazole and oxadiazole compounds in this study were measured by *S. Kaur (University of Manchester)* and *A. Ferrarini (University of Padua)* performed the calculations on the compounds. My contribution was to measure the elastic constants of the mixtures, investigating appropriate methods to measure the twist and measuring the twist elastic constants in the pure and mixtures of bent core materials. The difficulty in measuring the twist elastic constant means that there are almost no other such measurements in bent-core materials. Measuring the twist elastic constant is vital for providing a complete picture of the bent core behaviour. The results of this work have already been published in two papers in the Journal of Material Chemistry [13, 14]

Bent core liquid crystal properties

Bent core liquid crystal phases

As briefly introduced in chapter 1, bent core liquid crystals are commonly composed of long molecules which, rather than being rod-like, are bent at the core with a particular bend angle depending on the molecular structure. The bend breaks the symmetry of the system and can introduce polar ordering in conventional liquid crystal phases, such as the polar ordered smectic phases [15-24]. Even in nematic phases, polar ordering can potentially manifest with bi-axiality [25-27] (noting that bi-axiality in nematic phases is hotly debated). While the main focus of this study is within the nematic phase of the bent core liquid crystals, the behaviour of the nematic phase can be heavily influenced by the phase below its temperature range. The structure of underlying phase may disallow particular kinds of behaviour, e.g. smectic phases are unable to sustain twist or bend distortions, causing the twist and bend elastic constants to diverge near the nematic to smectic phase transition, referred to as pre-transitional divergence. In addition to conventional smectic phases, bent core liquid crystals can form a variety of other phases with higher order than the nematic phase, known as the “B” phases. These are reviewed in the paper by Takazoe and Takanishi [28]; of these only the Dark

Conglomerate (DC) phase is relevant to this study. Thus an overview of the DC formed by bent core liquid crystals used in this study is required to gain a full picture of the behaviour of elastic constants.

Dark Conglomerate Phase

As previously mentioned with phenomena such as pre-transitional divergence due to underlying smectic phases, it is important to understand some of the unique phases seen in bent core liquid crystals. A phase that is seen in a bent core liquid crystal in this study is the DC phase, occurring below the temperature range of the nematic phase.

The DC phase appears as an isotropic phase, thus the texture through cross polarised microscopy is a completely dark texture. However by slightly uncrossing the polarisers, domains can be seen in the texture which contain opposite-handed-chirality [29-33]. The macroscopic chirality is seen even in cases where the molecules are achiral [34, 35]. Freeze Fracture Microscopy is a method imaging involving quenching a liquid crystalline phase to very low temperature, where the speed of the cooling can preserve and 'freeze in' the liquid crystal structure in the solid phase. Then, using various imaging techniques such as Transmission Electron Microscope (TEM), Scanning Electron Microscope (SEM), and Atomic Force Microscope (AFM), the structure can be seen. Such imaging studies, in conjunction with x-ray studies [36-39], has revealed a sponge like saddle-splay layered structure such as that shown in Figure 29. The dimensions of this structure are sub-optical, explaining why it appears optically isotropic rather than birefringent.

Figure 29 Sponge like saddle splay structure which exists in layers in the DC phase [40].

Recently there have been further studies into the structural deformations of DC phase under electric fields. Behaviour such as the coalescence of chiral domain under electric fields [40] and electrically tunable refractive index in the DC phase [41] occur while retaining the DC structure. While understanding of the structure is growing, currently, this is still a relatively poorly understood phase. Relevant to the discussion of the elastic constants, it has been suggested that the saddle-splay structure can occur if the splay-bend elastic constant becomes very small [13].

Nematic Phases

Much of the discussion of the nematic phases assumes uniaxial order, i.e. there is only orientation ordering of one axis of the nematic phase. It was theorized in 1970 that a biaxial nematic phase can exist, where there is orientation ordering along two orthogonal axes while still having no positional order [25] shown schematically in Figure 30. It has been suggested that bent core nematic liquid crystals have the potential to display biaxial properties [1, 2].

Figure 30 A cartoon of a biaxial nematic phase with orientation along both vertical and horizontal axis.

However, as already mentioned, the evidence for biaxial properties observed in nematic phases has been hotly contested. Studies have shown that cybotactic SmC clusters can display similar properties to those expected in a biaxial nematic phase [42]. Cybotactic clusters are small clusters of molecules with smectic ordering within a nematic phase. Cybotactic clusters only appear locally and can give the appearance of biaxial and polar ordering while maintaining a macroscopic nematic phase. Cybotactic clusters would normally be associated with critical divergence of the elastic constants in the nematic phase, emphasising the importance of understanding the elastic behaviour in such systems.

Recently, significant experimental and simulation work has been carried out to determine the elastic constants in nematic phases of pure bent-core liquid crystals and also in several mixtures of bent-core and calamitic materials [5-12, 43]. In almost all cases of pure bent core nematic phases there is an anomalous behaviour of the splay and bend elastic constants, where $K_3 < K_1$, contrasting what is commonly seen in the nematic phase of calamitic materials where $K_3 > K_1$. In mixtures of bent core and calamitic liquid crystals the studies have shown decreasing K_3 with increasing concentration of bent core dopant, while K_1 showed relatively small changes compared to K_3. However there are few pure bent-core compounds reported to show calamitic-like behaviour i.e. $K_3 >$

K_1 [44]. It was proposed by *Majumdar et al.* in 2011 that cybotactic clusters caused the lowering of K_2 and K_3 relative to K_1 [5]. However, another explanation for this phenomenon proposed by *Sathyanarayana et al.* [6], was to consider that coupling of the bent molecular shape with the bend distortions of the director causes $K_3 < K_1$. Very few of studies of elastic behaviour consider the twist elastic constant due to difficulties in manipulating the compounds and in measuring the twist elastic constant; indeed, apart from this work, in the few studies that exist, only the elastic constant for a single temperature is reported. This chapter first describes investigations of mixtures of bent-core and calamitic liquid crystals, giving an insight into how introducing bend into the system can influence the elastic properties. The later part of the chapter describes measurements of pure bent-core materials.

Elastic Constants in Bent Liquid Crystalline Systems

Mixtures of Oxadiazole and calamitic liquid crystals

As mentioned before, bent core compounds commonly have relatively high nematic temperature ranges and often have negative dielectric anisotropy making them difficult to work with. By mixing bent core compounds with calamitic liquid crystals in room temperature nematic phases, accessible nematic temperature ranges are obtained in systems with positive dielectric anisotropy. The mixtures can give insight into the effect of introducing bend into a nematic liquid crystal system. In other studies, an increase of K_1 as well as a decrease in K_3 are reported with increases in bent core dopant concentration [45]. In some mixtures the temperature dependence of K_1 and K_3 begins to exhibit contrasting behaviours at lower temperatures due to the appearance of cybotactic clusters at lower temperature; this causes K_3 to increase rapidly and K_1 to decrease rapidly [46].

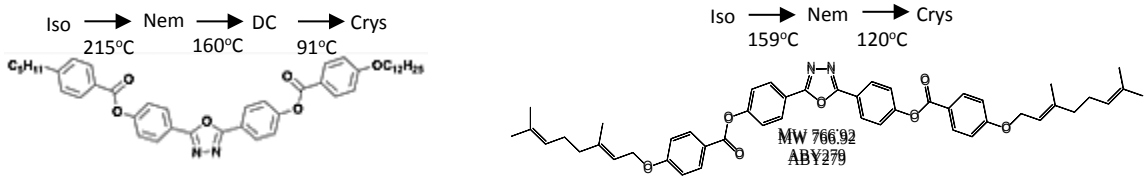

Figure 31 Molecular structure of the oxadiazole bent core compound (left) dopant 1 (right) dopant 2

In this study two bent core dopants were used in creating the mixtures. Dopant 1 was an oxadiazole compound with a dark conglomerate lying below the nematic phase, shown in Figure 31 (left). Dopant 2 is also an oxadiazole compound with only a nematic phase, shown in Figure 3 (right). Dopant 1 has a much higher nematic temperature range than dopant 2, thus mixtures made with dopant 2 have lower nematic temperature ranges than the mixtures with dopant 1. In all, 6 mixtures were made, shown in Table 1. All the mixtures exhibit only a nematic phase at room temperature except for mixture 2 which exhibits a unique phase that is discussed further, later in this thesis.

Mixture	Host	Dopant	Nematic to Isotropic (Heating)		Isotropic to Nematic (Cooling)
1	5CB – 95%	Dopant1 – 5%	37.5°C		39.9°C
2	5CB – 90%	Dopant1 – 10%	Initial Heating: 37.2°C	Subsequent Heating: 41.1°C	51.7°C
3	ZLI1132 – 95%	Dopant1 – 5%	75.6°C		75.3°C
4	ZLI1132 – 90%	Dopant1 – 10%	82.1°C		80.7°C
5	5CB – 95%	Dopant2 – 5%	37.4°C		37.3°C
6	5CB – 90%	Dopant2 – 10%	38.3°C		38.2°C

Table 1 Nematic to isotropic transition temperatures of the mixtures measured using DSC. Mixture 2 contains a filament growth which complicates the transition temperatures and which is discussed further later in the thesis.

The mixtures were made by measuring the appropriate weight percentages for each material then dissolving them using dichloromethane as a solvent, agitated in a sonic bath at room temperature for 1 hour. The solutions were then heated to 60° until all the dichloromethane had evaporated, leaving the liquid crystal mixture remaining. All the mixtures were checked using polarizing optical microscopy and Raman spectroscopy to ensure there was no phase separation. All the mixtures made exhibited only a nematic phase which existed from room temperature to the isotropic transition temperature range, with the exception of mixture 2. The temperature of the transition to isotropic is shown is shown in Table 1. The transition temperatures are measured from Differential Scanning Calorimetry (DSC). DSC is a method to analyse phase transitions by measuring the heat flow to the material compared to a reference sample. Depending on more or less heat flowed the transition is exothermic or endothermic and from the peak the transition temperature can be determined, and due to the wide peaks that exist for the transitions of the mixture the peak centre is taken as the transition temperatures. The unique phase seen for Mixture 2 has transition temperature sensitive to thermal history, with the initial transition on heating differing from the transition determined in subsequent heating runs. The discrepancy is attributed to a growth of a filament structure observed in the nematic of the mixture 2.

Mixture of Dopant 1 and 5CB

It is important to first briefly discuss the filament structure seen in the mixture, which will be investigated fully in chapter 5. The filament growth also eventually occurs in Mixture 1 but the process is much slower (~1 – 2 days) thus the measurements can be made within a stable, filament-

free nematic phase. For mixture 2, where there are significant filaments, a nematic-only phase can be achieved by melting the filaments at high temperature ~80°C then cooling to room temperature, with filaments forming on a much longer time scale (~0.5 hr) than the measurements (~5 minutes per temperature). To measure the splay and bend elastic constants, an Agilent Precision LCR Meter E4980A was used to determine the capacitance as a function of voltage, utilising the capacitance – voltage fitting method discussed in chapter 3. The twist elastic constant was measured using an IPS cell with planar alignment perpendicular to the electric field. As was explained in chapter 3, an in-house built photodiode measured the light transmission through the cell, while an AC voltage was applied from an Agilent 33220A waveform generator. The photodiode intensity was monitored using an Agilent 34410A multi-meter and the optical Fréedericksz transition used to determine the twist elastic constant.

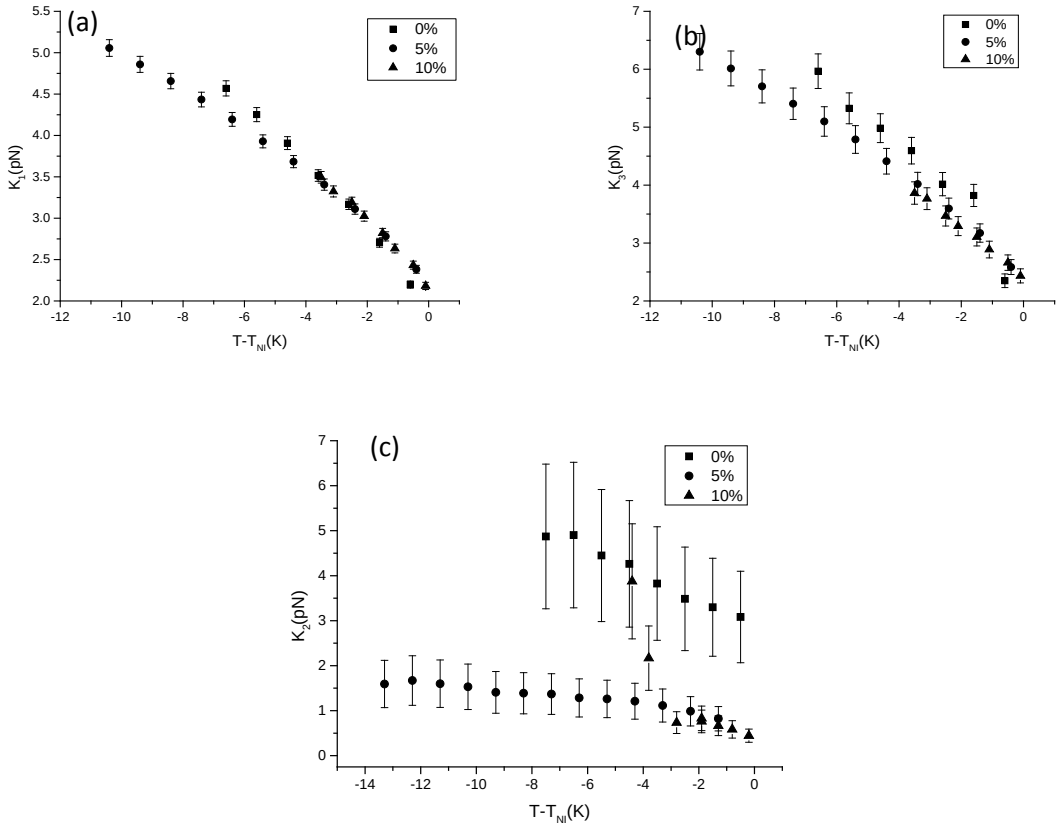

Figure 32 Mixtures 1 and 2 elastic constants compared with pure 5CB (a) splay elastic constant (b) bend elastic constant and (c) twist elastic constant.

Figure 32 presents the temperature dependence of all three elastic constants as a function of temperature below the nematic to isotropic transition temperature (T_{NI}) for Mixtures 1 and 2. In all cases, the elastic constants are behaving as expected, increasing with decreasing temperature. Figure

32(a) indicates that the inclusion of dopant 1 in the 5CB host seems to have very little effect on the splay elastic constant. Even with 10wt% of dopant 1, there is no significant change in K_1. Surprisingly K_3 also shows relatively small changes due to inclusion of bent core dopants. There is a slight decrease in K_3 of ~0.5pN for 5wt% of dopant, shown in Figure 32(b); however there is no further significant decrease in K_3 on increasing the amount of dopant 1 to 10wt%. For K_2, Figure 32(c) shows a significant decrease with the inclusion of the bent core dopant 1, decreasing by ~3.5pN. This change is much more significant than that seen in the other elastic constants. For the 10wt% of dopant 1 there is little further change close to T_{NI}, however at ~3K below the transition temperature significant divergence of K_2 occurs. Such divergence is more commonly seen in K_3 in calamitic nematic phases on approaching a smectic phase transition, as pretransitional divergence. In the case of mixture 2 it is most likely that the divergence of K_2 is associated with the filament growth. The filament structure either doesn't support the twist deformation or its growth alters the nematic phase so significantly that the usual Fréedericksz transition no longer applies fully.

To summarise, increases in dopant 1 concentration have relatively small effect on the splay and bend elastic constants. The lowering of K_2 is significant not only in terms of its magnitude but also is not seen in other similar mixture studies. Importantly, Mixture 1 also shows a consistent, significantly lower K_2, even though there is no filament growth observed. The lowering of K_2 is greater than K_3. This is surprising since the expected effect of including bent core dopants is to lower K_3. The divergence of K_2 is difficult to assess due to the unique nature of a phase with filament growth, but we can see the absolute value is initially very similar to the mixture 1, suggesting that lowering K_2 is repeatable. Therefore, it is difficult to generalise whether this phenomenon occurs for all bent core compounds. The presence of the filament structure also makes it difficult to generalise the results from mixture 1 and 2, however some further insight can be gained by considering these data in conjunction with results from the other mixtures.

Mixture of Dopant 1 and ZLI 1132

Initially, we speculated that the filament structure in Mixture 2 may be phase separation, resulting from the great discrepancy between the nematic phase temperatures of the host 5CB (T_{NI}=34.5ºC) and the bent core dopant 1 (T_{NI}=215ºC). Consequently, a nematic host with a much higher nematic range, ZLI 1132 (T_{NI} = 71.2ºC) was chosen for additional mixtures. Interestingly, there was no significant filament growth at any temperature in the nematic range of these mixtures.

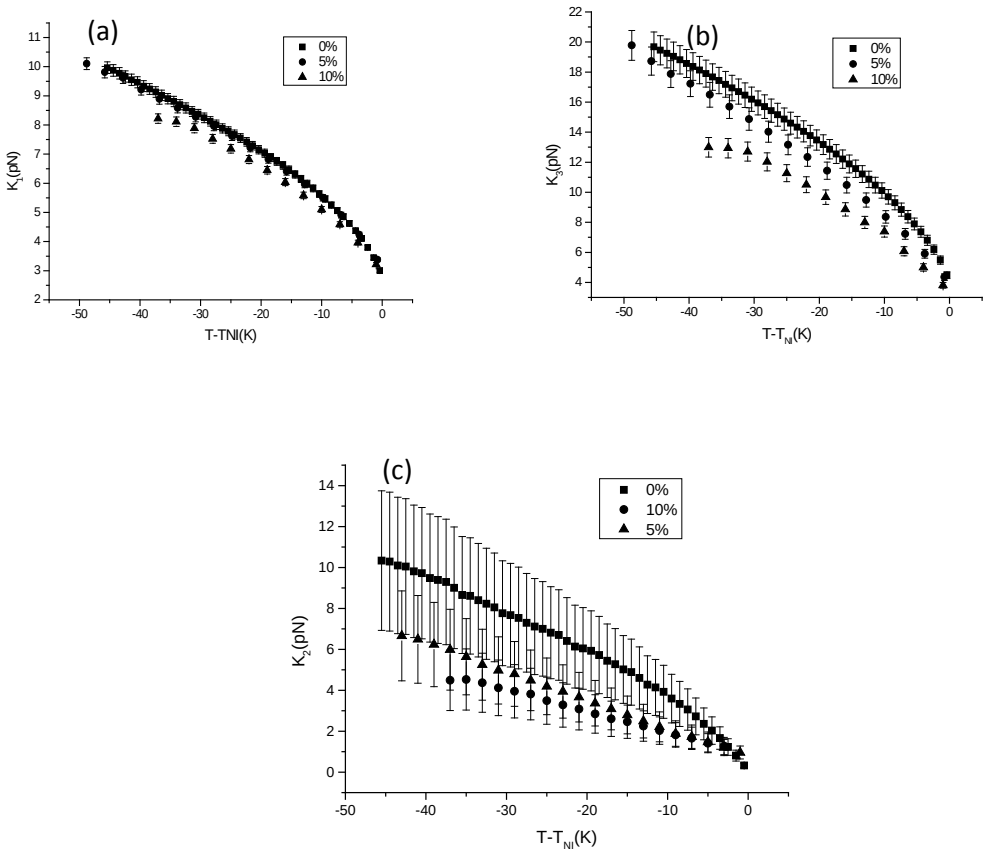

Figure 33 Mixtures of dopant 1 with ZLI1132 as host (a) splay elastic constant (b) bend elastic constant and (c) twist elastic constant

Mixtures 3 and 4 behave much more predictability due to the lack of filaments in these mixtures. Figure 33(a) shows that K_1 does not change much due to the addition of 5wt% bent core dopant. However on increasing dopant 1 to 10wt%, a slight decrease of ~0.5pN in K_1 is observed. The changes observed are very small and consistent with observations in mixtures 1 and 2. For K_3, shown in Figure 33(b), there is a significant decrease of ~2pN after adding 5wt% bent core dopant and there is a decrease of a further ~2pN with 10wt% dopant. These changes are very significant compared to those seen in K_1. The decrease in K_3 is expected, and is similar to that seen in other studies of bent core mixtures where the bend elastic constant significantly reduces with increasing bent core dopant concentration [47-49] Figure 33(c) also shows that K_2 is also significantly influenced; on including 5wt% of dopant 1 a change of ~3pN is observed and a further decrease of ~1.5pN occurs with 10wt% of dopant 1. Such large changes in K_2 are consistent with observations in Mixtures 1 and 2. The change in elastic behaviour in mixtures 3 and 4 is much more significant than in mixtures 1 and 2.

To summarise, K_3 reduces significantly; a ~20% decrease occurs with 10wt% of dopant 1, while K_1 shows only 5% change for the same dopant concentration. Again, the most significant change is in K_2, with a ~50% decrease at 10wt% dopant concentration, much more significant than the variation in

K_3. Indeed, while K_1 and K_3 behave largely as expected, it is K_2 that has the most significant decrease. While K_3 has been the focus of many of the studies of anomalous elastic behaviour in mixtures, this significant behaviour of K_2 has not been reported previously, indicating a significant gap in the literature with respect to understanding the elastic behaviour of mixtures of bent-core materials.

Mixture of Dopant 2 and 5CB

The suggestion that the filaments observed in mixtures 1 and 2 were due to discrepancies between the nematic ranges, of the host and dopant materials, led to the use of dopant 2 (T_{NI}=159°C) with its much lower nematic temperature range. It is noteworthy that even lower nematic ranges would be desirable, but high temperature nematic phases are a feature of bent-core compounds. Interestingly, the filament growth is not seen with dopant 2 in mixtures at either concentration.

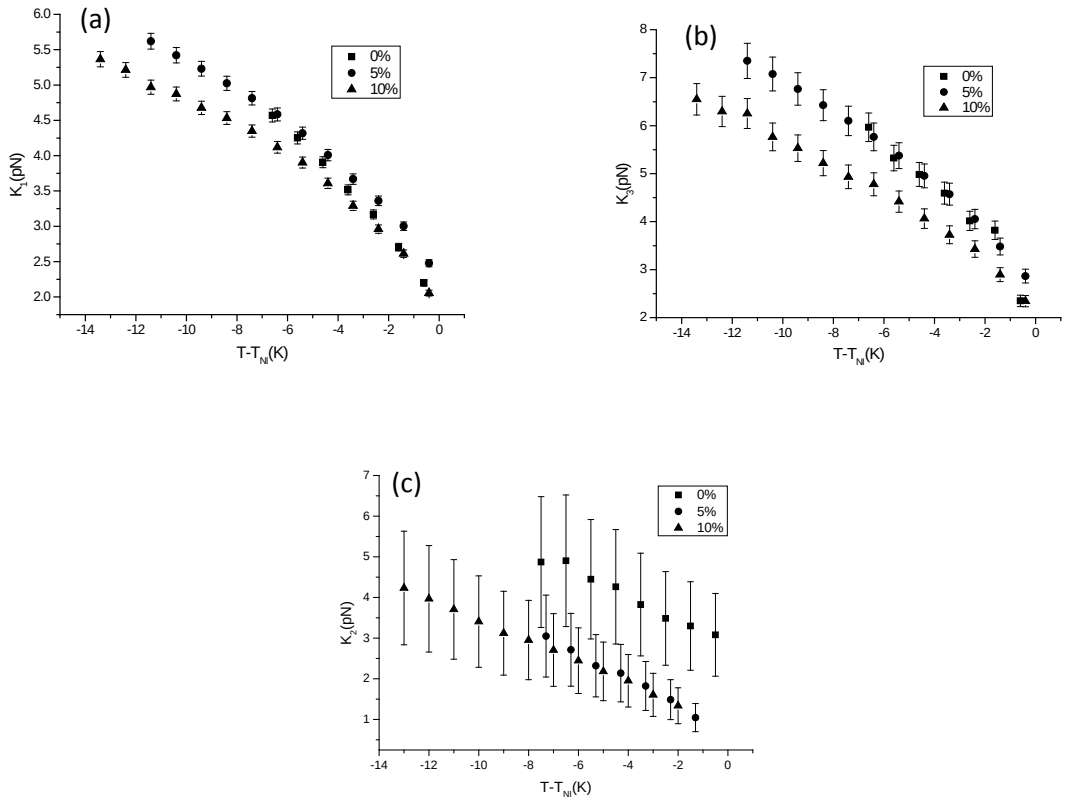

Figure 34 Mixtures of dopant 2 with 5CB as host (a) splay elastic constant (b) bend elastic constant and (c) twist elastic constant

Figure 34 shows the elastic properties of mixtures 5 and 6, which include dopant 2. Figure 34 (a) shows that $\boldsymbol{K_1}$ does not change on inclusion of 5wt% dopant, and only when the dopant concentration is increased to 10wt% is a decrease of ~0.5pN observed. For $\boldsymbol{K_3}$, shown in Figure 34 (b), there is

again no change on adding 5wt%, similar to the effect seen in $\boldsymbol{K_1}$. A significant change arises from adding 10wt% of dopant 2, however, leading to a significant decrease of ~2pN. This is much greater than the effect seen for $\boldsymbol{K_1}$ shown in Figure 34 (a). For $\boldsymbol{K_2}$, shown in Figure 34(c), there is a significant decrease of ~2pN even at 5wt%, unlike $\boldsymbol{K_1}$ and $\boldsymbol{K_3}$, and there is very little further change with 10wt% of dopant 2. The behaviour seen in the previous mixtures was largely repeated for these mixtures with changes in $\boldsymbol{K_3}$ (~20%), much more significant compared to $\boldsymbol{K_1}$ (~8%). Again, a much more significant reduction in $\boldsymbol{K_2}$ (~33%) is observed than in the other elastic constants.

Gruler [50] has suggested that the magnitude of the elastic constant can be influenced by the molecular shape, with a reduction in bend for bent molecules reported in many studies. In the mixture the elastic constant behaviour seems to be very consistent over different hosts and dopants lowering both K_3 and K_2 which decreases K_2 much more significantly. Although mixture 2 contains a filament growth, which limits the measureable temperature range of nematics, the elastic constants still behave similarly to the other mixtures. The consistency, despite the filament growth, means that it is likely that the filaments do not significantly affect the measurements of the nematic phase at low voltages, with the exception of the divergence of K_2. The results do suggest that the discrepancy in the nematic range between the host and dopant may be the cause of filament growth. With both measure taken to decrease the decrease discrepancy succeeded in removing the filament structure.

The mixtures measured have shown very similar behaviour as seen in other studies with mixtures of bent core and calamitic liquid crystals [47-49]. Specifically, increasing bent core dopants decreases the K_3 while K_1 remains relatively unchanged. There are no comparable studies of the influence on the twist elastic constant. It is clear from this study, however that for each of the different combinations of bent core dopant and hosts, there is a significant reduction of K_2 with increasing bent core dopant. Qualitatively, this behaviour is similar to that seen in K_3, but quantitatively large effects are seen in K_2. It is reasonable to generalise that the inclusion of intrinsic bend into liquid crystalline systems decreases both the K_3 and K_2 with K_2 decreasing much more significantly than K_3.

The Pure Oxadiazole Compound

The molecular shape is an important factor in determining the elasticity even in calamitic materials. Structural factors such as molecular length have been investigated in various studies of calamitic nematic liquid crystals [51-54]. There are many ways in which the molecular length can change, at one end [53-56] and both ends [51, 52] of the long molecular chain and molecules with the variable central group [57]. It is generally found that increasing terminal lengths increases the elastic constants.

In this study the changes to the terminal chain length are analysed for their effect on the elastic constants. In order to investigate the effect of terminal chains on elasticity, the elastic constants of a series of oxadiazole compounds with different terminal chain lengths were measured. The molecular structure and phase transitions are shown in Figure 35. The compound 1 – 4 decrease in terminal chain lengths, compound 2 also includes fluorination, and compound 4 has replaced an alkoxy with an alkyl lateral chain making it asymmetric. Compound 4 was also used in the previous mixtures studies as dopant 1. This study was performed in collaboration with *Sarabjot Kaur*, who measured the splay and bend elastic constant values for these materials and *Alberta Ferrarini* who performed the theoretical calculations on the materials. My contribution in this study was to measure the twist elastic constant, so far very few studies on bent core liquid crystals have been looked at due to the difficulty in measuring it. The results of this study have been already published in [13]. The elastic constants of the mixture is measured using the same setup as in the section 3.1, with capacitance – voltage fitting to obtain K_3 and K_1, and K_2 was measured using an IPS cell used.

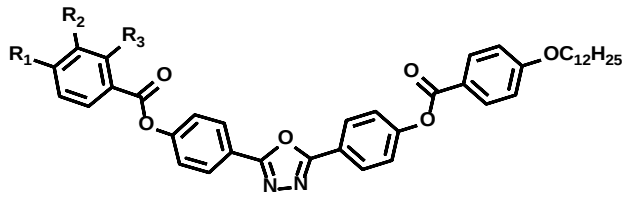

Compound 1: $R_1 = C_{12}H_{25}O$, $R_2 = R_3 = H$	Iso 217.7°C N 203.6°C SmC
Compound 2: $R_1 = C_9H_{19}O$, $R_2 = R_3 = F$	Iso 221.4°C N 206.0°C SmC
Compound 3: $R_1 = C_9H_{19}O$, $R_2 = R_3 = H$	Iso 236.6°C N 204.6°C SmX
Compound 4: $R_1 = C_5H_{11}$, $R_2 = R_3 = H$	Iso 239.6°C N 184.6°C DC

Figure 35 Molecular structure of four oxadiazole base molecules with different terminal chain length [58].

This series of oxadiazole liquid crystal all have a bend angle of 143°, determined from Raman and x-ray scattering[59], negative dielectric anisotropy, and high nematic temperatures, again making it difficult to measure the properties of the nematic phase. Homemade homeotropic cell had to be constructed to measure the splay and bend constants of these materials. Homeotropic alignment was achieved using trichloro-octadecyl silane in heptane for the complete nematic range of compounds 2 and 4, for limited range of temperatures compounds 1 and 3. Compound 1 and 2 have an underlying smectic C phase, while compound 3 have an unidentified smectic phase below the nematic phase referred to as smectic X in Figure 35. Compound 4 has a DC phase below the nematic phase, compound 4 have shown many unique properties in previous studies [58, 60, 61].

Elastic constants

The capacitance-voltage fitting method is used on homeotropic cells to obtain K_3 and K_1; the threshold voltage determines K_3, while the whole curve analysis determines K_1. The twist elastic constant was measured using an IPS cell, with the measurement differing from the previous measurement, as the alignment of the director is perpendicular to the interdigitated electrodes, as opposed to parallel in previous setups due to the negative dielectric anisotropy. In this configuration the liquid crystal director is orientated parallel to the electric field; this in turn causes the twist of the director towards a direction perpendicular to the electric field, due to the negative dielectric anisotropy.

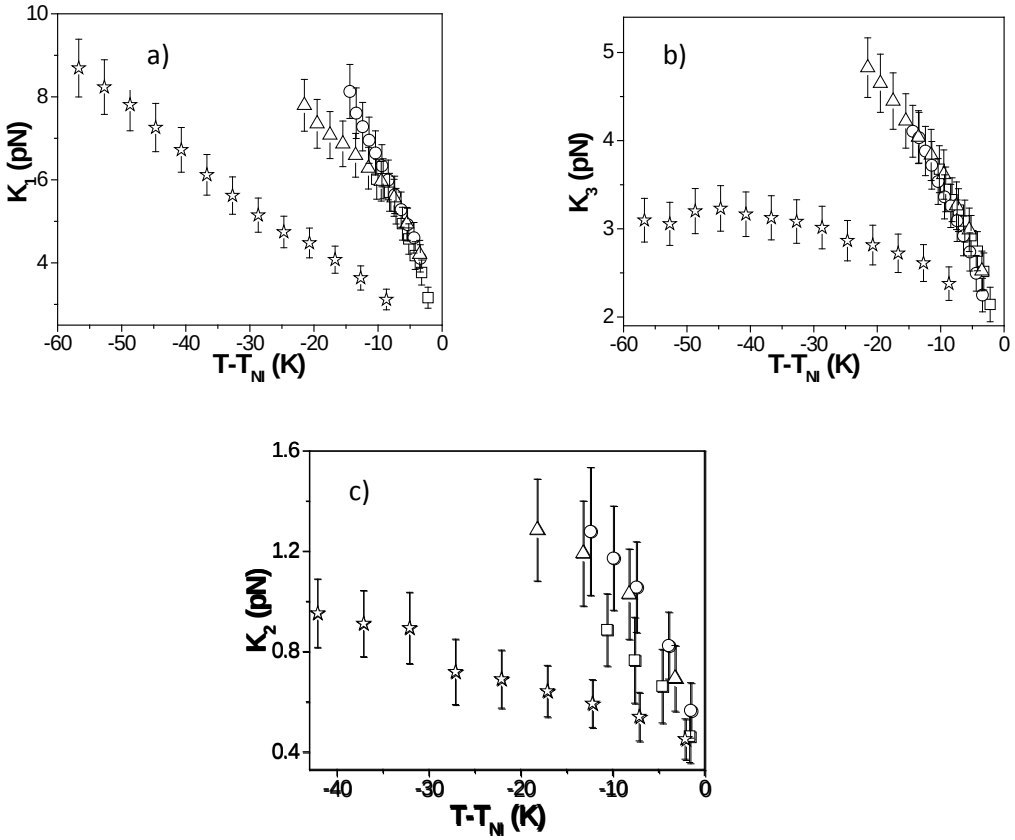

Figure 36 Elastic constant of compound 1(open squares), compound 2(open circles), compound 3(open triangle), and compound 4 (open star) and a) is the measured K_1, b) is the measured K_3, c) is the measured K_2 [58].

Figure 36 shows that all the oxadiazole compounds exhibit the anomalous behaviour where $K_3 < K_1$. Compounds 2 and 3 could not be measure accurately across the full range of the nematic phase due to deteriorating alignment. The temperature dependence of K_1 is as expected for all compounds increasing with decreasing temperature. For K_3, compounds 1-3 behave as expected with increasing

values on decreasing the temperature. However, for compound 4, while K_3 behaves largely similarly to the other compounds, a slight decrease is observed below $T - T_{NI} = -45^{o}C$. The decrease in K_3 with decreasing temperature is actually seen in several other studies regarding mixtures [43, 62, 63]. It is proposed in those studies that the decrease in K_3 is attributed to the coupling of the bent shape with the bend distortion becoming stronger at lower temperatures. In the mixtures, higher bent core dopant concentrations begin to lower K_3 deep in the nematic phase. Although there exists a smectic C phase below the nematic range in compound 1 and 2, no obvious divergence is seen in any of the elastic constants (it would be expected particularly in the bend constant). Similar to the behaviour seen in mixtures, K_2 again has very low values < $1pN$, and although K_2 is generally lower than K_1 and K_3, K_2 has been consistently very low throughout our studies into liquid crystalline systems with intrinsic bend. With many studies focusing on K_3 this unique behaviour of K_2 has largely been missed.

It is clear that there is no significant change in the behaviour any of the three elastic constants on decreasing the length of the side chains compound 1-3. Compound 4 however has consistently shown much lower elastic constants, reduced by a factor of ~ 75% across all three elastic constants in comparison to the other compounds. The main structural change is the removal of the oxygen in one of the side chains. Oxygen has a very strong dipole associated with the molecule so removal of a strong dipole might cause significant changes in the elastic properties because of the influence on the intermolecular interactions. However, the inclusion of fluorine, which also induces a large dipole, does not produce similar behaviour. The conformations adopted by the alkoxy chain are different from alkyl chains. Thus the origin of this behaviour may be conformational in nature.

Modelling

Atomistic modelling was performed by *Ferrarini et al* [14]. The atomistic calculations are based on mean field theory, which predicts the dependence of the elastic constants on the order parameter. In the calculations, the elastic constants were derived from the molecular shape, since many conformations exist for a particular molecular shape. The elastic properties for each conformation are calculated and a weighted averaged with respect to the probability of each conformation is employed.

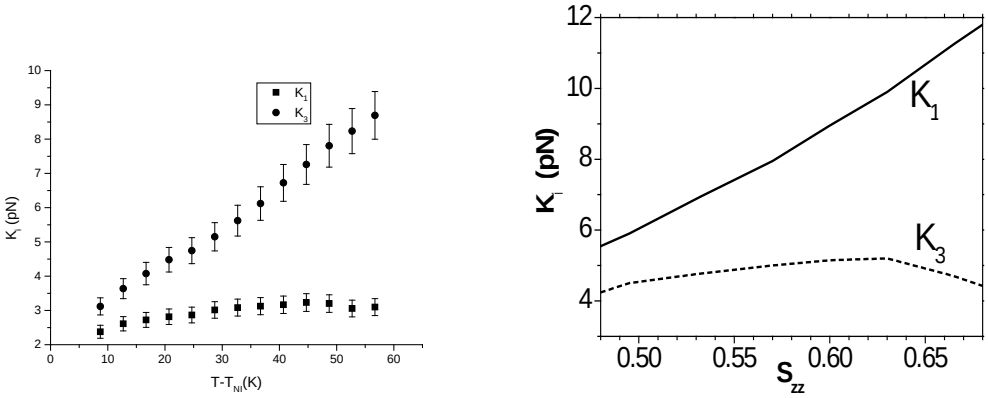

Figure 37 (left) Experimentally determined of compound 4 (left) compared with calculation (right) [58]

Figure 37 shows the experimental and calculated values for splay and bend elastic constants for compound 4. The calculated data are ~3pN larger than the values obtained experimentally, however the temperature dependence is in excellent agreement, even showing that at ~ -55ºC (S=0.63) the bend elastic constant begins to decrease with decreasing temperature. A detailed look at each conformation can reveal details in the exact origin of the anomalous behaviour.

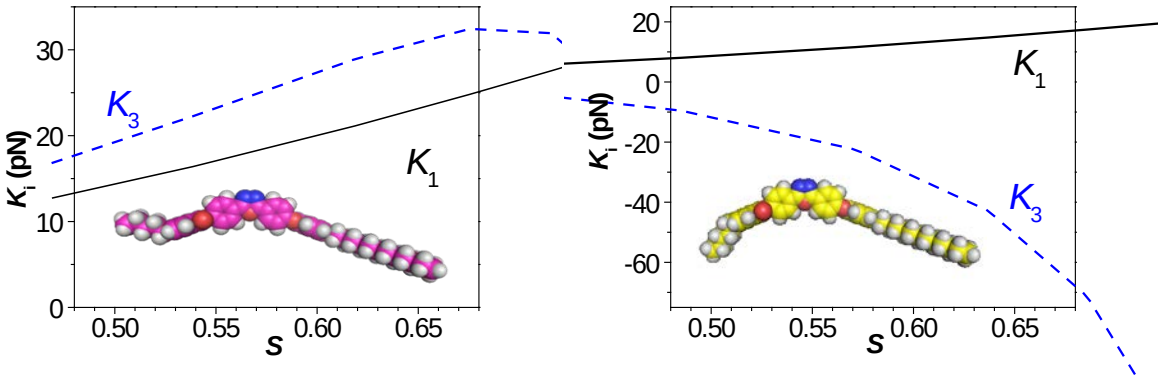

Figure 38 Calculations of elastic constants for different conformations of oxadiazole compound more elongated (left) less elongated (right) [14].

The calculations of the different conformations show that the more elongated conformations are closer in shape to calamitic molecules, shown in Figure 38 (left). Here the behaviour of $K_3 > K_1$ often seen in conventional calamitic materials, is recovered. The less elongated conformation in Figure 38 (right) is closer in shape to that expected in bent core molecules, and in this situation the anomalous behaviour $K_3 < K_1$ is seen. This further confirms the importance of the bend angle in determining the elastic constants. The sensitivity of K_3 to the bend angle has been confirmed by calculations performed for nematic systems as a function of the bend angle, especially in the range around 150°. The lateral chains of the molecule are claimed by some to have a key influence on the elastic

properties of bent core liquid crystals [44] but the calculations show a more complex scenario. The lateral chains may instead be of great importance in the stability of the nematic phase [64], and only directly influence the elastic properties depending on the conformations adopted.

Indeed, since the calculations consider the conformation of the molecules, the shape of the molecule is shown to be especially important for determining the elastic properties of a bent core liquid crystal. We can conclude that the anomalous behaviour seen in most bent core liquid crystals where $K_3 < K_1$; this is purely due to the coupling of the bent molecular shape and the bend deformation.

Elastic constants of a thiadiazole compound

Although many bent core liquid crystals have the unusual elastic behaviour, recent results on a bent-core thiadiazole material, shown in Figure 39, showed $K_3 > K_1$ at a single temperature that is analogous to the behaviour found in calamitic nematics [65].

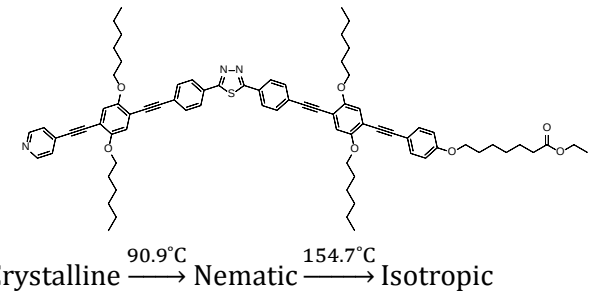

Figure 39 Thiadiazole bent core molecule. The phase transitions of the thiadiazole compound determined on heating via a DSC at a scan rate of 10°C/min [66].

Although a vast majority of bent core liquid crystals have shown the property where $K_3 < K_1$, the behaviour seen in the thiadiazole materials suggests that these properties are not universal for all bent core liquid crystals. The study of oxadiazole compounds in the previous section, in conjunction with the calculations, showed the importance of the bend angle. In fact in the calculations for sufficiently elongated conformations recovered the calamitic behaviour of $K_3 > K_1$. The thaidiazole compound has a bend angle of 164°, which is larger than that of the oxadiazole compounds (143°). In an attempt to confirm the cause of the anomalous behaviour, the temperature dependence of the elastic constants of the same thiadiazole materials used in [65], provided by *J. Seltmann and M. Lehmann* is measured and compared to those calculated from the atomistic modelling performed by *Ferrarini* [14]. This study was again in collaboration with *Sarabjot Kaur*, who measured the splay and bend elastic constant values for the thaidiazole compound and *Alberta Ferrarini* who again performed the

theoretical calculations on the materials. My contribution was to again measure the twist elastic constant. The results of this study have been already published in [14].

Another property of the thiadiazole compound is that it is a dual frequency material. Dual frequency materials display both $\Delta\varepsilon < 0$ and $\Delta\varepsilon > 0$ at different applied frequencies. This property overcomes some of the problems with measuring elastic constants experienced in bent core liquid crystals with $\Delta\varepsilon < 0$. The splay and bend elastic constants were measured using the capacitance – voltage fitting method explained in chapter 3. Due to being a dual frequency material, the measurements were only performed for the region where the material is $\Delta\varepsilon > 0$; hence a homogeneously aligned sample is used. The orientation order parameter, S, can be deduced from the refractive index data following the well-known Haller method [67]. In these data, an order parameter is used rather than temperature to directly compare experimental data with the theoretical predictions.

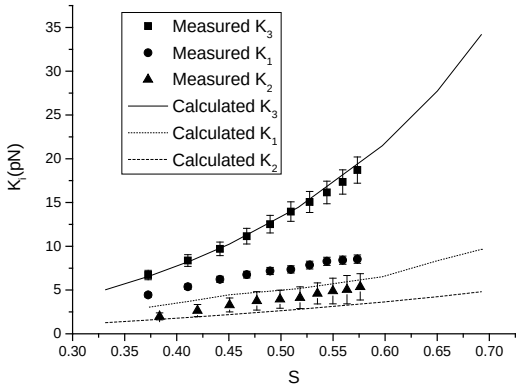

Figure 40 Points represent the experimentally determined elastic constants of the thiadiazole compound as a function of order parameter. Lines represent the calculated behaviour of the elastic constants of the thiadiazole compound.

Figure 40 shows the behaviour of the elastic constants, represented as points, as a function of the order parameter S. It is clear to see that $K_3 > K_1$ as seen in calamitic systems such as 5CB, measured in chapter 3. All of the elastic constants increase with increasing order parameter (decreasing temperature). Such behaviour is expected since as a system becomes more highly ordered, increased energy is needed to cause distortions.

A study performed by Salamon *et al* [65] on the same material using magnetic field Fréedericksz measurements also reports, K_3=10 pN, K_1=5.4 pN and K_2=2.2 pN at a single temperature of T-T_{NI}= -24 K. From Figure 40 (considering the order parameter at the equivalent temperature), K_3, K_1 and K_2

at T-T_{NI}= -24 K are seen to be 11.7±1.0pN, 6.9±0.4pN and 3.7±1.9pN respectively. The values are in excellent agreement within error.

Again, the calculations performed agree well with the experimental results, being only slightly lower in absolute values and with the temperature dependence reproduced extremely well. We do not expect the calculations and experimental results to agree exactly as the calculations are necessarily simplified. The strength of the calculation is nevertheless seen as the results reproduce the elastic behaviour as a function of temperature very well. Again this points to the importance of the molecular shape, in particular the bend angle, on the elastic properties of the nematic liquid crystal. In cases where the bend angle is sufficiently large, the elastic properties are not influenced sufficiently to reduce K_3 to below K_1.

Here the low values of K_2 and the temperature dependence is again replicated well in the calculations, pointing to the importance of the bend angle not only on K_3 but K_2. In this thaidiazole bent core compound, with a relatively large bend angle, bigger K_2 values are seen compared to the oxadiazole compounds. Thus this suggests both K_3, K_2 are strongly influenced by the bend angle. The low K_2 is observed for several bent core compounds and mixtures and, importantly, is also seen in the calculations. It is fair to extend this behaviour to all sufficiently bent liquid crystal systems.

Studies of the Thiadiazole compound in a TN cell

Initially, it was thought that a TN cell would be a convenient way of measuring the twist constant in the thiadiazole material since the compound can have positive dielectric anisotropy. However the results were both complicated and interesting with the appearance of domains, shown in Figure 41.

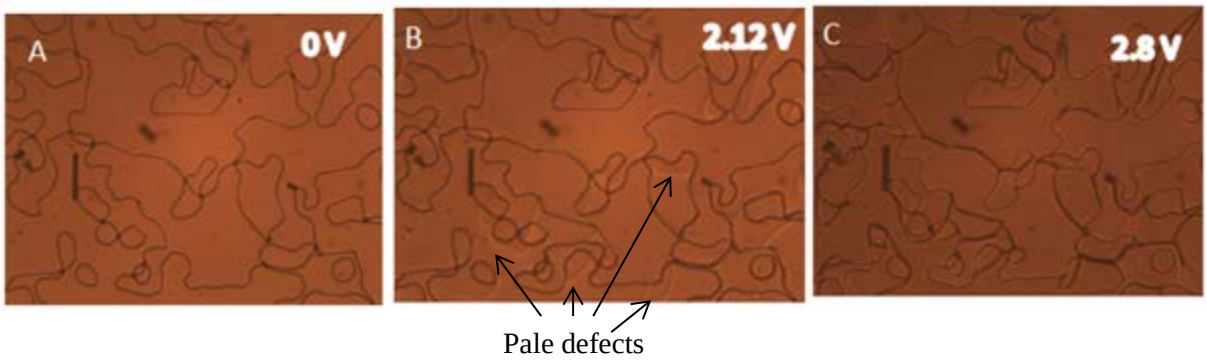

Figure 41 The domains of thiadiazole based compound in TN cell. An applied voltage creates extra pale defects

These domains seem to be different domains of chiral handedness, though unfortunately the check for chirality could not be made before the materials degraded. What is of interest are the pale defects separating the domains. On application of an electric field (Figure 41 (B)) extra (pale) defects nucleate from the original (dark) defects. These extra defects do not appear to be related to the Fréedericksz transition and appear before the Fréedericksz threshold voltage. Under higher applied voltages, as shown in Figure 41(C) when the threshold is exceeded, the entire cell darkens, presumably due to the tilting of the director.

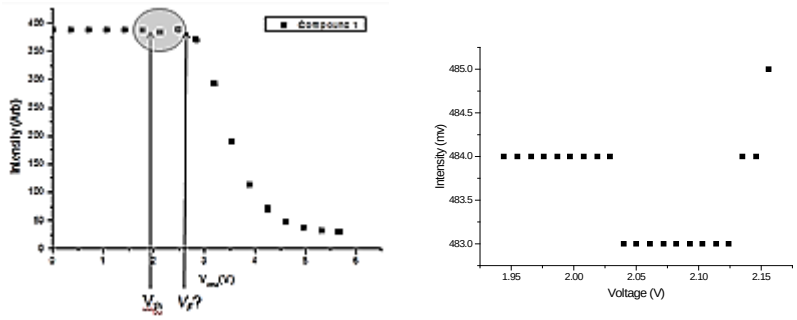

Figure 42 (Left)Transmitted intensity from the thiadiazole compound in a TN cell where V_{th} is the initial threshold and V_F is the threshold due to the Fréedericksz transition. (Right) the highlighted region in more detail.

In Figure 42 (left) the Fréedericksz transition seen in the transmitted intensity is shown, in the highlighted region there is a small decrease and increase in intensity before the actual Fréedericksz transition (V_F) corresponding to the appearance of the extra defects in Figure 41 (B). This initial threshold is consistent over the whole nematic temperature range and is shown in more detailed measurements in Figure 42(right).

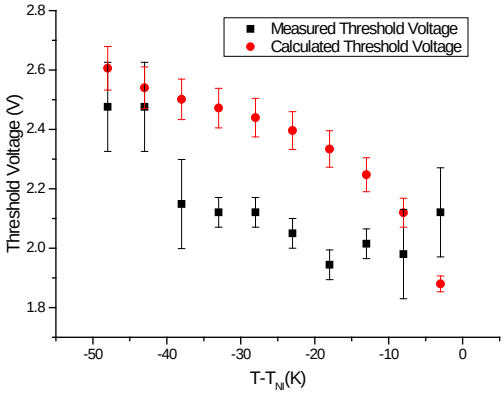

Figure 43 The threshold voltage calculated from measure elastic constant compared to the V_{th}

If the threshold voltage is calculated from the measured elastic constants and compared to the initial threshold seen in Figure 43, it is clear that the initial threshold occurs before the Fréedericksz transition. This is very unusual since in chapter 2 we saw that the threshold is the minimum field strength needed to cause any elastic distortions. The creation of the extra defects must be occurring from other electric field induced phenomenon such as flexoelectricity. Unfortunately, the thiadiazole material is light-sensitive and this sample eventually degraded. As we were unable to obtain any more of this material, no further investigations could be performed. Nonetheless, it would seem to be very interesting to propose measurements of the flexoelectric constants in this material.

Summary

In this chapter the elastic properties of pure bent core compounds and mixtures of bent core materials with calamitic hosts was examined. Mixtures of the oxadiazole materials with calamitic liquid crystals showed a lowering of both K_3 and K_2 with increasing oxadiazole dopant concentration. The observation of the reduction in K_2 the phenomenon is seen to be much more significant than the lowering of K_3 for same concentration of dopant. One mixture in particular is unique, with a significant filament growth that hindered the elastic constant study, but which is investigated further in chapter 5.

It was found that the bend angle of the bent core compound is extremely important in dictating the bend and twist elastic properties of the nematic liquid crystals. With a bend angle of ~160^o, such as in the thiadiazole compound, the closer shape to calamitic molecules results in similar behaviour, i.e. the bend elastic constant is larger than the splay elastic constant. A smaller bend angle of ~140^o, as seen in the oxadiazole compounds, results in the bend elastic constant being smaller than the splay elastic constant. A critical angle of ~150^o is suggested, where the bend and splay elastic constants would be expected to be equal.

The other structural changes studied in this section are terminal chain lengths, fluorination, and changing one terminal chain from alkoxy to alkyl. Most of these changes the to the molecular structure seem to have little effect on the elastic constants, and the most significant effect comes from changing one terminal chain from alkoxy to alkyl which significantly lowers the all elastic constants. In fact, in that particular oxadiazole compound with one alkyl chain has shown many unique properties such as a DC phase.

Reference

1. Madsen, L.A., Dingemans, T.J., Nakata, M., and Samulski, E.T., *Thermotropic Biaxial Nematic Liquid Crystals.* Physical Review Letters, 2004. **92**(14) 145505: p. 1-4.
2. Acharya, B.R., A. Primak, and S. Kumar, *Biaxial nematic phase in bent-core thermotropic mesogens.* Physical Review Letters, 2004. **92**(14) 145506: p. 1-4.
3. Dhara, S., Araoka, F., Lee, M., Le, K.V., Sadashiva, B.K., Song, K., Ishikawa, K., and Takezoe, H., *Kerr constant and third-order nonlinear optic susceptibility measurements in a liquid crystal composed of bent-shaped molecules.* Physical Review E, 2008. **78**(5) 050701: p. 1-4.
4. Wiant, D., Gleeson, J.T., Ěber, N., Fodor-Csorba, K., Jákli, A., and Tóth-Katona, T., *Nonstandard electroconvection in a bent-core nematic liquid crystal.* Physical Review E, 2005. **72**(4) 041712: p. 1-12.
5. Majumdar, M., Salamon, P., Jakli, A., Gleeson, J.T., and Sprunt, S., *Elastic constants and orientational viscosities of a bent-core nematic liquid crystal.* Phys. Rev. E, 2011. **83**(3) 031701: p. 1-8.
6. Sathyanarayana, P., Mathew, M., Li, Q., Sastry, V.S.S., Kundu, B., Le, K.V., Takezoe, H., and Dhara, S., *Splay bend elasticity of a bent-core nematic liquid crystal.* Phys. Rev. E, 2010. **81**(1) 010702: p. 1-4.
7. Tadapatri, P., Hiremath, U.S., Yelamaggad, C.V., and Krishnamurthy, K.S., *Permittivity, Conductivity, Elasticity, and Viscosity Measurements in the Nematic Phase of bent core LC.* J. Phys. Chem. B 2010. **114**: p. 1745-1750.
8. S. Kaur, Addis, J., Greco, C., Ferrarini, A., Gortz, V., Gooby, J.W., and Gleeson, H.F., *Understanding the distinctive elastic constants in an oxadiazole bent-core nematic liquid crystal.* Phys. Rev. E, 2012. **86**041703: p. 1-11.
9. Dodge, M.R., Rosenblatt, C., Petschek, R.G., Neubert, M.E., and Walsh ,M.E., *Bend elasticity of mixtures of V-shaped molecules in ordinary nematogens.* Phys. Rev. E 2000. **62**: p. 5056-5063.
10. Kundu, B., R. Pratibha, and N. Madhusudana, *Anomalous Temperature Dependence of Elastic Constants in the Nematic Phase of Binary Mixtures Made of Rodlike and Bent-Core Molecules.* Phys. Rev. Lett., 2007. **99**(24) 247802: p. 1-4.
11. Sathyanarayana, P., B.K. Sadashiva, and S. Dhara, *Splay-bend elasticity and rotational viscosity of liquid crystal mixtures of rod-like and bent-core molecules.* Soft Matter, 2011. **7**(18): p. 8556-8560.
12. Sathyanarayana, P., Jampani, V.S.R., Skarabot, M., Musevic, I., Le, K.V., Takezoe, H., and Dhara, S., *Viscoelasticity of ambient-temperature nematic binary mixtures of bent-core and rodlike molecules.* Phys. Rev. E, 2012. **85**(1) 011702: p. 1-9.
13. Kaur, S., Liu, H., Addis, J., Greco, C., Ferrarini, A., Gortz, V., Goodby, J.W., and Gleeson, H.F., *The influence of structure on the elastic, optical and dielectric properties of nematic phases formed from bent-core molecules.* Journal of Materials Chemistry C, 2013. **1**(40): p. 6667-6676.
14. Kaur, S., Tian, L., Liu, H., Greco, C., Ferrarini, A., Seltmann, J., Lehmannd, M., and Gleeson, H.F., *The elastic and optical properties of a bent-core thiadiazole nematic liquid crystal: the role of the bend angle.* Journal of Materials Chemistry C, 2013. **1**(13): p. 2416-2425.
15. Watanabe, J., Niori, T., Choi, S.W., Takanishi, Y., and Takezoe, H., *Antiferroelectric smectic liquid crystal formed by achiral twin dimer with two mesogenic groups linked by alkylene spacer.* Japanese Journal of Applied Physics Part 2-Letters, 1998. **37**(4A): p. L401-L403.
16. Shen, D., Diele, S., Pelzl, G., Wirth, I., and Tschierske, C., *Designing banana-shaped liquid crystals without Schiff's base units: m-terphenyls, 2,6-diphenylpyridines and V-shaped tolane derivatives.* Journal of Materials Chemistry, 1999. **9**(3): p. 661-672.

17. Niori, T., Sekine, T., Watanabe, J., Furukawa, T., and Takezoe, H., *Distinct ferroelectric smectic liquid crystals consisting of banana shaped achiral molecules.* Journal of Materials Chemistry, 1996. **6**(7): p. 1231-1233.
18. Weissflog, W., Lischka, C., Benne, L., Scharf, T., Pelzl, G., Diele, S., and Kruth, H., *New banana-shaped mesogens.* Liquid Crystals: Chemistry and Structure, 1998. **3319**: p. 14-19.
19. Kentischer, F., Macdonald, R., Warnick, P., Heppke, G., and Rauch, S., *Second harmonic generation in liquid crystals of nonchiral, banana shaped molecules.* Liquid Crystals, 1997. **3143**: p. 128-135.
20. Walba, D.M., Korblova, E., Shao, R., Maclennan, J.E., Link, D.R., Glaser, M.A., and Clark, N.A., *A ferroelectric liquid crystal conglomerate composed of racemic molecules.* Science, 2000. **288**(5474): p. 2181-2184.
21. Nadasi, H., Weissflog, W., Eremin, A,m Pelzl, G., Diele, S., Das, B., and Grande, S., *Ferroelectric and antiferroelectric "banana phases" of new fluorinated five-ring bent-core mesogens.* Journal of Materials Chemistry, 2002. **12**(5): p. 1316-1324.
22. Diele, S., Grande, S., Kruth, H., Lische, C.H., Pelzi, G., Weissflog, W., and Wirth, I., *Structure and properties of liquid crystalline phases formed by achiral banana-shaped molecules.* Ferroelectrics, 1998. **212**(1-4): p. 169-177.
23. Sekine, T., Takanishi, Y., Niori, T., Watanabe, J., and Takezoe, H., *Ferroelectric properties in banana-shaped achiral liquid crystalline molecular systems.* Japanese Journal of Applied Physics Part 2-Letters, 1997. **36**(9ab): p. L1201-L1203.
24. Weissflog, W.,Wirth, I., Diele, S., Pelzl, G., Schmalfuss, H., Schoss, T., and Wurflinger, A., *The N,N '-bis[4-(4-n-alkyloxybenzoyloxy)benzylidene]phenylene-1,3-diamines: mesophase behaviour and physical properties.* Liquid Crystals, 2001. **28**(11): p. 1603-1609.
25. Freiser, M.J., *Ordered States of a Nematic Liquid.* Physical Review Letters, 1970. **24**(19): p. 1041-1043.
26. Yu, L.J. and A. Saupe, *Observation of a Biaxial Nematic Phase in Potassium Laurate-1-Decanol-Water Mixtures.* Physical Review Letters, 1980. **45**(12): p. 1000-1003.
27. Malthete, J., N.H. Tinh, and A.M. Levelut, *New Mesogens with 6-Paraffinic, 4-Paraffinic, or 3-Paraffinic Chains.* Journal of the Chemical Society-Chemical Communications, 1986(20): p. 1548-1549.
28. Hideo, T. and T. Yoichi, *Bent-Core Liquid Crystals: Their Mysterious and Attractive World.* Japanese Journal of Applied Physics, 2006. **45**(2R): p. 597-625.
29. Thisayukta, J., Y. Nakayama, and J. Watanabe, *Effect of chemical structure on the liquid crystallinity of banana-shaped molecules.* Liquid Crystals, 2000. **27**(9): p. 1129-1135.
30. Shih, C.S. and R. Alben, *Lattice Model for Biaxial Liquid-Crystals.* Journal of Chemical Physics, 1972. **57**(8): p. 3055-3061.
31. Ortega, J., Folcia, C.L., Etxebarria, J., Gimena, N. and Ros, M.B., *Interpretation of unusual textures in the B-2 phase of a liquid crystal composed of bent-core molecules.* Physical Review E, 2003. **68**(1) 011707: p. 1-4.
32. Etxebarria, J., Folcia, C.L., Ortega, J., and Ros, M.B., *Induction of ferroelectricity in the B-2 phase of a liquid crystal composed of achiral bent-core molecules.* Physical Review E, 2003. **67**(4) 042702: p. 1-4.
33. Eremin, A. and A. Jakli, *Polar bent-shape liquid crystals - from molecular bend to layer splay and chirality.* Soft Matter, 2013. **9**(3): p. 615-637.
34. Gortz, V., Southern ,C., Roberts, N.W., Gleeson, H.F., and Gooby, J.W., *Unusual properties of a bent-core liquid-crystalline fluid.* Soft Matter, 2009. **5**(2): p. 463-471.
35. Link, D.R., Natale, G., Shao, R., Maclennan, J.E., Clark, N.A., Korblova, E., and Walba, D.M., *Spontaneous formation of macroscopic chiral domains in a fluid smectic phase of achiral molecules.* Science, 1997. **278**(5345): p. 1924-1927.
36. Weissflog, W., Sokolowski, S., Dehne, H., Das, B., Grande, S., Schroder, M.W., Eremin, A., Siele, S., Pelzl, G., and Kresse, H., *Chiral ordering in the nematic and an optically isotropic mesophase of bent-core mesogens with a halogen substituent at the central core.* Liquid Crystals, 2004. **31**(7): p. 923-933.
37. Chen, D., Shen, Y.Q., Zhu, C.H., Hough, L.E., Ros, M.B., and Clark, N.A., *Interface structure of the dark conglomerate liquid crystal phase.* Soft Matter, 2011. **7**(5): p. 1879-1883.

38. Ortega, J., Folcia, C.L., Etxebarria, L., Gimeno, N., and Ros, M.B., *Interpretation of unusual textures in the B_2 phase of a liquid crystal composed of bent-core molecules.* Physical Review E, 2003. **68**(1) 011707: p.1-4.
39. Liao, G., Stojadinovic, S., Pelzl, G., Weissflog, W., Sprunt, S., and Jakli, A., *Optically isotropic liquid-crystal phase of bent-core molecules with polar nanostructure.* Physical Review E, 2005. **72**(2) 021710: p. 1-6.
40. Nagaraj, M., Jones, J.C., Panov, V.P. Liu, H., Portale, G., Bras, W., and Gleeson, H.F., *Understanding the unusual reorganization of the nanostructure of a dark conglomerate phase.* Physical Review E, 2015. **91**(4) 042504: p.1-13.
41. Nagaraj, M., Gortz, V., Goodby, J.W., and Gleeson, H.F., *Electrically tunable refractive index in the dark conglomerate phase of a bent-core liquid crystal.* Applied Physics Letters, 2014. **104**(2) 021903: p.1-5.
42. Francescangeli, O., Vita, F., Ferrero, C., Dingemans, T., and Samulski, E.T., *Cybotaxis dominates the nematic phase of bent-core mesogens: a small-angle diffuse X-ray diffraction study.* Soft Matter, 2011. **7**(3): p. 895-901.
43. Parthasarathi, S., Rao, D.S.S., Csorba, K.F., Prasad, S.K., *Viscoelastic Behavior of a Binary System of Strongly Polar Bent-Core and Rodlike Nematic Liquid Crystals.* The Journal of Physical Chemistry B, 2014. **118**(49): p. 14526-14535.
44. Salamon, P., Eber, N., Seltmann, J., Lehmann, M., Gleeson, J., Sprunt, S., and Jakli, A., *Dielectric technique to measure the twist elastic constant of liquid crystals: The case of a bent-core material.* Physical Review E, 2012. **85**(6) 061704: p. 1-9.
45. Sathyanarayana, P., Jampani, V.S.R., Skarabot, M., Musevic, I., Le, K.V., Takezoe, H., Dhara, S., *Viscoelasticity of ambient-temperature nematic binary mixtures of bent-core and rodlike molecules.* Physical Review E, 2012. **85**(1) 011702: p.1-9.
46. Lee, J.H., T.H. Yoon, and E.J. Choi, *Unusual temperature dependence of the splay elastic constant of a rodlike nematic liquid crystal doped with a highly kinked bent-core molecule.* Physical Review E, 2013. **88**(6) 062511 p.1-5.
47. Sathyanarayana, P., B.K. Sadashiva, and S. Dhara, *Splay-bend elasticity and rotational viscosity of liquid crystal mixtures of rod-like and bent-core molecules.* Soft Matter, 2011. **7**(18): p. 8556-8560.
48. Dodge, M.R., Rosenblatt, C., Petschek, R.G., Neubert, M.E., and Walsh, M.E., *Bend elasticity of mixtures of V-shaped molecules in ordinary nematogens.* Physical Review E, 2000. **62**(4): p. 5056-5063.
49. Dodge, M.R., Petschek, R.G., Rosenblatt, C., Neubert, M.E. and Walsh, M.E., *Light scattering investigation above the nematic-smectic-A phase transition in binary mixtures of calamitic and bent-core mesogens.* Physical Review E, 2003. **68**(3) 031703: p. 1-6.
50. Gruler, H., *Elastic properties of the nematic phase influenced by molecular properties.* The Journal of Chemical Physics, 1974. **61**(12): p. 5408-5412.
51. Gruler, H. and G. Meier, *Investigations on the Elastic Constants of the Nematic Homologous Series of 4,4'-Di(n-Alkoxy) Azoxybenzene.* Mol. Cryst. Liq. Cryst., 1973. **23**(3-4): p. 261-270.
52. de Jeu, W.H. and Claassen W.A.P., *The elastic constants of nematic liquid crystalline terminally substituted azoxybenzenes.* J. Chem. Phys., 1977. **67**(8): p. 3705-3712.
53. Leenhouts, F., Roebers, H.J., Dekker, A.J., and Jonker, J.J., *Relation between Elasticity and Molecular Structure of Nematic Liquid Crystals.* J. Phys. Colloq., 1979. **40**(C3): p. 291-297.
54. Schad, H., G. Baur, and G. Meier, *Elastic constants and diamagnetic anisotropy of p-disubstituted phenylcyclohexanes (PCH).* J. Chem. Phys., 1979. **70**(6): p. 2770-2774.
55. Schad, H. and M.A. Osman, *Elastic constants and molecular association of cyano-substituted nematic liquid crystals.* J. Chem. Phys., 1981. **75**(2): p. 880-885.
56. Karat, P.P. and N.V. Madhusudana, *Elastic and Optical Properties of Some 4'-n-Alkyl-4-Cyanobiphenyls.* Mol. Cryst. Liq. Cryst., 1976. **36**(1-2): p. 51-64.
57. Bradshaw, M.J. and E.P. Raynes, *Electric Permittivities and Elastic Constants of the Cyano Bi-Cyclohexanes (CCH).* Mol. Cryst. Liq. Cryst., 1981. **72**(2-3): p. 35-42.
58. Kaur, S., Addis, J., Grecoc, C., Ferrarini, A., Gortz, V., Gooby, J.W., and Gleeson, H.F., *Understanding the distinctive elastic constants in an oxadiazole bent-core nematic liquid crystal.* Physical Review E, 2012. **86**(4) 041703: p. 1-11.

59. Southern, C.D., Brimicombe, P.D., Siemianowski, S.D., Jaradat, S., Roberts, N., Gortz, V., Gooby, J.W., and Gleeson, H.F., *Thermotropic biaxial nematic order parameters and phase transitions deduced by Raman scattering.* EPL (Europhysics Letters), 2008. **82**(5) 56001: p. 1-6.
60. Kaur, S., Panov, V.P., Greco, C., Ferrarini, A., Gortz, V., Goodby, J.W., and Gleeson, H.F., *Flexoelectricity in an oxadiazole bent-core nematic liquid crystal.* Applied Physics Letters, 2014. **105**(22) 223505: p. 1-4.
61. Kaur, S., Belasissaoui, A., Goodby, J.W., Gortz, V., and Gleeson, H.F., *Nonstandard electroconvection in a bent-core oxadiazole material.* Physical Review E, 2011. **83**(4) 041704: p. 1-12.
62. Kundu, B., R. Pratibha, and N.V. Madhusudana, *Anomalous Temperature Dependence of Elastic Constants in the Nematic Phase of Binary Mixtures Made of Rodlike and Bent-Core Molecules.* Physical Review Letters, 2007. **99**(24) 247802: p. 1-4.
63. Sathyanarayana, P., Jampani, V.S.R., Skarabot, M., Musevic, I., and Le, K.V., Takezoe, H., and Dhara, S., *Viscoelasticity of ambient-temperature nematic binary mixtures of bent-core and rodlike molecules.* Physical Review E, 2012. **85**(1) 011702: p. 1-9.
64. Kim, Y.K., Majumdar, M., Senyuk, B.I., Tortora, L., Seltmann, J., Lehmann, M., Jakli, A., Gleeson, J.T., Lavrentovich, O.D., and Sprunt, S., *Search for biaxiality in a shape-persistent bent-core nematic liquid crystal.* Soft Matter, 2012. **8**(34): p. 8880-8890.
65. Salamon, P., Eber, N., Seltmann, J., Gleeson, J., Sprunt, S., and Jakli, A., *Dielectric technique to measure the twist elastic constant of liquid crystals: The case of a bent-core material.* Phys. Rev. E, 2012. **85**(6) 061704: p. 1-9.
66. Seltmann, J., Marini, A., Mennucci, B., Dey, S., Kumar, S., and Lehmann, M., *Nonsymmetric bent-core liquid crystals based on a 1,3,4-thiadiazole core unit and their nematic mesomorphism.* Chemistry of Materials, 2011. **23**(10): p. 2630-2636.
67. Haller, I., *Thermodynamic n static properties of LCs.* Prog Solid State Chem, 1975. **10**.

Chapter 5 Investigating Filament Structure in Mixture of Bent Core and Calamitic liquid crystals

Introduction

In chapter 4, when measuring the elastic properties of a mixture composed of 10% oxadiazole compound 4 as the dopant 1 and with 90% 5CB as the host, difficulties in measurements arose from the growth of a filament structure. The filaments seem to not directly affect the nematic phase as birefringence of the nematic phase can still be seen in background, and can be shown to switch although under much higher voltage. The filaments also manifest other unique properties such as the different transition temperatures on initial heating and subsequent heating, and time dependence of the filament formation. This chapter's aim is to investigate whether the filament structure is some form of phase separation and crystallisation of the bent core dopant or some form of hybrid phase of the two compounds. The phase transitions will be analysed by polarising microscopy and DSC. Then the dielectric properties will be examined. Finally, SAXS will be performed on a bulk sample of the mixture to find any periodicities within the structure of the filaments.

Phase observation

Optical observation of filament phases

The mixture is composed of two components 5CB and an oxadiazole compound shown in

Figure 44 molecular structure of bent core compound (left), 5CB (right).

The phases the mixture exhibits are complicated as the system is not a uniform continuous phase. There are two elements to the phase, the filament structure and the background nematic phase. The filaments are attribute to a phase separation of the bent core dopant compound In Figure 45 (a) the

filaments exhibited are the orange fan like structures spiralling out from nucleation points, while the background nematic is shown as the green background surrounding the structure. In this state the "phase" is referred to as the nematic – filament phase.

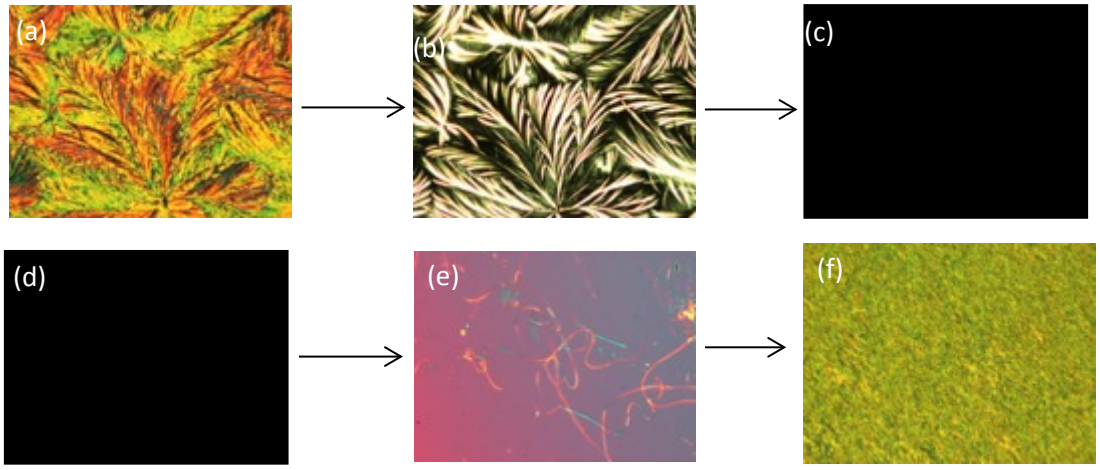

Figure 45 (a) a nematic filament phase at room temperature (b) the background nematic transitions into an isotropic phase, while the filament remains unchanged forming an isotropic filament phase at 50°C (c) a pure isotropic phase at 80°C (d) pure isotropic phase at 80°C (e) A nematic phase occurs at 50.3°C however the filament that grows in is difficult to get nematic phase below ~5°C the transition (f) nematic filament phase where filament grows throughout the sample

Initially after filling, the cell the mixture is in a nematic phase and covered with filament (nematic – filament phase) at room temperature as shown in Figure 45 (a). Upon heating, the nematic phase in the background transitions into an isotropic phase, while the filament remains unchanged forming an isotropic – filament phase at 37.2°C as shown in Figure 45 (b). Finally, a complete isotropic phase occurs at 80°C as shown in Figure 45 (d) and (e). The melting of the filaments is not seen clearly in the DSC and the DSC signal is dependent on the heating rate, thus the DSC is unable to measure the transition of the isotropic-filament phase to the complete isotropic phase. On cooling, a nematic phase occurs at 51.7°C however the nematic phase is unstable. Filaments quickly grow in and a nematic phase below ~5°C the transition is difficult to obtain, as shown in Figure 45 (e). Eventually a filament grows throughout the sample giving the final nematic – filament state shown in Figure 45 (f). The other property that makes mixture-2 unique is that on subsequent heating, the transition temperature of the nematic-filament to isotropic-filament changes as shown in Table 1. When the mixture enters the unstable nematic phase, filament growth exists but is slower than those seen at lower temperatures. If this is left at the same temperature, the filament will continue to grow throughout the mixture. The filament growth in the mixture affects the dielectric properties and the response of the nematic phase to electric field.

Upon heating to 38.7°C the background nematic phase undergoes a phase transition to the isotropic phase while the filament structure remains unchanged, referred to as the isotropic – filament phase shown in Figure 45 (b). Finally upon heating to relatively high temperatures the filament structure melts slowly over a temperature range from 65.7°C – 72.2°C culminating into the pure isotropic phase shown in Figure 45 (c).

The mixture displays different phases on cooling than on heating. There is no filament structure forming in the isotropic phase. Instead the mixture cools from an isotropic phase into a nematic phase, with filaments forming in the nematic phase as shown in Figure 45 (e). What is interesting to note is that the filaments cannot form in the isotropic phase and can only form in the nematic phase. The filament growth is slow and is dependent on time and the growth speed is dependent on the temperature, at lower temperatures the filament growth is relatively faster with filaments formed through the system in ~1 minute. Once the filament dominates the mixture, the system returns to the initial nematic – filament phase seen in Figure 45 (f).

The difference between the nematic – filament phase textures seen in Figure 45 (f) and Figure 45 (a) is the cooling rate. Figure 45(a) shows a system that is quenched from the isotropic phase whereas the in Figure 45(f) the system is cooled slowly at a rate of 2°C/min. Uniquely, when the mixture is cooled slowly like in Figure 45 (f) the filament growth is aligned with the nematic phase and the alignment layer, the texture observed is relatively uniform and has dark states when parallel or perpendicular to the polarisers. The same effect can be seen in a cell with homeotropic alignment as shown in Figure 46 (left). This is similar to the quenched system with branched out filament structure from several nucleation points. Figure 46 (right) cooled at 2°C/min giving a relatively uniform dark texture indicating that the alignment are perpendicular to the plane of the cell.

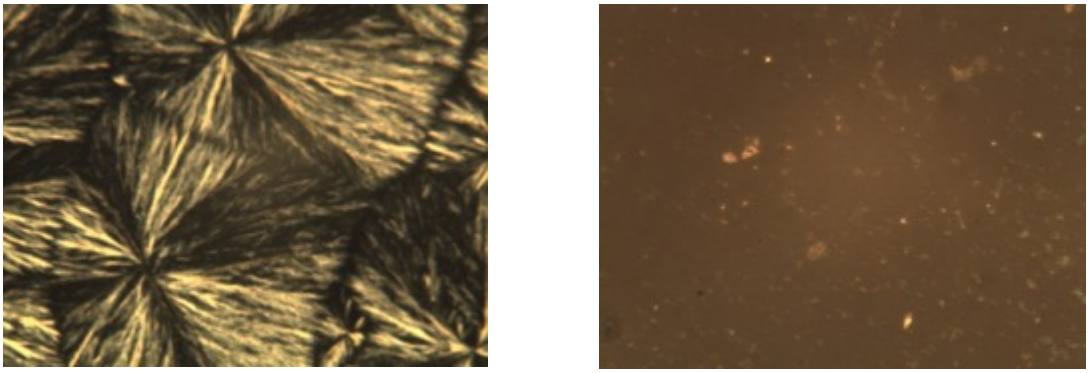

Figure 46 (left) The mixture quenched from isotropic phase. (right) The mixture cooled at 2°C/min from isotropic phase

This ability to align the filaments is a result of the filament dependency on the nematic phase. In the nematic phase, the mixture is influenced by the alignment layer with a slow enough cooling rate

the filament growth can follow the alignment. At faster cooling rates, the growth is fast enough to not be completely influenced by the alignment of the nematic phase.

There also exists a difference in phase transition temperatures on initial heating and the immediate subsequent heating which is unexpected. On initial heating, with a well-established filament structure, the transition from nematic to isotropic – filament phase is found to be 37.7^{o}C. After a subsequent heating run, and after the system has cooled from a pure isotropic phase, the nematic to isotropic – filament phase transition is higher 42.8^{o}C. When the mixture is left for ~24 hours, however, the mixture reverts back to the initial system. The discrepancy in the heating runs suggests that the phase is altered in some way in the initial system and the immediate subsequent system. The most obvious difference between the two systems is the amount of time for which the filaments have grown. It is sensible to speculate that the filaments are composed mainly of the bent core dopant; this means for a system that has just cooled from an isotropic phase, there is still a large amount of bent core compounds within the mixture that has not had time to form into the filaments yet. Therefore, the mixture, in the immediate subsequent systems, has higher bent core content than the initial system. Since the nematic phase of the pure bent core compound is much higher than the nematic temperature of 5CB, with higher bent core content leads to higher nematic to isotropic transition temperatures.

Of all the mixtures made only this one has shown significant changes to the nematic from adding small amount of bent core dopant. One reason could be great discrepancy in nematic temperature ranges, which in the other mixtures was avoided and could have also avoided the filament growths. The bent core compound has a DC phase below the nematic temperature range, the DC phase is still relative not well understood, and underlying phases can have effects on the nematic phase. From Raman scattering the mixture seem well mixed not showing any obvious phase separation, however there is an obvious phase separation occurring.

Optical observations of the filament structure in the mixture have revealed many interesting features of the filaments in the mixture. Firstly, the mixture seems to be composed of two components, the filament structure and the background nematic phase. The filament structure possesses many unique properties too. The filament growth is time dependent, attributed to the bent core dopants, and only grows in the nematic phase. Due to these properties the background nematic phase's exact content percentages is different depending on the amount of time given for the filament formation. The phases the mixture displays have already shown to be extremely complex and DSC will be used to investigate the phase in more detail.

DSC investigation of phase transition

The DSC was performed at a rate of 2ºC/min from room temperature to 100ºC as shown in Figure 47(left). Again the obvious discrepancy in the initial heating run and immediate subsequent heating run is seen.

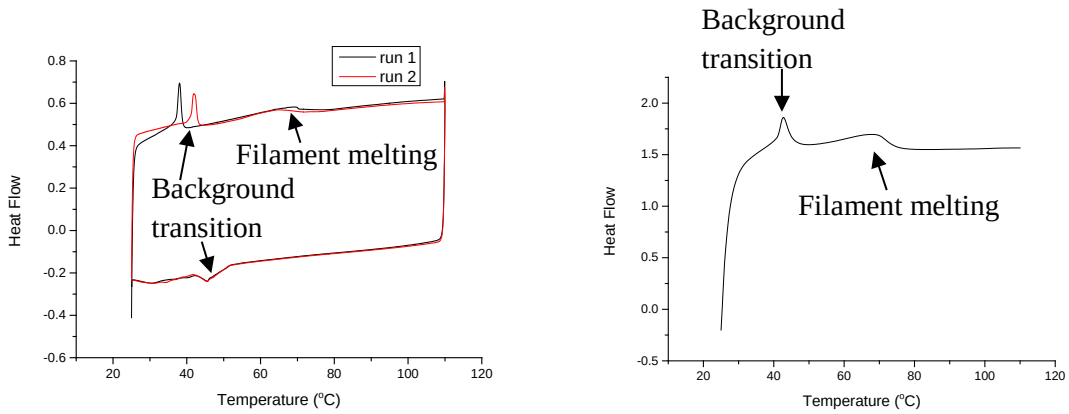

Figure 47 (left) DSC of the mixture at heating rate of 2ºC/min (Right) DSC on heating at 20ºC/min

During the initial heating, shown in Figure 47 (left) run 1 gives a background transition of 38.7ºC, and on the subsequent cooling run 43.1ºC. The second heating run gives a background transition onset of 41.2ºC and the subsequent cooling run gives an onset of 42.9ºC. There is clear discrepancy between the heating run 1 and run 2 phase transitions, the origin seems to be the amount of filaments established in the system. There is no discrepancy seen in the cooling runs as there are no filament formations in either system thus displaying similar properties.

The melting of the filaments is observed from 65.7ºC to 72.2ºC optically, this melting is not clearly seen in the DSC slight indication are shown in Figure 47 (left) of a very small wide peak near 65ºC. The peak does not change in intensity with increased sample size or amount. However there is a significant change when changing the heating rate to 20ºC/min, as shown in Figure 47 (right). The peak becomes much more prominent with increased heating rates. The phase transition, which is sensitive to heating rates, is typically seen in dynamic phase transitions such as gel transitions, suggesting that the system is a gel or gel-like system.

The DSC confirms what was seen optically in the phase transitions and suggests that a gel system is what is formed from the mixture. This is in fact confirmed optically with two relative independent systems co-existing, the background nematic and the filament structure. In the next section, we will investigate whether the mixture is a gel.

Gel-like properties

The mixture has shown to have unique properties not seen in conventional liquid crystal phases. These properties are, however, quite common in gel materials. Gels in general are a 3D network with a continuous phase mixed in between the network. Chemical and physical organogels are formed through self-assembly of the molecules into 3D networks mixed with solvents to make a gel. Chemical gels are self-assembled through chemical bonding using covalent bonds, whereas physical gels self-assemble through physical processes such as hydrogen bonding [1-5], lipophilic [6], dipole-dipole [7], and donor-acceptor interactions [8]. Liquid crystals have been shown to be able to form gels through doping a liquid crystal with a self-assembling of gelators, forming a self-assembled 3D structure with a liquid crystal acting as the continuous phase. The self-assembling of a liquid crystal phase forming a 3D structure added to organic solvent also enabled liquid crystal gel formation [9-12].

There have been recent studies showing other complex liquid crystal phases displaying gelation abilities in organic solvents, with smectic liquid crystal phases forming self-assembled 3-D structures to form gels [7]. There are also disc-like liquid crystal compounds forming gels with 3-D structures showing columnar ordering [13-15]. A helical-nano-filament phase (B4) can also form a gel with the 3-D structure showing similar x-ray patterns as the pure B4 phase x-ray pattern [16], and in the same study, a DC phase was found not able to form gels with solvents.

The mixture is actually a soft malleable material but it does not flow or possess any of the typical liquid crystal properties. Yet the nematic phase can be observed in the background while the system shows more mechanical properties seen in solid or more ordered liquid crystal phases. This is consistent and expected if the mixture has formed a gel where the 3D network gives the system a mechanical stability while maintaining a more fluid phase. In Figure 48 (left and middle) the mixture can be shown to hold its own weight another common property of the gel.

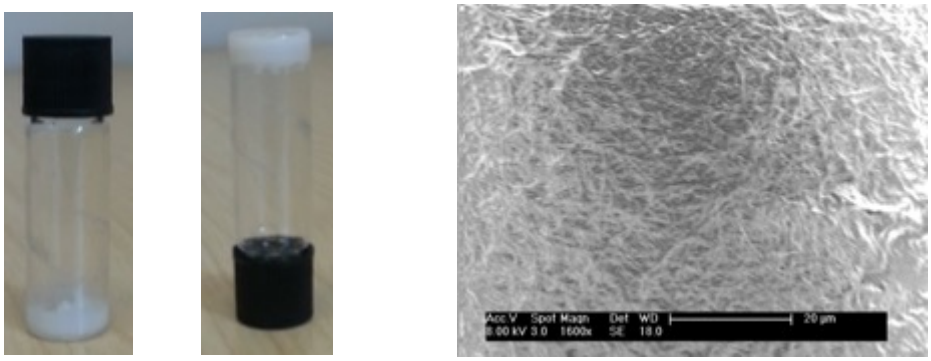

Figure 48 A bottle of the mixture upright (left) and upside down (middle) at room temperature. (right) SEM of the mixture with 1600 X magnification.

Utilising a Scanning Electron Microscope (SEM) the 3D network formed by the filaments structure can be imaged as shown in Figure 48 (right). Figure 48 (right) is similar to other organogel networks imaged with SEM. The filament network can be attributed to that of a gel 3D network. In this gel system has already been shown to be unique and different from the conventional gel networks. Firstly, both the filament network and the background phase are both made from liquid crystalline materials; previous liquid crystal gels only have the liquid crystal forming one component of the gel. In fact, very few gels form from only two components. Secondly the filament network can be aligned, something previously not capable in any gel system. The filament formation mechanism is still not clear and need further investigations

The evidence seems to suggest that the mixture is a gel material and potentially a completely new system with liquid crystal components forming both the elements of the gel, with anisotropy in both the network and the background nematic adding another dimension in which the gel can be manipulated. To investigate this material further, the dielectric properties will be studied. The dielectric properties the mixture exhibited were only studied with relation to the nematic phase in chapter 4. The dielectric properties of the filaments with the nematic phase were not investigated in any detail.

Dielectric investigations

Similar to the dielectric measurements made in chapter 4, a device was constructed with 2 glass substrates to contain a liquid crystal layer 5 μm thick. An Indium-Tin-Oxide transparent electrode area that measures 30 mm^2 and indium is used to attach the wires to the electrode surfaces. The electrical properties of the devices were calibrated using air as a standard reference for all of the temperatures studied, and the devices were capillary-filled at 100˚C. The devices were held in a Linkam THMS600 hot stage equipped with a TMS 93 controller which allowed temperature control of the samples with a relative accuracy of ±0.1˚C. The apparatus includes an Agilent Precision LCR Meter E4980A which measures the dielectric permittivity across the frequency range 20 Hz – 2 MHz using a 0.05 V_{ac} probe voltage, where necessary in the presence of an AC electric field of up to 10 *V*.

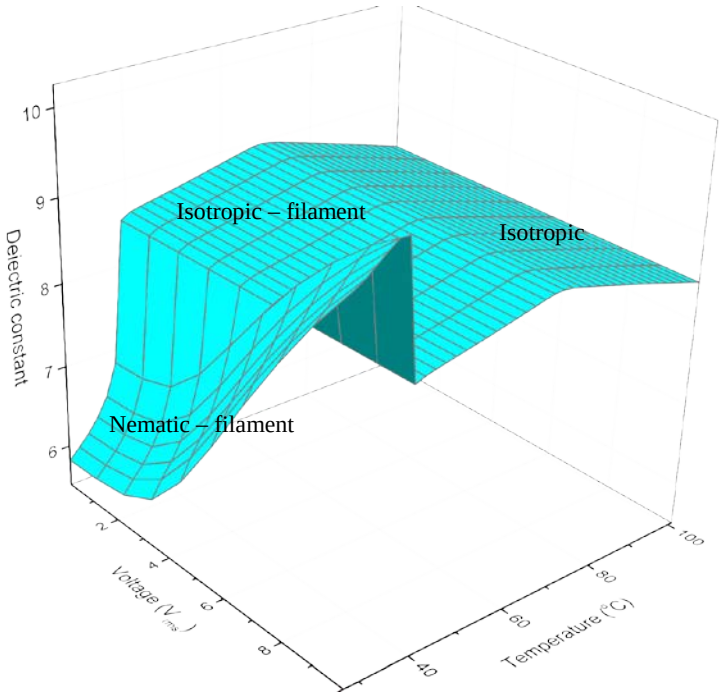

Figure 49 Dielectric constant vs Voltage vs Temperature of mixture on heating

From Figure 49 for the isotropic – filament and the pure isotropic phase there is no change in the dielectric constant with increasing voltage application. The filaments have no dielectric response meaning any response observed should purely arise from the background nematic phase. The responses seen at the lower temperatures in the nematic – filament phase are suppressed with respect to the pure 5CB response with a threshold voltage increased from 0.7V to ~3V. There is little response in the isotropic-filament phase; however there is temperature dependence in the isotropic phase decreasing uniformly with increasing temperature.

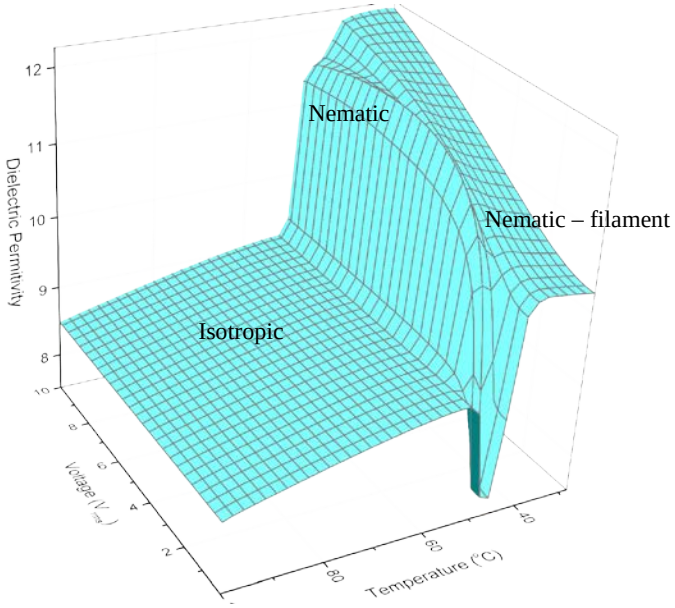

Figure 50 Dielectric constant vs Voltage vs Temperature on cooling

The same effects are seen on cooling the mixture as shown in Figure 50 the isotropic range there has no effect from the electric field. There is the temperature dependence with the isotropic phase again of increasing uniformly with decreasing temperature. Upon entering the non-stable narrow nematic range where there is a typical nematic response to electric fields, the values of the dielectric constants go from the perpendicular and parallel dielectric constants. This indicates that the director is reorienting in the electric field. The nematic phase exhibited is unstable and quickly the mixture is dominated by the filament growths. Once the filaments have grown, the reaction to electric fields of the nematic phase is supressed, again similar to the effects on the heating. The dielectric constant in the presence of the well-established filaments has also increased from the value at unstable nematic phase.

The filaments seem to have no influence on the dielectric properties. When the mixture enters the isotropic – filament phase, the mixture behaves similar to the complete isotropic phase under presence of an electric field. There is temperature dependence in the isotropic phase that is not seen in the filaments phase. Since the effects of electric field are suppressed in the nematic – filament phase, two cell geometries are used to observed the effect of reorienting the mixture.

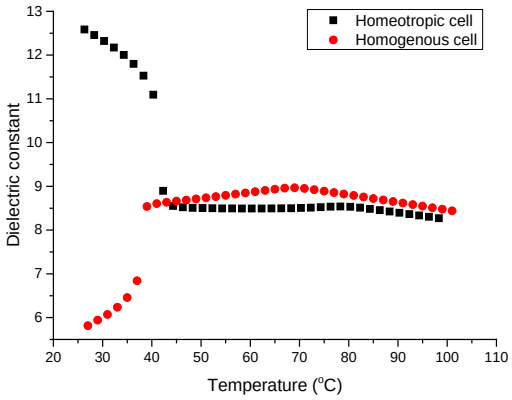

Figure 51 The dielectric constant at 0.05V temperature dependence in two different cell geometries, planar and homeotropic.

In Figure 51 the dielectric constant responses to temperature are what is typically seen in nematic phase at high and low voltage application, i.e. homeotropic and planar alignments of the molecules. The dielectric constant converging ~45°C at the transition temperature of the background nematic to the value at the filament and isotropic phases which is very similar in two different cells. The homogenous aligned cell can be considered as the $\varepsilon_{\perp}$, and homeotropic aligned cell can be consider as the $\varepsilon_{\parallel}$. This means the background nematic phase can be aligned and the network has little effect on the alignment of the nematic phase. To further investigate the structure of the filament growth, small

angle x-ray scattering (SAXS) was employed to look for any periodic structures within the filament network.

SAXS investigation of the filaments

SAXS can be used to probe the periodicity within the filaments network and reveal any periodic structure in which the molecules are arranged in. In the pure samples of similar oxadiazole bent core compounds, there is a DC phase at the temperature ranges below the nematic phase. The DC phase under SAXS investigations have shown a layer spacing of 3.7nm which increases with decreasing temperature [17]. By using SAXS, any periodic structures like layer spacing can be probed in the filament structure, and compared with the known periodic structure of the pure material.

SAXS experiments were conducted using a bulk sample of the mixture contained within a homemade Kapton packet. The temperature of the device was controlled using a Linkam heating stage with an absolute accuracy of $\pm 1^{o}$C and a relative accuracy of $\pm 0.1^{o}$C. The X-ray scattering was conducted at ESRF synchrotron, Grenoble, France. An X-ray beam win an energy of 12KeV, make it sensitive to features from 1.5nm to 9nm, and a beam size of 0.2 x 0.2 mm. Typically a short accumulation time was used ~3 seconds. By analysing the radial distribution of the scattering pattern of silver behenate, which has well defined peaks for which the spacing is known, the spacing of the mixture can be found.

Mixture's periodic structure behaviour on heating

The typical image obtained from SAXS on the mixture at initially before any heating or cooling is shown in Figure 52. Since a bulk sample was measured, there is no expected angular dependence in the scattering pattern. Due to short accumulation time there is insufficient signal to noise to be able see scattering from liquid – like phases, such as the nematic phase, therefore the nematic 5CB scattering is not present in Figure 52.

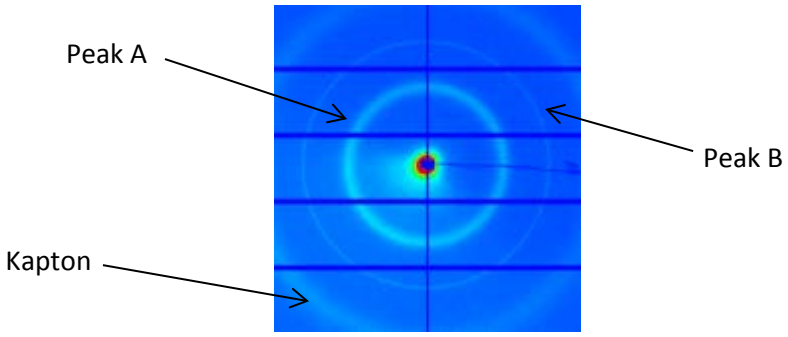

Figure 52 X-ray pattern of mixture 2 at room temperature before any heating or cooling is performed on the sample.

The middle ring (peak B) is thin, indicating a well-defined periodic structure. The inner-most (peak A) is a more diffuse ring that is less defined and has a larger spacing than peak B. The furthest ring from the centre is a diffuse ring originating from the Kapton packet label as Kapton in Figure 52. Thus this Kapton signal is unrelated to the mixture and is omitted from the rest of the discussions.

Peaks A and B are both attributed to the filament structure. These peaks also display the same temperature dependence as seen optically and with DSC. Both peaks exist to well beyond the temperature range of the nematic – filament phase of the mixture, into the isotropic – filament phase, and thus are not caused from the nematic phase, and the diffuse outer peak exists beyond 100ºC. To analyse these rings in more detail the image is integrated over all angles, and the fitting methods discussed chapter 3 will be employed to find the ring attributes. Signals from the nematic phase are not seen in the current setup.

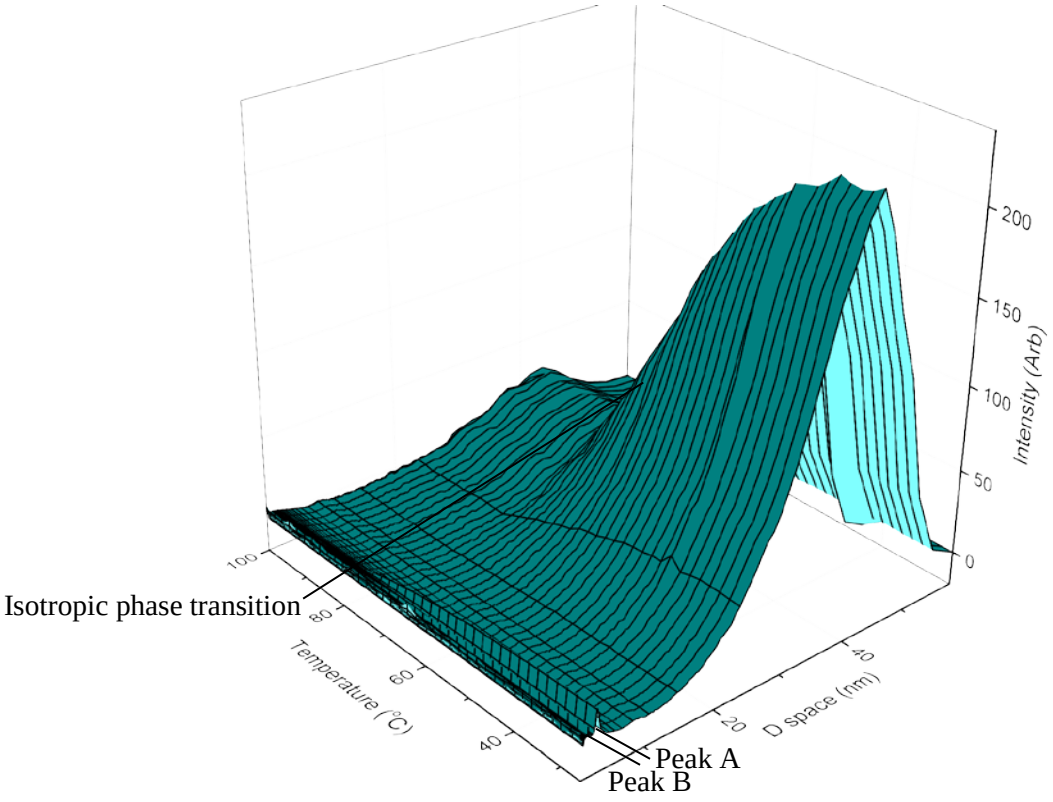

Figure 53 The integrated x-ray pattern vs temperature vs distance on heating.

In Figure 53, the most prominent feature is the significant long range scattering signal, the signal can be attributed to the filament structure, from the behaviour of this signal with temperature. The long range scattered signal disappears at the same temperature as peak A and peak B at the temperatures where the filament network is melted. The exact nature of the signal could not be further investigated with the current setup, but warrant further SAXS studies.

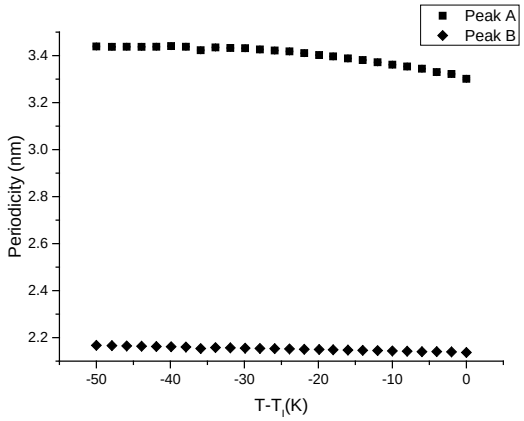

Figure 54 Temperature dependence of the peak positions the transition into the isotropic – filament phase occurs at ~37.19°C according to DSC.

Upon heating, at a rate of 2°C/min, the periodicity of peak A and peak B does not have any significant changes as shown in Figure 54. Peak A shows the trend, seen in the pure bent core compound, of increasing periodicity with decreasing temperature. Peak A decreases very slightly from a periodicity of 3.43nm to 3.30nm, and peak B decreases very slightly from a periodicity of 2.17nm to 2.14nm. From optical and DSC analysis, the mixture enters the isotropic-filament phase at ~38°C. Peaks A and B shows no significant change at that temperature range. Thus peaks A and B are both attributed to the filament structure, this is consistent with what is seen optically as the filaments does not show any significant change even across phase transitions of the background nematic. Both the layer spacing has shown a very small decrease with increase in temperature, similar to the pure bent core compound which shows a decrease of layer spacing with increase in temperature [17].

The system was initially suspected to be crystallization of the dopant, however the periodicities seen are different to the periodicities of the crystal phase of the dopant. In fact the periodicity of 3.4nm exhibited by Peak A that is similar to what is observed in the SAXS performed on the DC phase in the pure sample with the layer spacing of 3.7nm[17]. Peak A structure must be derived from a bent core molecule to bent core molecule periodic structure, since the molecular length of the bent core molecule is ~3.9nm. Peak B, with a corresponding periodicity of 2.2nm, is similar to the molecular length of 5CB of ~1.8nm [18] this peak is derived from a 5CB to 5CB molecular spacing. The periodic structure of 5CB is $\sim\frac{1}{2}$ of the periodicity of the bent core molecule, this could be due to the 5CB forming a similar structure to the pure dopant structure with two 5CB structures forming with one bent core molecule structure.

Since peaks A and B are both attributed to the filament structure, this suggests that within the filaments there is 5CB content forming a periodic structure to fit with the structure from bent core molecules. The 5CB content remains even beyond the normal isotropic temperature range of 5CB

which is incredibly unusual. It is interesting to note that for peak A, the fitting from the split pseudo-Voigt is not as good as the fitting for peak B suggests that peak A is more complicated. This indicates that the periodicity is not well-defined and can be attributed to the presence of the 5CB, which may not exactly match the periodicity of the bent core compound. While the cooling of mixtures behave differently than heating runs, during optical and DSC observations, there may be significant differences in periodicity in the cooling runs also.

Mixture's periodic structure behaviour on cooling

Upon cooling at the same rate of 2°C/min, the mixtures exhibit a transition temperature similar to what was seen optically and through DSC. Initially, in the nematic phase, the scattering image shows a split of peak A into 2 rings, while peak B remains relatively unchanged as shown in Figure 55.

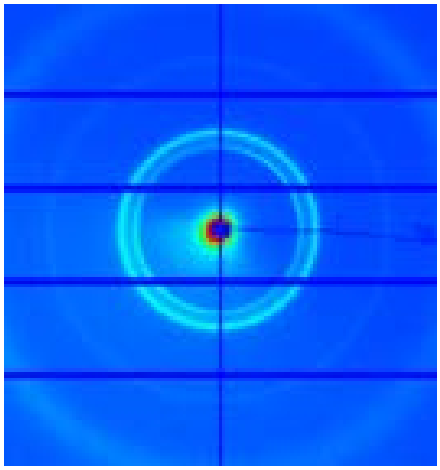

Figure 55 x-ray image on cooling from the isotropic region

Upon integrating the intensity of the image shown in Figure 55, the double ring occurs near 3.7nm and has shifted significantly from the original peak A. To differentiate it from the initial peak A, these peaks have been named A′ and A″. These peaks are close to each other and are convoluting each other in the fitting process, so analysis on these peaks using the same split pseudo-Viogt function used previously is not possible. A simple Lorentz function was employed and only fit the data around the peak centres. A good fit can be obtained for the peak centre, but with unreliable FWHM and amplitude.

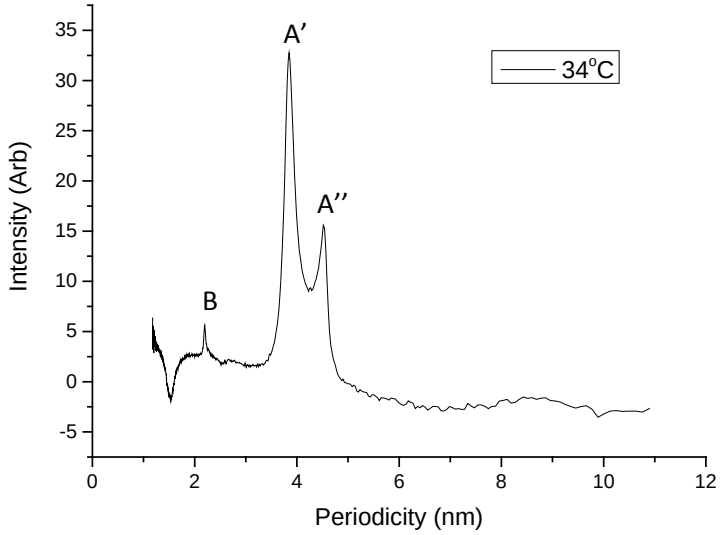

Figure 56 peak A split into two peaks labelled A′ and A′′ while peak B remains unchanged.

From the fitting in Figure 56 peak B is present again at 2.2nm with very little change due to temperature. Peaks A′ and A′′, also remain constant at 3.85nm and 4.54nm, respectively, with changes in temperature. Peak A′ of 3.85nm is of closer in size to the molecular length of bent core compound of 3.9nm is mostly likely a shifted peak A and originates from the bent core compound. For peak A′′, there are no single molecules with molecular lengths in the mixtures to which this spacing can be attributed to.

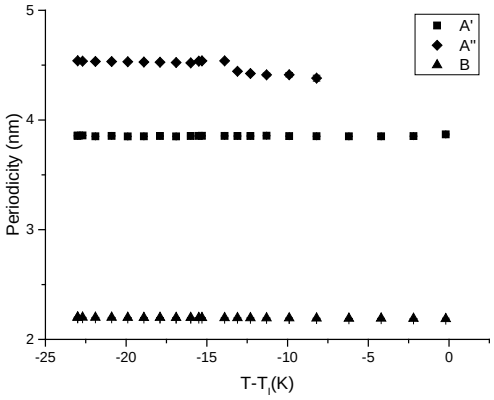

Figure 57 the temperature dependence of the peak positions on cooling

From Figure 57 the temperature dependence of the peak positions are shown. There is very little temperature dependence in the peak positions. Peak A′′ comes into existence at the same temperature as the other periodicities, however the resultant peak is weak and convoluted, so analysis of this peak position is not possible until $T - T_I = -7K$ and not completely well defined until $T - T_I = -12K$.

Peak A″ can be derived from a coupled molecular structure of 5CB. 5CB is known to often form dimers in the nematic phase [18-20]. Commonly 5CB dimers form in an anti-parallel configuration giving a spacing ~1.4 times the molecular length. I speculate that this structure, however, may support an end-to-end configuration [21] of the 5CB dimer. The end-to-end dimer size is similar to the periodicity of A″, and so it is possible that within the filaments, 5CB is also forming dimers to co-exist with other spacing.

The peak A″ is not seen in the initial SAXS shown in Figure 52. This means that peak A″ must be eventually destroyed as the filament formation is stabilized over time. The peaks A″ and A′ must merge with time to recover the initial values.

Time dependence of the filament structure

The mixture has repeatedly shown it has a very time dependent growth associated with the filament network. To check the time dependence of the filament structure, a sample is left a room temperature over several hours, periodically placed back on SAXS setup to measure how the peaks have changed. There was no obvious change to peak B as expected, however peak A seems to be very sensitive to time.

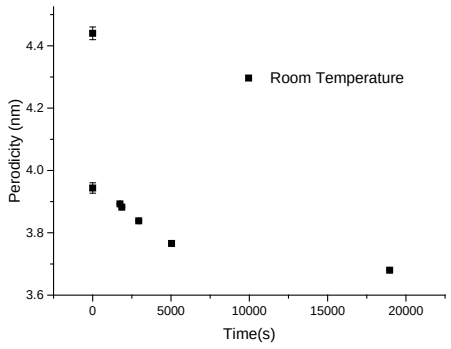

Figure 58 Time dependence of peak A

From Figure 58 peaks A′ and A″ quickly converge into one peak in ~1 hr. The periodicity decreases from 3.95nm to 3.68nm in ~5 hours at room temperature. This is a significant shift in the periodic structure of the filaments and much closer to the initial values seen. This would explain why the system never recovers to the initial layer spacing in peak A as not enough time have been given to the system to recover, and further confirms the time dependence of the filament formation.

This means that, although optically the filament phase is stable, there is still some dynamic process happening, this in fact is consistent with the discrepancy in the transition temperature between the initial heating and subsequent heating. The exact process cannot be revealed in this experiment;

however it is likely to be a process which incorporates more bent core dopant content into the filament structure judging from the discrepancy of transition temperature. From the existence of 5CB dimers initially in system leads me to believe initially that the filament structure phase is similar to that of nematic, or is surrounded by a nematic – like phase. As the bent core content in the filaments is increased over time the phase of the filament structure changes, with the relative stability of peak B can infer that the phase change "freezes" the 5CB within its structure. This process can in turn leading to the alignment of the filaments seen with slow cooling and quenching.

Mixture's periodic structure behaviour on subsequent heating

There are already differences seen in systems with well-established filaments and initial filaments in transition temperature differences, periodicity differences. There are also exists a region shift of the peak A position similar to that of the DC phase is shown by the black circled region in Figure 59.

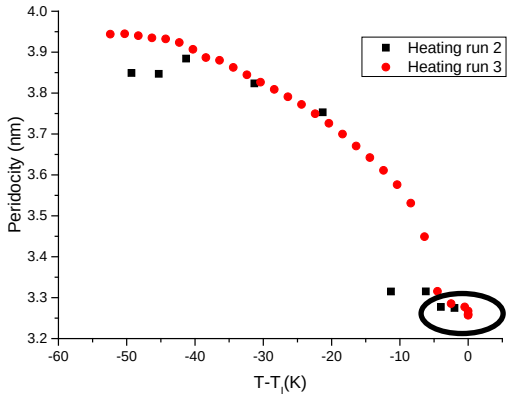

Figure 59 Temperature dependence of peak A on subsequent heating runs, black circle represent a stable region which displays DC phase properties.

The two subsequent heating's initial periodicity is dependent on how long the sample remained at a particular temperature giving the difference seen in Figure 59 on the initial position. The two heating runs also have different heating rates as heat 3 has a continuous heating rate while heat 2 has a static stop at every temperature. The static measurements give more time for the time dependent system to react to the changes in temperature, giving the slight discrepancy seen between the two heating runs. In the two subsequent heating runs there is a region of ~5^{o}C range just below the isotropic phase transition where there is stabilization of the periodic structure from 3.32 nm to 3.27 nm. This stabilization in periodic structure appears to be a phase transition in material and the x-ray pattern becomes broad and diffuse similar to those observed in the DC phase of the pure material.

This would be not seen optically due to the DC phase being an isotropic phase. There was however no indication of this phase transition in the DSC with, but warrants further investigations.

Summary

Initially what appears to be a phase separation and crystallization of the dopant from the host, is actually a much more complicated system. There is phase separation but the phase is not crystal and likely to be liquid crystalline in nature, possibly the DC phase. There are two further separate phenomena occurring in this mixture. Firstly, the gel formation. The filament network is different phase separated from the nematic phase and self-assembled into a 3D network seen as the filament structure. This causes a gel to form from the network and the nematic. The exact nature of the filament phase is unknown at the moment but it contains some periodic structure. A filament phase has been observed in several other materials in the same family of oxadiazole bent core liquid crystals and most exhibit both a DC phase and a filament phase suggesting that these phases could be linked in some way [22]. To the author's knowledge this is the first case where a gel was formed with liquid crystal based 3D network and with a liquid crystal phase acting as the continuous phase in between.

The second phenomenon occurring in this mixture is the incorporation of the 5CB into the 3D gel network for from the bent core dopant. From the SAXS studies 5CB content is always included in the filament structure and is supported by the fact the filament is only formed in the nematic phase of the mixture. 5CB is necessary for the filament structure which is the reason the filament can be aligned as the nematic 5CB can be aligned and thus influences the growth of the filaments when formed slowly.

Liquid crystal gels have been shown to exhibit fast switching in twisted nematic cell [11], have light scattering and transmission modes switchable with electric field, and have the potential to be used in flexible liquid crystal displays [23]. This unique 'double' liquid crystal gel, where the gelator and the host both are liquid crystalline, can be manipulated independently. Further studies into these materials may yield many unique properties yet to be observed.

There are unique properties associated with this double liquid crystal gel such as the ability to align the gel network, incorporation of host into the network, and maintaining 5CB periodic structure well beyond within isotropic temperature. The filaments network has already shown ability to suppress the dielectric response in the current alignment, it is possible that bi-stability can be achieved in certain orientations of the network. Unique the DC-like phases seen in the SAXS experiment, the extremely large long distance scattering which is dependent on the filament network, all warrant further studies into this unique system.

References

1. Hanabusa, K., Yamada, M., Kimura, M., and Shirai, H., *Prominent gelation and chiral aggregation of alkylamides derived from trans-1,2-diaminocyclohexane.* Angewandte Chemie-International Edition in English, 1996. **35**(17): p. 1949-1951.
2. Van Esch, J., Schoonbeen, F., de Loos, M., Kooijman, H., Spek, A.L., Kellogg, R.M., and Feringa, B.L., *Cyclic bis-urea compounds as gelators for organic solvents.* Chemistry-a European Journal, 1999. **5**(3): p. 937-950.
3. Yoza, K., Amanokura, N., Ono, Y., Akao, T., Shinmori, H., Takeuchi, M., Shinkai, S., and Reinhoudt, D.N., *Sugar-integrated gelators of organic solvents - Their remarkable diversity in gelation ability and aggregate structure.* Chemistry-a European Journal, 1999. **5**(9): p. 2722-2729.
4. Aggeli, A., Bell, M., Boden, N., Keen, J.N., Knowles, P.F., Mcleish, T.C.B., Pitkeathly, M., and Radford, S.E., *Responsive gels formed by the spontaneous self-assembly of peptides into polymeric beta-sheet tapes.* Nature, 1997. **386**(6622): p. 259-262.
5. Hafkamp, R.J.H., M.C. Feiters, and R.J.M. Nolte, *Organogels from carbohydrate amphiphiles.* Journal of Organic Chemistry, 1999. **64**(2): p. 412-426.
6. Murata, K., Aoki, M., Suzuki, T., Harada, T., Kawabata, H., Komori, T., Ohseto, F., Ueda, K., and Shinkai, S., *Thermal and Light Control of the Sol-Gel Phase-Transition in Cholesterol-Based Organic Gels - Novel Helical Aggregation Modes as Detected by Circular-Dichroism and Electron-Microscopic Observation.* Journal of the American Chemical Society, 1994. **116**(15): p. 6664-6676.
7. Mamiya, J., Kanie, K., Hiyama, T., Ikeda, T., and Kato, T., *A rodlike organogelator: fibrous aggregation of azobenzene derivatives with a syn-chiral carbonate moiety.* Chemical Communications, 2002(17): p. 1870-1871.
8. Rizkov, D., Gun, J., Lev, O., Sicsic, R., Melman, A., *Donor-acceptor-promoted gelation of polyaromatic compounds.* Langmuir, 2005. **21**(26): p. 12130-12138.
9. Kato, T., et al., *Anisotropic self-aggregation of an anthracene derivative: Formation of liquid-crystalline physical gels in oriented states.* Langmuir, 2002. **18**(18): p. 7086-7088.
10. Kato, T., et al., *Gelation of room-temperature liquid crystals by the association of a trans-1,2-bis(amino)cyclohexane derivative.* Advanced Materials, 1998. **10**(8): p. 606-608.
11. Mizoshita, N., K. Hanabusa, and T. Kato, *Self-aggregation of an amino acid derivative as a route to liquid-crystalline physical gels - Faster response to electric fields.* Advanced Materials, 1999. **11**(5): p. 392-394.
12. Kato, T., Kutsuna, T., Yabuuchi, K., and Mizoshita, N., *Liquid-crystalline physical gels: Electro-optic properties and phase behavior.* Abstracts of Papers of the American Chemical Society, 1999. **218**: p. U502-U502.
13. Hashimoto, M., S. Ujiie, and A. Mori, *Low molecular weight gelators with hexagonal order in their liquid-crystal phases and gel states: 5-cyano-2-(3,4,5-trialkoxybenzoylamino)tropones.* Advanced Materials, 2003. **15**(10): p. 797-800.
14. Isoda, K., T. Yasuda, and T. Kato, *Dipole-driven self-assembly of redox-active mesogenic tetracyanoanthraquinodimethanes.* Journal of Materials Chemistry, 2008. **18**(38): p. 4522-4528.
15. Yoshio, M., Konishi, R., Sakamoto, T., and Kato, T., *Bisphenylsulfone-based molecular assemblies: polar columnar liquid crystals aligned in electric fields and fibrous aggregates in organic solvents.* New Journal of Chemistry, 2013. **37**(1): p. 143-147.
16. Zep, A., Salamonczyk, M., Vaupotic, N., Pociecha, D., and Gorecka, E., *Physical gels made of liquid crystalline B-4 phase.* Chemical Communications, 2013. **49**(30): p. 3119-3121.
17. Southern, C.D., *Order Parameter Measurements and phase behaviour in bent core liquid crytal systems*, in *Physics*. 2008, University of manchester: manchester. p. 177.
18. Leadbetter, A., R. Richardson, and C. Colling, *The structure of a number of nematogens.* Le Journal de Physique Colloques, 1975. **36**(C1): p. C1-37-C1-43.

19. Kedziora, P. and J. Jadzyn, *Dimerization of Polar Mesogenic Molecules.* Molecular Crystals and Liquid Crystals, 1990. **192**: p. 31-37.
20. Dbrowski, R., Janik, J.A., Janik, J.M., and Otnes, K., *A neutron scattering study of dimerization and pairing of molecules in liquid crystal mixtures.* Liquid Crystals, 1988. **3**(4): p. 443-452.
21. Guillon, D. and A. Skoulios, *Conjectures on the Smectic-a Behavior of Dissymmetric and Strongly Polar Mesogens.* Journal De Physique, 1984. **45**(3): p. 607-621.
22. Gortz, V., Southern, C., Robert, N.W., Gleeson, H.F., and Goodby, J.W., *Unusual properties of a bent-core liquid-crystalline fluid.* Soft Matter, 2009. **5**(2): p. 463-471.
23. Kato, T., *Self-assembly of phase-segregated liquid crystal structures.* Science, 2002. **295**(5564): p. 2414-2418.

Chapter 6 Unusual Flexoelectric Switching

Introduction

Recently, there have been developments of display devices utilising the flexoelectro-optic effect, as described in chapter 2, can create fast switching displays. The flexoelectro-optic effect is a naturally fast-switching mechanism seen in short-pitch chiral nematics, and sub millisecond switching has been shown to be possible [1-3]. Bent core molecules have been postulated to have prominent flexoelectric co-efficients [4]. Recent studies into oxadiazole bent core liquid crystals have measured the flexoelectric coefficient through the entire nematic range [5]. The flexoelectric coefficient was found to be ~3 times larger than those seen in calamitic liquid crystal, suggesting bent systems can exhibit larger flexoelectric effects. Dimeric liquid crystals have shown the capability of forming extremely bent systems and can form new bent phases, the twist bend phase [6]. Mixing calamitic liquid crystals and dimers, with a strong chiral dopant, created suitable materials to be used in a flexoelectric display device that exhibited unusual switching behaviour when switching. Under AC voltage, between two states, the intensity exhibited does not reduce the value at zero field at any point. This chapter aims to investigate the cause of the unusual switching behaviour

Flexoelectric switching

As discussed in chapter 2, a chiral nematic phase can manifest the flexoelectric effect during a tilt of the optical axis. This can occur in two geometries, a Uniform Lying Helix (ULH) where the optical axis is in the plane of the cell and in Uniform Standing Helix (USH) where the optical axis is perpendicular to the plane of the cell. The difficulty with the ULH mode is with achieving a stable alignment of the optic axis. Chiral nematic (N*) liquid crystals generally do not spontaneously align to the ULH configuration in conventional cells. The periodic structure of the chiral nematic phase does not match the anchoring conditions imposed by the rubbed polyimide or homeotropic surfactants [7]. An alignment can be achieved by cooling to the N* phase in the presence of an electric field perpendicular to the plane of a planar cell. The helix of the N* phase, through the cooling process, will orient itself parallel to the cell's plane. To achieve a uniform orientation of the helix in the plane of the cell, a gentle shearing of the cell is performed as described by Rudquist et al [8]. However the

alignment is not completely uniform and small domains arise from different alignments as shown in Figure 60 (left). The alignment is also unstable and reverts to a USH structure once the electric field is removed.

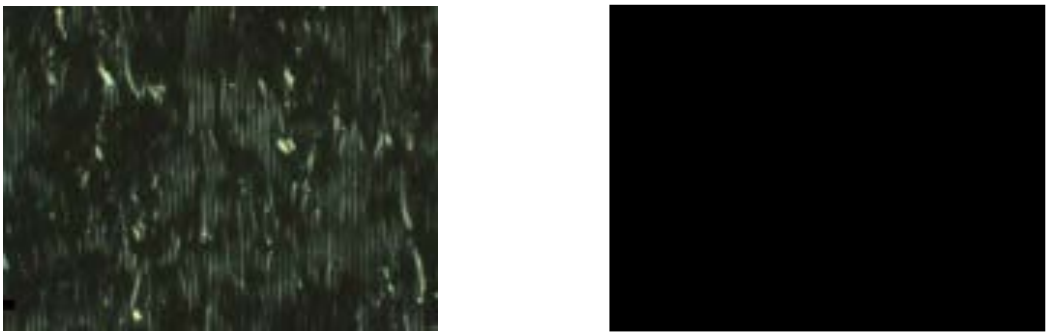

Figure 60 (left) ULH texture with the optical axis parallel to the polariser. (Right) USH texture with the optical axis perpendicular to the plane of the cell at magnificent 50×.

In ULH systems, the optical axis lies in the plane of the cell, to obtain the dark state needed. The optical axis must be oriented parallel or perpendicular to the polarisers in order to switch. We see in Figure 60 (left) that a completely uniform texture is extremely difficult to obtain. This process is not ideal for making display devices [9].

A major advantage of the USH mode is that the alignment is trivial. The USH structure is the lowest energy configuration when using rubbed polyimide alignment layers. A comparison of flexoelectro-optic switching in both the ULH and USH modes revealed that the tilt angles:

$$tan(\Psi) = \frac{(e_1 - e_3)pE}{2\pi(K_1 + K_3)}.$$

are comparable for the two modes [9]. The actual tilt angle required is dependent on a number of factors such as the flexo-elastic ratio, birefringence, and cell thickness [10]. Another significant benefit of USH is the off state, since light is travelling along the optical axis the system exhibits no birefringence, thus a good dark texture can be achieved for short pitches (typically less than 200 nm) [7]. In order to obtain the required switching, a field needs to be applied in the plane of the cell, perpendicular to the optical axis, again an IPS cell can be utilised to achieve this. A similar setup is demonstrated in chapter 3 is used.

The intensity is measured using an in-house built photodiode. An AC square voltage of 100 V_{rms} was applied from an Agilent 33220A waveform generator, the photodiode output was measured from a Tektronix 2024C oscilloscope. The expected behaviour is that the USH device under a square voltage

application would have an optical axis that would tilt back and forth, tilting through the ground state. This would result in a delayed square wave like response; when there is a positive voltage, there would be a rapid rise in intensity until it reaches maximum that would be maintained until a change in polarity of the voltage occurs. When the voltage changes there will be a rapid decay of transmitted intensity to the minimum transmission and then rapidly increase again to a maximum intensity.

When analysing the system, the unusual switching is apparent in Figure 61 (left) where the intensity never reaches a minimum at any point. The obvious cause of transmitted intensity never reaching minimum is that the photodiode is not fast enough to detect the sudden change in intensity, since a square wave is used to drive the system there is a discontinuity in the voltage application. By using a relatively faster photodiode, more of the switching can be detected, however there was no significant difference between the 5μs response time photodiode, Figure 61 (right), and the 250 μs response time photodiode, Figure 61 (left).

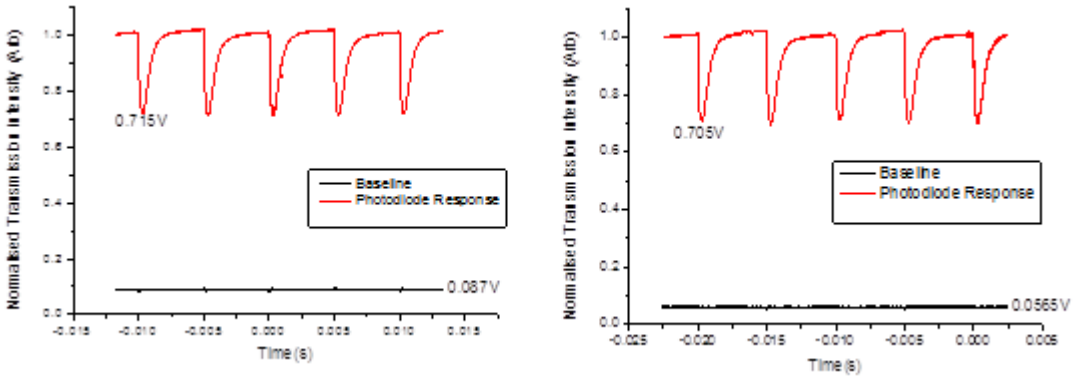

Figure 61 (left) The measured transmission using a 250 μs response time photodiode under 100 Vrms voltage. (right) The measured transmission using a 5 μs response time photodiode under 100 V_{rms} voltage.

The non-zero switching is unlikely to be due to the photodiode response and it is more likely that it is a property of the switching mechanism itself. In order to investigate further, a detailed optical analysis of the switching processes will performed.

Optical observation

Since the switching is expected to consist of tilting of the optical axis back and forth perpendicular to the electric field, the resulting texture should consist of a uniform uniaxial system aligned parallel to the electric field. The origin of the unusual switching mechanism must be within the switching processes itself, any a deviation from a uniaxial texture could indicate a non-standard switching mechanism in this device.

The system is behaving like a uniaxial system when it should be rotating the cell between cross polarisers and the intensity relations.

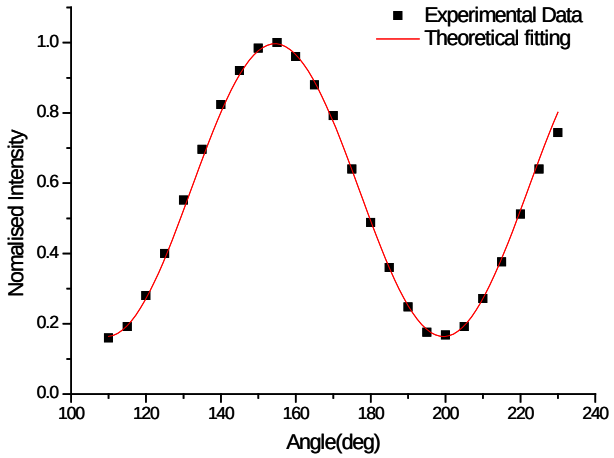

Figure 62 Transmitted intensity of the IPS cell rotating between crossed polarisers.

Fitting the data in Figure 62 to a uniaxial system rotating under cross polarisers shows an excellent fit, and thus the unusual switching is unlikely to be an unusual switch process such as distortions in the helix.

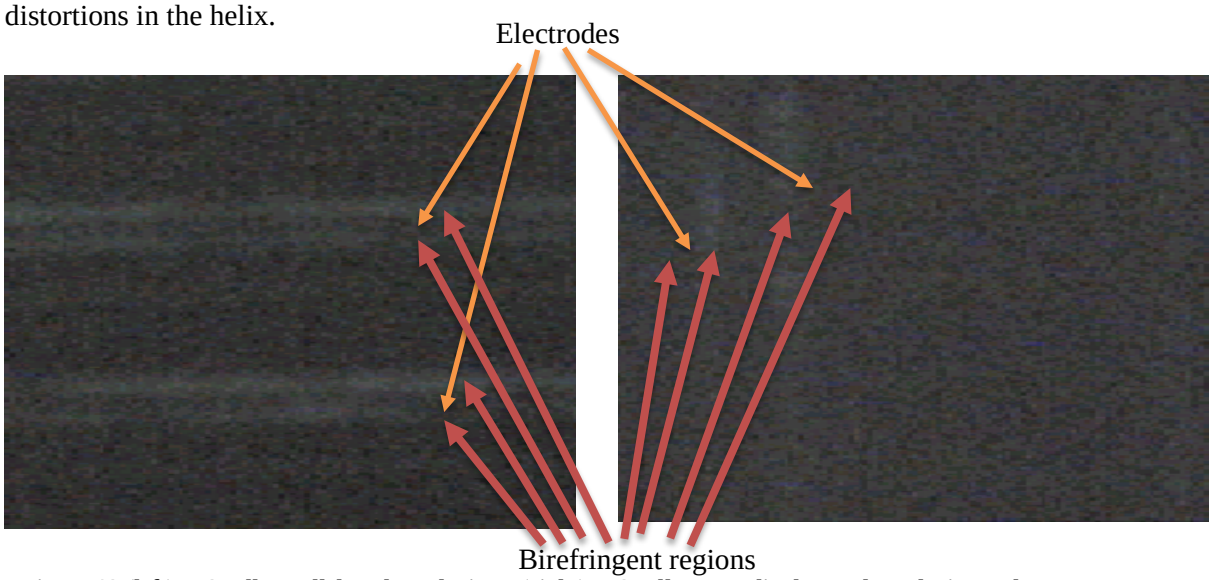

Figure 63 (left) IPS cell parallel to the polarisers (right) IPS cell perpendicular to the polariser. The orange arrows points to the dark regions of the electrodes and the red arrows points to the birefringent regions.

There is only a slight deviation from the expected texture in the dark state where there is birefringence near the electrodes as shown in Figure 63. The region near the electrodes has a much more inhomogeneous electric field relative to the centre in between the electrodes; such complex components are unsurprising. The lack of unusual texture in between the electrodes suggests that the switching behaviour is as expected throughout the majority of the cell and the origin of the unusual switching must be derived from other aspects, possibly the inhomogeneous area of the electric field.

There is also a physical discontinuity of the director field at the electrodes surface which can greatly influence the flexoelectric response.

We analyse if the unusual switching is due to changes in the electric field, such as a square wave modulated with another square wave with amplitudes alternating between 120V to 80V.

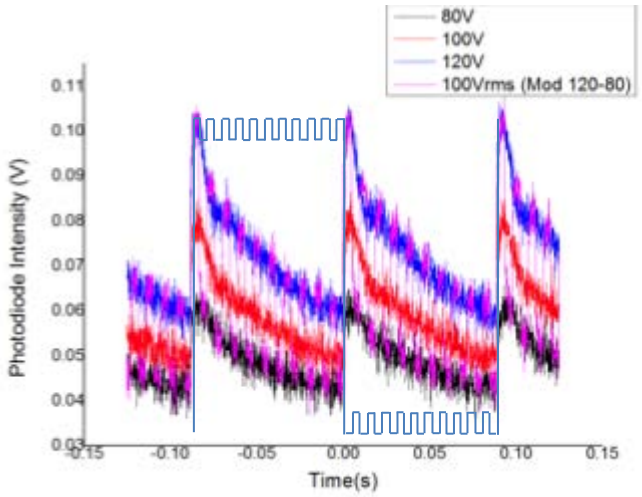

Figure 64 The intensity response of the USH device from a modulated square wave at $100V_{rms}$ and standard square waves at different voltages.

Figure 64 shows a modulated square wave alternating between 120V and 80V and the corresponding intensity response in the pink. The intensity response from the modulated wave alternated, between the values shown, to an unmodulated square wave at 120V and 80V. This shows that there is no complex switching due to the changing of the field strengths. However, the complex switching may be attributed to the changing of polarity of the field seen in the square wave. By analysing the system with a bipolar pulse the sensitivity to any polarity of the field may be found. If the source of the unusual switching is due to the polarity change, then the response from different polarity pulses should result in different transmitted intensity.

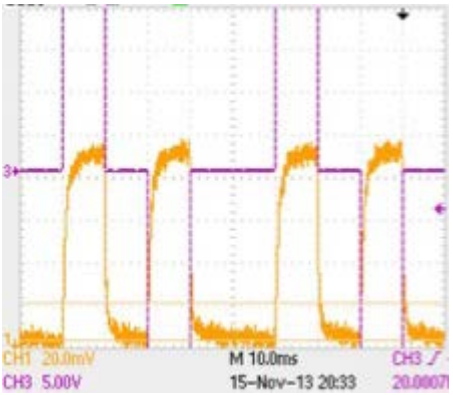

Figure 65 Photodiode response from the USH device using bi-polar pulses.

Figure 65 shows the response from a bi-polar pulse, here the usual response is seen, where the intensity drops to zero at zero electric field, with no significant difference between the two polarities seen; this suggests that polarity does not play a part in the unusual switching.

The experiments performed in this section only looks at the system over a large area and shows that the response to electric field is as expected. The only unusual aspect seen so far is in the small regions near the electrodes showing birefringence in the dark state. To analyse fully how the director is behaving near the electrode, Raman spectroscopy can be employed to investigate the regions.

Time Resolved Raman scattering

Raman spectroscopy is a powerful tool to analyse the director profile in small regions and has been used to map the director profile even in complex systems such as around colloids [11]. This is done by analysing the Raman scattering that is polarised along the molecular long axis; thus by scanning through a material, the director in the material can be found. Raman utilises the inelastic scattering of the photons due to the molecular vibrational modes, thus the signals are commonly extremely weak and need to be collected over a specific time period. Rotating a sample between cross polarisers, the Raman signal is strongest when the molecular vibrational mode is parallel to the analyser, and simply comparing the intensities at different angles, the alignment of the molecules can be inferred. Using this simple technique, the director profile near the electrodes can be analysed for director formations, and possibly the cause of the unusual switching mechanism. The time dependent nature of the Raman signal poses a difficulty in measuring a dynamic system during the switching process. Therefore, a time resolved Raman technique is proposed to obtain a Raman signal for only static portions of the switching process, at the final tilt angle. A Renishaw 1000 Raman spectrometer with a solid state laser with a maximum output power of 50mW at 515.4nm was used in the experiment.

A Raman signal is taken over a period of time; however, the switching process is dynamic. Initially, upon field application, the molecules will be reorienting themselves until they reach their final position. The Raman signal taken during the switching process will be composed of the dynamic reorientation and the final static position. Only the final static orientation is of interest as it can reveal the orientation of the director. By simply eliminating the light source with a mechanical chopper during the dynamic portions of the switching process, only the signal from the static portions of the switching process will be accumulated. Due to the chopper having a physical start up time to get to the required frequency, the waveform applied is triggered from the light source.

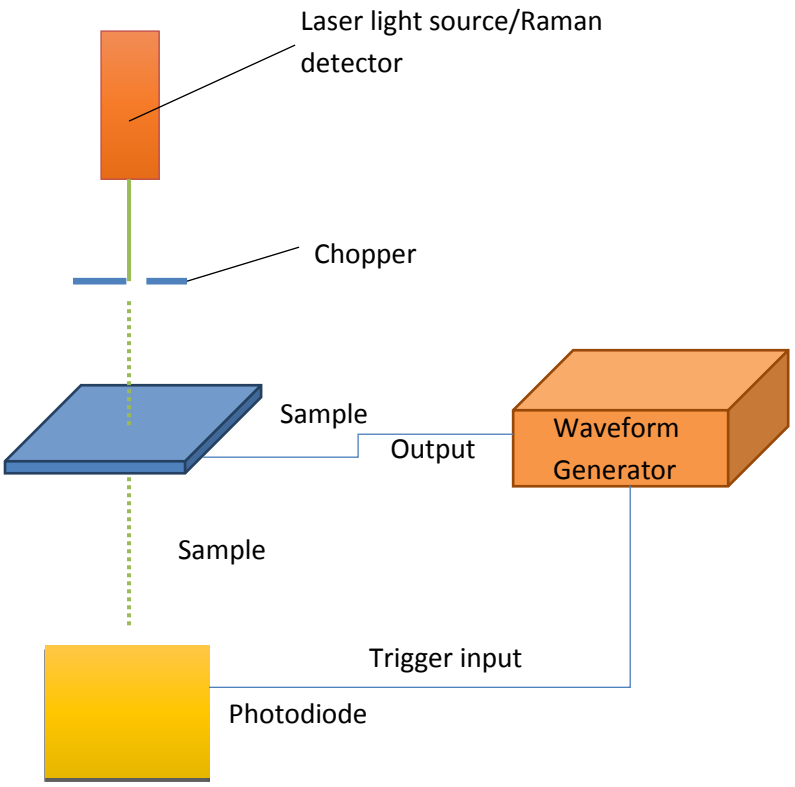

Figure 66 Setup of the electro-optic equipment.

The experimental setup is shown in Figure 66. The experimental setup is operating in parallel with the Raman spectrometer, with the chopper is set to cut of 70% of the light at the same frequency of the output square wave. The waveform generator is triggered from a photodiode to detect when light is present to produce the square wave that's needed. The end result is that the static switching, from the Raman signal, is observed and collected.

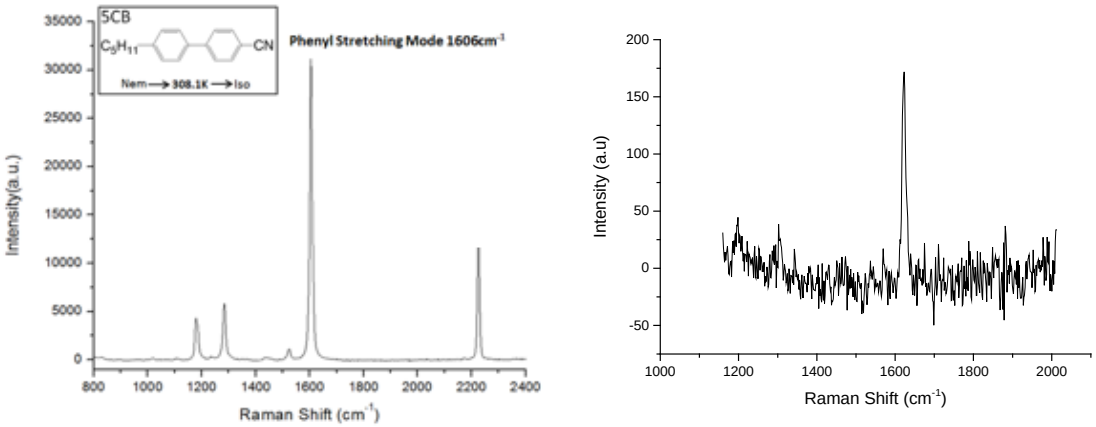

Figure 67 (left) Raman spectrum of 5CB from a non-chopped source [12] (right) Raman spectrum of 5CB from a chopped source.

Figure 67 (left) shows the signal from 5CB using an un-chopped light source, the signal strength is strong compared to a low background noise. The spectrum obtained from a chopped source

has a much reduced signal strength but displays the phenyl stretching mode clearly with the same Raman shift of 1606cm^{-1}. This method can be used on the dimeric mixture during switching in order to analyse the molecular alignment near the electrodes. This is done by rotating the sample and finding the orientations with maximum Raman signal. This indicates that the molecular alignment is parallel to the orientation.

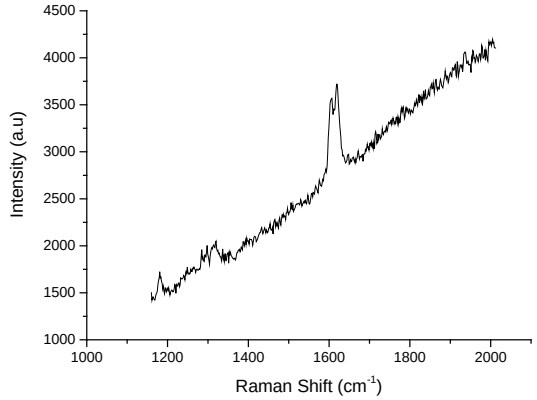

Figure 68 Raman spectrum of USH device with chopped source

Figure 68 shows the Raman spectrum of the USH device signal, however it is in the presence of a strong background, and difficulties quickly arose as the material exhibited fluorescence and the background grew stronger and overcame the signal from the device as shown in Figure 69.

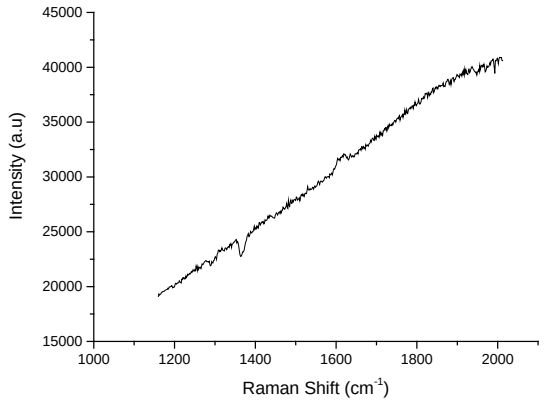

Figure 69 Raman spectrum of the USH device with chopped source and florescence

The sudden increase in fluorescence is quick, ~10-20 minutes, and as a result, there weren't enough measurements made to make any analysis of the director profile. Fluorescence is the absorption and re-emission of light, by using different wavelength light sources. The absorption and, in turn, the re-emission can be reduced allowing enough time to collect a series of Raman spectrums.

Summary

The USH system studied in this chapter appears to display unusual switching under square electric fields, however many aspects of the switching seem to be behaving as expected. The switching directions seem to obey the back and forth tilting of the optical axis and the response to changing electric field strengths and polarity also exhibits the expected behaviour. There are however small complex regions near the electrodes during the switching, these regions are likely to be the cause of the unusual switching.

Attempts to analyse the exact structure with time resolved Raman spectroscopy was not successful due to the high amount of fluorescence. This may be overcome by using different wavelength light sources, which is an avenue that we lacked time to pursue, but warrants further investigation.

References

1. Musgrave, B., P. Lehmann, and H.J. Coles, *Flexoelectro-Optic Properties of a Series of Novel Chiral Nematic Liquid Crystals.* Molecular Crystals and Liquid Crystals Science and Technology. Section A. Molecular Crystals and Liquid Crystals, 1999. **328**(1): p. 309-316.
2. Broughton, B.J., Clark, M.J., Blatch, A.E., and Coles, H.J., *Optimized flexoelectric response in a chiral liquid-crystal phase device.* Journal of Applied Physics, 2005. **98**(3) 034109: p. 1-6.
3. Morris, S.M., Clarke, M.J., Blatch, A.E., and Coles, H.J., *Structure-flexoelastic properties of bimesogenic liquid crystals.* Physical Review E, 2007. **75**(4) 041701: p. 1-9.
4. Patel, J.S. and R.B. Meyer, *Flexoelectric Electrooptics of a Cholesteric Liquid-Crystal.* Physical Review Letters, 1987. **58**(15): p. 1538-1540.
5. Kaur, S., Panov, V.P., Greco, C., Ferrarini, A., Gortz, V., Goodby, J.W., and Gleeson H.F., *Flexoelectricity in an oxadiazole bent-core nematic liquid crystal.* Applied Physics Letters, 2014. **105**(22) 223505: p. 1-4.
6. Cestari, M., Diez-Berart, S., Dunmar, D.A., Ferrarini, A., de la Fuente, M.R., Jackson, D.J.B., Lopez, D.O., Luchkhurst, G.R., Perez-Jubindo, M.A., Richardson, R.M., Salud, J., Timimi, B.A., and Zimmermann, H., *Phase behavior and properties of the liquid-crystal dimer bis(4-cyanobiphenyl-4-yl) heptane: A twist-bend nematic liquid crystal.* Physical Review E, 2011. **84**(3) 031704: p. 1-20.
7. Chen, J.e., W.e. Cranton, and M.e. Fihn, *Handbook of visual display technology*.
8. Rudquist, P., Buivydas, M., Komitov, L., and Lagerwall, S.T., *Linear Electrooptic Effect Based on Flexoelectricity in a Cholesteric with Sign Change of Dielectric Anisotropy.* Journal of Applied Physics, 1994. **76**(12): p. 7778-7783.
9. Salter, P.S., Kischka, C., Elston, S.J., and Raynes, E.P., *The influence of chirality on the difference in flexoelectric coefficients investigated in uniform lying helix, Grandjean and twisted nematic structures.* Liquid Crystals, 2009. **36**(12): p. 1355-1364.
10. Castles, F., S.M. Morris, and H.J. Coles, *Flexoelectro-optic properties of chiral nematic liquid crystals in the uniform standing helix configuration.* Physical Review E, 2009. **80**(3) 031709: p. 1-9.
11. Lee, T., Mundoor, H., Gann, D.G., Callahan, T.J., Smalyukh, I.I., *Imaging of director fields in liquid crystals using stimulated Raman scattering microscopy.* Optics Express, 2013. **21**(10): p. 12129-12134.
12. Zhang, Z., Thesis in *School of Phyiscs and Astronomy*. 2014, University of Manchester: Manchester.

Chapter 7 Summary and Future Work

Introduction

The recent interest in bent core liquid crystals has led to discovery of many unusual behaviours, such as an apparent biaxial nematic phase [1, 2], large Kerr effect [3], large flexoelectricity [4, 5] and unusual elastic properties [6-10]. It is apparent from the current research that liquid crystalline system which contains an intrinsic bend in the bent core liquid crystals which is the primary cause of the many unique behaviours. This thesis investigated further liquid crystalline systems with intrinsic bend, and the effect of introducing the intrinsic bend to conventional liquid crystalline systems. It is found that the bend angle of molecules with intrinsic bend has a significant effect on the physical properties, resulting in the anomalous elastic behaviour [11, 12]. Interestingly anomalous behaviour occurs as a natural consequence of the natural conformation of the molecule with intrinsic bend. Further complex systems were investigated by introducing intrinsic bend into conventional liquid crystalline systems resulting in mixtures. The mixtures had the predicted result of altering the elastic behaviour the anomalous behaviour. However there was also a unique mixture which were unpredicted and found to form a new phase, which led to further studies suggesting that it is a new unique gel phase. Prominent flexoelectric properties was postulated [13] and seen in some bent core liquid crystals [4, 5]. Large flexoelectric effect are of particular interest in developing display devices due to the relatively fast switching speeds. Some mixtures with intrinsic bend however showed an unusual switching. Investigations into the unusual switching were attempted, but was ultimately hindered by the fluorescence of the mixture. Overall it is found that molecules and liquid crystalline systems with intrinsic bend can be altered from systems without intrinsic bend. The differences range from minor alterations to the physical properties to forming completely new phases.

Elastic properties in bent core liquid crystals

The elasticity dictates how liquid crystals respond to external fields, which is important factor in practical devices and in understanding the physical properties. The splay and bend elastic constants are investigated using the well-known method of fitting capacitance and voltage. The difficulty came in measuring the twist elastic constant, this was overcome in this thesis by utilising an In-Plane Switching (IPS) cell, combined with an extrapolation method to find the threshold voltage. This

proved to replicate results well in conventional calamitic liquid crystals, but is associated with large errors. Using these methods, the elastic properties of complex bent core liquid crystal compounds and mixtures of bent core and calamitic liquid crystal was then examined.

The bend elastic constant, in pure bent core compounds, was commonly greater than the splay elastic constant, contrary to calamitic liquid crystals [6-10]. Some bent core compounds exhibited elastic properties similar to calamitic liquid crystals [11, 14]. In order to understand this disparity, first the elastic constants of mixtures of oxadiazole bent core liquid crystals and calamitic liquid crystals were found. The bent elastic constant and the twist elastic constant have shown drastic reductions in values throughout the nematic temperature range which increases with dopant concentration. The splay elastic constant showed consistently small changes relative to the other elastic constants even with increasing dopant concentration. The K_3 results confirms what has been seen in other studies which suggests the bent core liquid crystals heavily influence the K_3 values, while there is a lack information for the K_2 value due to the difficulty in measurement techniques. Surprisingly in the mixtures K_2 values also showed significant decreases with increases in dopant concentration, often greater changes that those seen in K_3. In fact in mixtures of 5CB and a oxadiazole compound, the 5wt% inclusion of bent core compound resulted in a change of ~3.5pN or ~80% reduction in K_2. This revealed a previously unseen and unpredicted property of the intrinsic bend angle heavily influencing the twist deformation also.

For further investigation a series of oxadiazole and thiadiazole based bent core liquid crystal were measured in conjunctions with atomistic calculations, performed by *A. Ferrarini*. The experimental results obtained were in collaboration with *S. Kaur*, who measured the bend and splay elastic constants, results published in [11, 12]. The atomistic calculations were based solely on the molecular conformations that the molecules adopted. The experimental results were in excellent agreement with atomistic calculations indicating the importance of the bend angle. The bend angle of the bent core compound is extremely important for dictating the bend and twist elastic properties in the nematic phase. A bend angle ~160^o, like those seen in the thiadiazole compound, is large and closer in shape to calamitic molecules thus displays the property where the bend elastic constant is larger than the splay elastic constant. The bend angle of ~140^o, like those seen in the oxadiazole compound is small, displays the property of the bend elastic constant, and is smaller than the splay elastic constant. Inclusions of intrinsic bend into a liquid crystal system also dramatically reduced the twist elastic constant in almost all cases. The twist elastic constant reduces as the temperature increases; this is expected behaviour as the nematic phase is approaching isotropic phase where there are no elastic properties. The values of the K_2 for series of oxadiazole compounds $T - T_{NI} = -8^oC$ is <1.5pN. This is very low compared to those seen in 5CB which shows K_2 of 5pN.

The other structural changes we studied included terminal chain lengths, fluorination of terminal chains, and changing one terminal chain from alkoxy to alkyl. Most of these changes to the molecular shape seem to have little effect on the elastic constants; the most significant effect comes from changing one terminal chain from alkoxy to alkyl which significantly lowers the all elastic constants, however this is expected from the strong dipole associated with the oxygen.

In all the unique behaviour of bent core liquid crystal seems to be heavily influenced by only the bend angle, where the size will determine the properties the nematic phase displays. This can be may prove useful in the future in designing liquid crystal with certain physical properties.

Further investigations

The changing of one terminal chain from alkoxy to alkyl appears induce the greatest change in elastic properties. One clear difference is the asymmetry caused by changing one of the terminal chains from alkoxy to alkyl. In particular the oxadiazole compound with the asymmetric molecular structure displayed the most drastic difference to conventional liquid crystals, such as displaying a DC phase. Investigating different asymmetric bent core compounds may produce similar significant changes to the physical properties. The nature of such asymmetry also needs further investigation, such as physical asymmetric molecules, hockey shaped molecules, warrants further investigations into these asymmetric compounds.

New double liquid crystal gels

A new phase was formed from a mixture of 10% a bent core oxadiazole compound with 5CB as host. Through optical observations, differential scanning calorimetry, and Small Angle X-ray Scattering (SAXS), it was determined that the phase was a double liquid crystal gel phase. The double liquid gel is unique due to a liquid crystal phase based network with another liquid crystal phase acting as the continuous phase in between. The system is further complicated by two separate phenomena occurring in this mixture. Firstly, the gel formation is a phase separation, of elements from the mixtures from the nematic phase, self-assembled into a 3D network seen as a filament structure. This causes a gel to form from the network and the nematic phase. The filament formation can only form in the nematic phase, which is an extremely time-dependent process. The dependence of the filaments on the nematic phase can also lead to some unique properties such as the ability to align the filaments. The exact nature of the filament phase is unknown at the moment but it contains

some periodic structure seen in the SAXS pattern but could be linked to a Dark Conglomerate (DC) phase.

The second phenomenon occurring in this mixture is the incorporation of the 5CB into the 3D gel network to from the bent core dopant. From the SAXS studies, 5CB content is always included in the filament structure and is supported by the fact the filament is only formed in the nematic phase of the mixture. 5CB is necessary for the filament structure which is the reason the filament can be aligned in the same way the nematic 5CB can be aligned, and thus influences the growth of the filaments when formed slowly.

Further investigations

In SAXS studies of the double liquid crystal gel, there exists significant long range scattering. This is heavily linked to the filament structure in the phase, mostly likely due to the filament to filament interactions. Investigations into the long range scattering by adjusting the SAXS setup can reveal more of how the filaments are interacting with each other and any orientation preference it may have with and without alignment.

The exact phase of the 3D network which is phase separating in the mixture is also unknown. The phase of the 3D network is similar to a filament phase seen in other oxadiazole bent core compounds, and could be linked in some way. There is a brief region where the periodicity observed is very similar to the spacing seen in DC phases (seen at high temperatures) in subsequent heating runs of the mixture, suggesting a possible DC phase in the 3D network. The exact mechanism by which some host material is incorporated in the network has never been seen before and requires detailed studies into the system. The periodic structure seen in 3D network matching relatively well seems to suggest that the molecule shape is an important factor the incorporation process. Using 8CB as the host may lead to understanding how the molecular shape is important in the mechanism if a similar gel phase forms.

There may also be application potential for the new double liquid crystal gel. Liquid crystal gels in twisted nematic cells have been shown to exhibit fast switching [15], have light scattering and transmission modes that are switchable with electric fields and have the potential to be used in flexible liquid crystal displays [16]. There is potential for non-conventional applications such as new battery devices using highly anisotropic ion conduction in liquid crystal materials [17]. Liquid crystal gels can also be used as bioactive membranes [18, 19], which may be used for drug delivery or tissue-healing applications. Self-assembled structures may also function as templates for the formation of nano – meter scale conduits and networks [20]. This unique ‘double’ liquid crystal gel, where the gelator and the host are both liquid crystalline, can be manipulated independently and have the ability

to align the gel network. Further studies into these materials may yield many unique properties yet to be observed.

Unusual flexoelectric switching in dimeric chiral nematics

Highly chiral dimeric mixtures in a Uniform Standing Helix (USH) system seem to display unusual switching under square electric fields, where the intensity never reduces to zero during any part of the switching process. Many aspects of the switching behave as expected. After examining the optical behaviour, the switching directions seem to obey the back and forth tilting of the optical axis. The response to a modulated square wave showed that changing electric field strength also exhibits the expected behaviour. In bipolar pulses the response to different polarities was the same and did not change depending on polarity of the field applied. There are however small complex regions near the electrodes during the switching; these regions are likely to be the cause of the unusual switching. The physical discontinuity of the director profile and the non-uniform electric field near the electrodes can form complex surfaces which may influence the flexoelectric properties of the mixture.

Further investigations

Raman spectroscopy can reveal the director profile in small areas, attempts to analyse the exact structure with time resolved Raman spectroscopy was not successful due to the high amount of fluorescence. The time resolved method was successful in measuring the final position within the dynamic switching process. The fluorescence may be overcome by using different wavelength light sources, then the exact director profile in the complex regions near the electrodes can then be analysed to see if it can cause the unusual switching.

Conclusion

It is seen that introducing bend into liquid crystal systems influences greatly the phase and can form new bent phases. This thesis mainly focuses on the simplest nematic phase, and even in this phase there are drastic changes to the properties from bent influences. Thus the bend deformation intrinsic to the molecule or system has a great effect in a wide range of liquid crystalline phases, even in the nematic phase. The unusual elastic property exhibited by many of the bent core liquids is found to be strongly influenced by the bend angle of the intrinsic bend in the system. Seen from mixtures the changes seen in the elastic properties are related to the intrinsic bend content, such as bend core dopants. What is not seen in a lot of current research is the drastic lowering of the twist elastic

constant, due to the difficulty of measurement there was few reports on the low values of twist elastic constant seen. In studies performed in this thesis, the drastically low values of twist elastic constant were repeatedly seen in mixture and pure compound alike.

New phases can be formed from mixing oxadiazole bent core compound with 5CB, which was found to be a double liquid crystal gel phase. The double liquid crystal gel has two phenomena of incorporation of host into rigid structure, and liquid crystalline properties of the structure. The exact nature of how the gel is formed and the resultant properties from the changes are still unknown and require additional research.

In further complex systems such as in USH and the corresponding flexoelectric effects. It is seen to produce further unique properties such as, the unusual switching. It is likely that the non-uniformity of the field with the discontinuity of the director profile in conjunction with the inclusion of intrinsic bend have caused complex molecular orientations to occur in the edge regions, and these region in turn influence the bulk orientation as a whole. However this could not be confirmed due to the material fluorescence, but the effect of introducing intrinsic bend again have a great effect on a previously known liquid crystal phenomena.

In conclusion the inclusion of intrinsic bend into liquid crystalline systems can have a dramatic effect on almost all liquid crystal phases. The parameter which dictates the differences seem to defined by the bend angle. However in more complex systems the introduction of intrinsic bend can further complicate the liquid crystal phase, with new molecular orientations formed at edge regions of electrodes, which can influence the bulk properties. Thus the introduction of bend can alter conventional understood liquid crystals and give rise to new effects and materials, and there is still much that needs to be understood in these bent systems. With further studies introducing bend to ever more complex system can reveal even more on how liquid crystal systems are responding to intrinsic bend.

References

1. Vanakaras, A.G. and D.J. Photinos, *Thermotropic biaxial nematic liquid crystals: Spontaneous or field stabilized?* J. Chem. Phys., 2008. **128**(15) 154512: p. 1-4.
2. Francescangeli, O., Vita, F., Ferrero, C., Dingemans, T., and Samulski, E.T., *Cybotaxis dominates the nematic phase of bent-core mesogens: a small-angle diffuse X-ray diffraction study.* Soft Matter, 2011. **7**(3): p. 895-901.
3. Dhara, S., Araoka, F., Lee, M., Le, K.V., Guo, L., Sadashiva, B.K., Song, K., Ishikawa, K., and Takezoe, H., *Kerr constant and third-order nonlinear optic susceptibility measurements in a liquid crystal composed of bent-shaped molecules.* Phys. Rev. E, 2008. **78**(5) 050701: p. 1-4.
4. Salter, P.S., Tschierske, C., Elston, S.J., and Raynes, E.P., *Flexoelectric measurements of a bent-core nematic liquid crystal.* Phys. Rev. E, 2011. **84**(3) 031708: p. 1-5.
5. Kaur, S., Panov, V.P., Greco, C., Ferrarini, A., Gortz, V., Goodby, J.W., and Gleeson, H.F., *Flexoelectricity in an oxadiazole bent-core nematic liquid crystal.* Applied Physics Letters, 2014. **105**(22) 223505: p. 1-4.
6. Majumdar, M., Salamon, P., Jakli, A., Gleeson, J.T., and Sprunt, S., *Elastic constants and orientational viscosities of a bent-core nematic liquid crystal.* Phys. Rev. E, 2011. **83**(3) 031701: p. 1-8.
7. S. Kaur, Addis, J., Greco, C., Ferrarini, A., Gortz, V., Goodby, J.W., and Gleeson, H.F., *Understanding the distinctive elastic constants in an oxadiazole bent-core nematic liquid crystal.* Phys. Rev. E, 2012. **86**041703: p. 1-11.
8. Sathyanarayana, P., Mathew, M., Li, Q., Sastry, V.S.S., Kundu, B., Le, K.V., Takezoe, H., and Dhara, S., *Splay bend elasticity of a bent-core nematic liquid crystal.* Phys. Rev. E, 2010. **81**(1) 010702: p. 1-4.
9. Tadapatri, P., Hiremath, U.S., Yelamaggad, C.V., and Krishnamurthy, K.S., *Permittivity, Conductivity, Elasticity, and Viscosity Measurements in the Nematic Phase of bent core LC.* J. Phys. Chem. B 2010. **114**: p. 1745-1750.
10. Salamon, P.,Eber, N., Seltmann, J., Lehnmann, M., Gleeson, J.T., Sprunt, S., and Jakli, A., *Dielectric technique to measure the twist elastic constant of liquid crystals: The case of a bent-core material.* Phys. Rev. E, 2012. **85**(6) 061704: p. 1-9.
11. Kaur, S., Tian, L., Liu, H., Greco, C., Ferrarini, A., Seltmann, J., Lehmann, M., and Gleeson, H.F., *The elastic and optical properties of a bent-core thiadiazole nematic liquid crystal: the role of the bend angle.* Journal of Materials Chemistry C, 2013. **1**(13): p. 2416-2425.
12. Kaur, S., Liu, H., Addism J., Greco, C., Ferrarini, A., Gortz, V., Goodby, J.W., and Gleeson, H.F., *The influence of structure on the elastic, optical and dielectric properties of nematic phases formed from bent-core molecules.* Journal of Materials Chemistry C, 2013. **1**(40): p. 6667-6676.
13. Patel, J.S. and R.B. Meyer, *Flexoelectric Electrooptics of a Cholesteric Liquid-Crystal.* Physical Review Letters, 1987. **58**(15): p. 1538-1540.
14. Salamon, P., Eber, N., Seltmann, J., Lehmann, M., Gleeson, J., Sprunt, S., and Jakli, A., *Dielectric technique to measure the twist elastic constant of liquid crystals: The case of a bent-core material.* Phys. Rev. E, 2012. **85**(6) 061704: p. 1-9.
15. Mizoshita, N., K. Hanabusa, and T. Kato, *Self-aggregation of an amino acid derivative as a route to liquid-crystalline physical gels - Faster response to electric fields.* Advanced Materials, 1999. **11**(5): p. 392-394.
16. Kato, T., *Self-assembly of phase-segregated liquid crystal structures.* Science, 2002. **295**(5564): p. 2414-2418.
17. Ohtake, T., Ogasawara, M., Ito-Akita, K., Nishina, N., Ujie, S., Ohno, H., and Kato, T., *Liquid-crystalline complexes of mesogenic dimers containing oxyethylene moieties with LiCF3SO3: Self-organized ion conductive materials.* Chemistry of Materials, 2000. **12**(3): p. 782-789.

18. Slack, N.L., Schellhorn, M., Eiselt, P., Chibbaro, M.A., Schulze, U., Warriner, H.E., Davidson, P., Schmidt, H.W., and Safinya, C.R., *Synthesis and phase behavior of new amphiphilic PEG-based triblock copolymers as gelling agents for lamellar liquid crystalline phases.* Macromolecules, 1998. **31**(24): p. 8503-8508.
19. Warriner, H.E., Idziak, S.H.J., Slack, N.L., Davidson, P., and Safinya, C.R., *Lamellar biogels: Fluid-membrane-based hydrogels containing polymer lipids.* Science, 1996. **271**(5251): p. 969-973.
20. Evans, E., Bowman, H., Leung, A., Needham, D., and Tirrellm, D., *Biomembrane templates for nanoscale conduits and networks.* Science, 1996. **273**(5277): p. 933-935.